SPINTRONICS IN TIME-DEPENDENT SYSTEMS: MANIPULATION AND DETECTION OF SPIN CURRENTS BY RASHBA SPIN-ORBIT INTERACTION

by

FAHRİYE NUR GÜRSOY

Submitted to the Graduate School of Engineering and Natural Sciences
in partial fulfillment of
the requirements for the degree of
Doctor of Philosophy

Sabancı University

December 2022

SPINTRONICS IN TIME-DEPENDENT SYSTEMS: MANIPULATION AND DETECTION OF SPIN CURRENTS BY RASHBA SPIN-ORBIT INTERACTION

Approved by:

Prof. Dr. İnanç Adagideli . . . .
(Dissertation Supervisor)

Prof. Dr. Zafer Gedik . . . .

Prof. Dr. Burç Mısırlıoğlu . . . .

Prof. Dr. Klaus Richter . . . .

Assoc. Prof. Ahmet Levent Subaşı . . . .

Date of Approval: December 16, 2022

ABSTRACT

SPINTRONICS IN TIME-DEPENDENT SYSTEMS: MANIPULATION AND
DETECTION OF SPIN CURRENTS BY RASHBA SPIN-ORBIT INTERACTION

Fahriye Nur Gürsoy

Ph.D. Thesis, December 2022

Thesis Supervisor: Prof. Dr. İnanç Adagideli

In this thesis, we focus on manipulating spin-orbit interaction to generate spin-dependent transport in two-dimensional electron gases (2DEG). Rashba spin-orbit interaction (SOI) can be modulated both spatially and temporally. Here, we explore how we can create spin currents in nano- or mesoscale conductors via periodically time-dependent Rashba SOI. We base our calculations on the Floquet scattering theory, which is the standard tool to study time dependent transport properties in these systems. In particular, we analyze AC and DC charge and spin currents generated by dynamical Rashba SOI in the absence of bias voltage, checking our analytical expressions and approximations with full numerical spin-dependent transport simulations and studying our numerical results in both low and high-frequency regimes. We also investigate high harmonic generation in a time-dependent Rashba coupling and study the pumping charge and spin current when the system involves one or two adjustable parameters in and beyond the adiabatic approximation. Spin-orbit coupling in 2DEGs can also be formulated using SU(2) gauge fields. Through an SU(2) gauge transformation, one can show that the time-dependent Rashba SOI induces spin-dependent voltages. Furthermore, this gauge transformation enables one to identify relevant Onsager symmetries. The latter can then be exploited for the realization of spin transistor devices, particularly when the spin-orbit interaction is inhomogeneous throughout the sample. Combining these two concepts, we propose a spin transistor that generates spin current by employing the dynamical SOI. Finally, we exploit spatially inhomogeneous Rashba SOI to convert spin currents into charge currents, providing an experimentally feasible detection mechanism.

ÖZET

ZAMANA BAĞLI SİSTEMLERDE SPİNTRONİK : RASHBA SPİN-YÖRÜNGE ETKİLEŞİMİ ILE SPİN AKIMLARININ MANİPÜLASYONU VE ÖLÇÜMÜ

Spintronics in time-dependent systems: Manipulation and detection of spin currents by Rashba spin-orbit interaction

FAHRİYE NUR GÜRSOY

FİZİK DOKTORA TEZİ, ARALIK 2022

Tez Danışmanı: Prof. Dr. İnanç Adagideli

Anahtar kelimeler: Meso ve nano ölçekli sistemler, spintronik, spinorbitronik, Rashba spin-yörünge etkileşimi, kuantum taşınım, yük ve spin pompalama, zamana bağlı taşınım, Floquet saçılma kuramı

Bu tezde iki boyutlu elektron gazlarında spine bağlı taşınım oluşturma amacıyla spin-yörünge etkileşiminin manipülasyonunu ele aldık. Rashba spin-yörünge etkileşimi hem uzamda hem de zamanda modüle olabilir. Burada biz nano ve mezo ölçekli iletkenlerde zamanda periyodik Rashba spin-yörünge etkileşimi yoluyla nasıl spin akımı oluşturulabileceği sorusuna odaklanıyoruz. Hesaplarımızı, bu sistemlerdeki zamanda periyodik taşınım özelliklerinin incelenmesinde standart bir yöntem olan Floquet saçınım kuramı ile yaptık. Analitik ve yaklaşıklık içeren hesaplarımızı nümerik spine bağlı taşınım simülasyonlarıyla kontrol ederek, bias gerilimi olmadığı durumda dinamik Rashba SOI ile oluşmuş AC ve DC yük ve spin akımlarını analiz ettik. Ayrıca, zamana bağlı Rashba etkileşimi halinde yüksek harmonik oluşumunu irdeleyip, sistem bir veya iki parametre içerdiği durumda adyabatik yaklaşıklıkta ve bunun ötesinde pompalanmış yük ve spin akımını inceledik. Öte yandan, 2 boyutta elektron gazlarında spin-yörünge etkileşimi SU(2) ayar alanları kullanılarak da formüle edilebilir. Bir ayar dönüşümü ile Rashba spin-yörünge etkileşiminin spine bağlı gerilimler oluşturduğu gösterilebilir. Bu ayar dönüşümü ayrıca ilgili Onsager simetrilerinin belirlenmesini sağlar. Bu da, özellikle spin-yörünge etkileşiminin materyal boyunca homojen olmadığı durumda, spin transistör gereçlerinin gerçekleştirilmesi yolunda kullanılabilir. Bu iki olguyu birleştirerek dinamik Rashba spin-yörünge etkileşimi kullanarak spin akımı oluşturan bir spin transistörü ileri sürüyoruz. Son olarak, spin akımlarını yük akımlarına çevirmek için uzamda homojen olmayan Rashba spin-yörünge etkileşiminden yararlandık ki bu da deneysel olarak spin akımlarını saptamayı mümkün kılan bir mekanizma sağlıyor.

ACKNOWLEDGEMENTS

First, I would like to express my gratitude to my advisor, Prof. İnanç Adagideli, for his support and guidance over the years.

I would like to extend my sincere thanks to Prof. Klaus Richter and his group, especially Dr. Cosimo Gorini and Dr. Phillipp Reck for their hospitality when I spent a year at Regensburg University. I had the pleasure of working with them in an excellent research environment.

My grateful thanks are also extended to thesis committee members Prof. Zafer Gedik, Prof. Burç Mısırlıoğlu, and Assoc. Prof. Levent Subaşı for their insightful comments.

I am also grateful to my colleagues Dr. Baris Pekerten, Dr. Aykut Teker, Dr. Mert Bozkurt and Dr. Ali Asgharpour for their help and valuable conversations during my studies.

I gratefully acknowledge financial support from the Scientific and Technological Research Council of Turkey (TUBITAK) under the program 2214-A. I appreciate Regensburg and Utrecht universities for hospitality, where I completed some parts of my research.

Secondly, I would like to offer my special thanks to my friends for their support: Cenk Yanık, Tuna Demircik, Deniz Özen, Tolga Çağlar, Güneş Aydındoğan, Zeynep Sungur, Özge Aldıkaçtı, Seda Aydın, Deniz Yıldız and Çağler Dede.

I am also very grateful to my family; special thanks to my mother and brother for their support and faith in me, and my daughter Leyla for making my life more beautiful. Lastly, I could not have undertaken this journey without my husband, Umut Gürsoy. I am deeply grateful to him for his endless support.

To Leyla

TABLE OF CONTENTS

LIST OF FIGURES

LIST OF ABBREVIATONS

Chapter 1

INTRODUCTION

The enormous progress in electronics technology in the last decades brings its limitations along with it: according to Moore's law [1], the number of transistors inside a computer chip doubles every year, then the transistor size should be made smaller with an exponential rate. Quantum mechanical effects need to be taken into account when this size reaches the nanoscale. Spintronics proposes a revolutionary solution to this problem. Spintronic devices are electronic devices that use both charge and spin properties of electrons to save and transport information. The main advantages of using the spin degree of freedom as a dynamical variable are that these devices are expected to be smaller, faster, and more energy-effective. Hence they would be able to keep up with the rapidly increasing need for more storage in information technology. They will require less power consumption and exhibit more memory, processing capabilities, and new functionalities because of the additional spin degree of freedom. As a result, spintronics has emerged as a promising new discipline over the last decades. However, realizing such spin-based devices requires solving various substantial problems, such as generation, manipulation, and detection of spin current [2]. Specifically, an approach to these issues based on electrical methods turns out to be promising. Such electrical methods, for example, side-steps major problems such as the conductivity mismatch [3, 4], a problem commonly arise when ferromagnetic materials are employed. Via these electrical methods, applying a gate voltage can adjust the spin-orbit coupling strength and provides the tunability of the system. This alternative means of manipulating spin-based systems through the spin-orbit interaction, sometimes called *spinorbitronics*, has become a rapidly emerging discipline. Of particular importance is a tunable Rashba type spin-orbit coupling [5] for realizing spintronic devices through only electric means.

In this thesis, we specifically concentrate on non-stationary aspects of the Rashba spin-orbit coupling. Through time-dependent effects, we study generation of phase-coherent

spin and charge transport in 2-dimensional noninteracting mesoscopic systems. Indeed, time-dependent potentials provide additional transport phenomena, such as the generation of a spin-dependent voltage and/or a spin and a charge current without a bias voltage, in addition to those in stationary systems. In particular, we develop Floquet scattering theory [6–8] for spin and charge transport in ballistic systems with periodically driven parameters. We then compute spin and charge currents using numerical simulations.

Chapter 2 presents an overview of quantum transport in stationary mesoscopic systems. We introduce basic features of our system, which is a reduced dimension semiconductor heterostructure, such as the Rashba spin-orbit interaction, essential length scales, together with the tools we will use to study these systems, namely the Landauer-Büttiker formalism.

Chapter 3 introduces quantum transport for systems periodically driven in time. Floquet scattering formalism which describes the dynamic quantum transport properties. The Floquet Hamiltonian allows expressing periodic time dependency as a multi-channel stationary matrix with Floquet channels. Apart from the Floquet scattering matrix, computed by the Floquet Hamiltonian, we also use the adiabatic approximation at low frequencies. Then, we show how to obtain time-dependent spin and charge current using Landauer-Büttiker formalism in the presence of a periodic in-time potential or applied voltage. We also derive formulas for AC and DC spin and charge currents without a bias voltage.

In Chapter 4, we investigate the AC spin current induced by a time-dependent Rashba SOI and vanishing bias voltage. We obtain time of flight using the Wigner-Smith time-delay matrix [9, 10], which helps us specify the low and high-frequency regimes. We then compare the Floquet scattering matrix and its adiabatic approximation in different frequencies. We also study high harmonic generation (HHG) in the presence of the time-dependent Rashba coupling. In the second part, we consider an appropriate SU(2) gauge transformation to express the time-dependent Rashba field in terms of two opposite spin-dependent electric fields. Moreover, we examine these fields as spin-dependent voltage applied to the system, which helps us to obtain spin current via this voltage and charge conductance. We also theoretically and numerically show this equivalence in adiabatic and high-frequency regimes.

In Chapter 5, we focus on a two-dimensional electron gas — which we abbreviate as 2DEG — with position and time-dependent Rashba SOI, rewriting it in terms of non-Abelian gauge fields. We devise a unitary transformation that approximates the desired spin-dependent quantities (such as AC spin currents and spin conductances) in terms of conventional charge transport quantities (such as AC charge currents and impedances). While the time-dependent Rashba coupling generates AC spin current, position-dependent

Rashba coupling converts it to an AC charge current, which vanishes in two terminal systems with time-reversal symmetry, Using Onsager relations, we show that opening a third terminal or breaking time-reversal symmetry gives a non-zero AC charge current. Then we propose a spin transistor in which on/off states are controlled by connecting a lead using a gate. Finally, we present our results both in low and high-frequency regimes.

Chapter 6 studies time averaged charge and spin currents when the system involves one or two adjustable parameters without a bias voltage. The latter case occurs with two time-dependent potentials out of phase. We show our result using the Floquet scattering matrix and its adiabatic approximation. While the adiabatic approximation yields non-vanishing currents only in the two-parameter case, we obtain, using the Floquet scattering matrix, a non-vanishing current even in a single-parameter case beyond the adiabatic approximation.

In Chapter 7, we discuss our conclusions.

Chapter 2

OVERVIEW

In this chapter, we provide overview of stationary mesoscopic transport. The next chapter investigates time-dependent effects on spin and charge transport. Mesoscopic systems, which are systems of intermediate scale between macroscopic and microscopic, may contain a large number of atoms as classical objects while still exhibiting quantum interference effects inherent to atomic scales. Below, we define some significant length scales in the mesoscopic regime and then introduce the mesoscopic systems studied in this thesis. These semiconductor heterostructures in reduced dimensions realize what is called two-dimensional electron gases (2DEG). We then introduce the Rashba spin-orbit interaction (SOI), which has a significant impact on these materials. Next, we show the computation of charge and spin currents using Landauer-Büttiker formalism.

2.1   Length Scales in Mesoscopic Regime

We will first introduce the relevant length scales in mesoscopic transport [11]. The limits of the mesoscopic scale depend on the material type and are strongly affected by temperature. Quantum interference effects are relevant until inelastic scattering events (electron-electron or electron-phonon) destroy the initial phase of an electron. At low temperatures, these inelastic scattering processes are suppressed, and, as a result, an electron can travel longer, keeping its initial phase. The length scale by which the electron phase coherence is conserved defines the phase coherence length L_ϕ

$$L_\phi = \sqrt{D\tau_\phi} \tag{2.1}$$

where τ_ϕ and D are, respectively, the phase breaking time and the diffusion constant. The system is considered in the mesoscopic regime when its length is smaller than L_ϕ. A second relevant length is the Fermi wavelength λ_F, which is determined by the electron's kinetic energy.

$$\lambda_F = \frac{2\pi}{k_F}, \qquad E_F = \frac{\hbar^2 k_F^2}{2m} \qquad (2.2)$$

where k_F is the Fermi wave vector and E_F is the Fermi energy. At low temperatures, $k_B T \ll E_F$, only the electrons nearby E_F can participate in the current; thus, the Fermi wavelength becomes the only relevant scale. Electrons obey quantum mechanics if the sample size is comparable to the Fermi wavelength. An elastic scattering process due to impurities of the system does not destroy the initial phase of the electron but changes its initial momentum. An electron travels a certain distance before its momentum changes by an elastic scattering event. That is called the mean free path L_m.

$$L_m = v_F \tau_m . \qquad (2.3)$$

where τ_m is the momentum relaxation time and v_F is the Fermi velocity. For an electron in a semiconductor, L_m is about 100 nm and could reach up to 10 μm [12]. Quantum transport in distances shorter than L_m is called ballistic transport.

Besides charge transport, we will consider transport properties of spin degrees of freedom in mesoscopic systems. The appropriate length scale for spin transport is the spin-diffusion length λ_s. It is defined as the average distance the electron's spin relaxes from its initial state. It is given as

$$\lambda_s = \sqrt{D_s \tau_s} \qquad (2.4)$$

where τ_s and D_s are, respectively the spin relaxation time and the spin diffusion constant. Semiconductor materials have longer phase coherence lengths compared to metals. At low temperatures, an electron in a semiconductor sample can travel with phase coherence up to micrometers [12]. Because of this large phase coherence length, semiconductor materials enable us to explore mesoscopic quantum transport in a wide range of length scales from a few nanometers to micrometers. Reduced dimensional systems, whereby electron motion is restricted to one or two dimensions, such as the 2D electron gases, are particularly suitable for this purpose due to large λ_F and large L_m .

2.2 Two-Dimensional Electron Gas (2DEG)

In this thesis, we will consider two-dimensional mesoscopic systems. Semiconductor heterostructures are commonly used to produce an effectively two-dimensional electron gas by confining the motion in one direction (usually taken to be z) [12]. For example, a layered system made by placing doped $AlGaAs$ and $GaAs$ semiconductors on top of each other produce a confining well perpendicular to their interface. Starting from the Hamiltonian,

$$H = \frac{\mathbf{p}^2}{2m} + U(z),\tag{2.5}$$

where m is the effective mass of the electron, the confining potential $U(z)$ can be made sufficiently deep such that electron dynamics are effectively described by a 2D Hamiltonian

$$H = \frac{p_x^2 + p_y^2}{2m} + E_k\tag{2.6}$$

where we used the lowest energy solution in the z-direction and replaced the z-dependent part of the Hamiltonian with its corresponding energy eigenvalue E_k with $k = 1$. Two-dimensional electron gases have long phase coherence lengths and allow for easy control of their electronic properties, which makes them attractive for technological applications. In particular, the spin dynamics can be tuned in these systems by electric means, which is an essential property for spintronic applications. In this thesis, we will consider a setting with a particular spin-orbit interaction called the Rashba coupling. An applied gate voltage can tune this coupling.

2.3 Spin Orbit Interaction (SOI)

Coupling of electrons' intrinsic spin with their orbital motion causes an interaction in these electronic systems. This spin-orbit interaction is understood as follows. Consider an electron moving in an electric field. The electron's rest frame transforms this field into a magnetic field $\vec{B}$. This magnetic field couples to the electron's spin due to the Zeeman coupling of the form $\vec{S} \cdot \vec{B}$. The general form of the Hamiltonian with SOI is [13]

$$H_{SO} = \frac{\hbar}{4m_0^2 c^2} \mathbf{p} \cdot (\sigma \times \nabla V),\tag{2.7}$$

where m_0 is free electron mass, c is the velocity of light, V is the electric potential, $\hbar$ is Planck's constant, $\sigma = (\sigma_x, \sigma_y, \sigma_z)$ is a vector of Pauli spin matrices. In the semiconductor quantum wells, SOI typically has two separate sources, which depend on the origin of the

electric field: absence of crystal inversion symmetry, which results in the Dresselhaus SOI [14], and asymmetry of electron confinement potential in heterostructures, which results in the Rashba SOI [15]. We focus on the latter type of interaction in this thesis.

2.3.1 Rashba SOI

Rashba SOI, first introduced by E. Rashba [15], originates from the structural inversion asymmetry of electrons' confinement potential in the heterostructure. In these quantum wells with no structural inversion symmetry, an energy split exists in the spin subbands. This band splitting was understood [16–18] to be originated from the Rashba SOI:

$$H_R = \alpha \left(\sigma \times \mathbf{p} \right) \cdot \hat{z} \,, \tag{2.8}$$

where $\mathbf{p} = -i\hbar\nabla$ is the momentum operator, $\hat{z}$ is the growth direction of the heterostructure, $\sigma = (\sigma_x, \sigma_y, \sigma_z)$ is a vector of the Pauli spin matrices and α gives the spin-orbit interaction strength. The effective Hamiltonian of an electron in 2DEG with Rashba SOI in the single electron approximation is given by

$$H = \frac{p_x^2 + p_y^2}{2m^*} + \frac{\alpha}{\hbar}(\sigma_x p_y - \sigma_y p_x) \,, \tag{2.9}$$

where m^* is an effective mass. Corresponding energy dispersion relation reduces to

$$E = \frac{\hbar^2 \mathbf{k}^2}{2m^*} \pm \alpha|\mathbf{k}| \,. \tag{2.10}$$

As shown in Fig.2.1, it follows from this dispersion relation that Rashba SOI lifts the spin-degeneracy in the conduction band, even in the absence of an external magnetic field. In particular, the Rashba SOI splits the energy of up and down spin states by a factor of 2α. Rashba SOI can be tuned during the growth process of the heterostructure [19] or controlled by an applied gate voltage [5, 19–21]. In narrow gap semiconductors, experimentally found the highest value of the Rashba SOI strength is $\alpha = 10^{-11}$eVm [13]. The feature that an applied gate voltage can control the Rashba SOI makes it very attractive for applications in spintronics. It allows for manipulating the spin direction without an applied magnetic field or using a ferromagnetic material. That also motivates the calculations presented in this thesis.
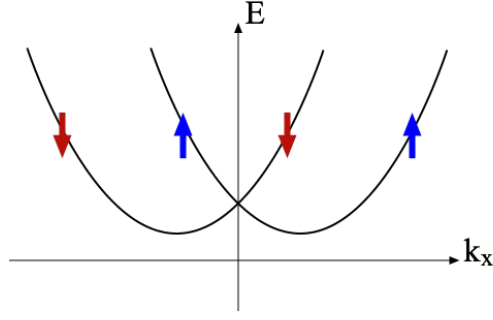
Figure 2.1: Splitting of spin energy eigenstates due to the Rashba SOI.

2.3.2 Tight-binding Hamiltonian for 2DEG with Rashba SOI

We use the discretized version of the Hamiltonian in our numerical simulations, given in
[22, 23]. In a 2DEG with spatially inhomogeneous Rashba coupling on the x-y-plane, the
continuum Hamiltonian we use for our analytical calculations is

$$H = \frac{\hbar^2}{2m^*}(k_x^2 + k_y^2) + \frac{1}{2}\{\alpha_R(\mathbf{x}), (\sigma^x p_y - \sigma^y p_x)\} \tag{2.11}$$

where $\alpha_R(\mathbf{x})$ is the Rashba SOI strength and σ denotes Pauli matrices. The corresponding
discretized version of this Hamiltonian on a 2D square lattice with a lattice constant a is

$$\begin{aligned}
H_{tb} &= \sum_{k,l,\sigma,\sigma'} 4t\,(c^\dagger_{k,l,\sigma}c_{k,l,\sigma'}) + \sum_{k,l,\sigma} t\,(c^\dagger_{k+1,l,\sigma}c_{k,l,\sigma} + c^\dagger_{k,l+1,\sigma}c_{k,l,\sigma}) + \\
&\quad \sum_{k,l,\sigma,\sigma'} \frac{1}{2a}\frac{1}{2}(\alpha_{R,k,l} + \alpha_{R,k+1,l})\,c^\dagger_{k+1,l,\sigma}(i\sigma_y)^{\sigma\sigma'}c_{k,l,\sigma'} + \\
&\quad \sum_{k,l,\sigma,\sigma'} -\frac{1}{2a}\frac{1}{2}(\alpha_{R,k,l} + \alpha_{R,k,l+1})\,c^\dagger_{k,l+1,\sigma}(i\sigma_x)^{\sigma\sigma'}c_{k,l,\sigma'}
\end{aligned} \tag{2.12}$$

where $c^\dagger_{k,l,\sigma}$ is the creation operator, which creates an electron with spin σ at the lattice
point (k,l). In this Hamiltonian, the hopping amplitude is $t = -\hbar^2/(2m^*a^2)$.

2.4 Landauer-Büttiker Formalism

This thesis is concerned with mesoscopic quantum systems, which are created on a 2DEG
by confinement potentials with arbitrary shape, as shown in Fig 2.2. Macroscopic contacts
are connected to the system via leads, as shown in the figure. We are mainly interested in
calculating conductance in such systems. In the ballistic regime where the system's size

L is smaller than L_m, the conductance is quantized in units of $\frac{2e^2}{h}$. The Landauer formula [24] gives the conductance as

$$G = \frac{2e^2}{h}\mathcal{T},$$ (2.13)

which is expressed in quantum transmission probabilities over all channels $\mathcal{T}$.
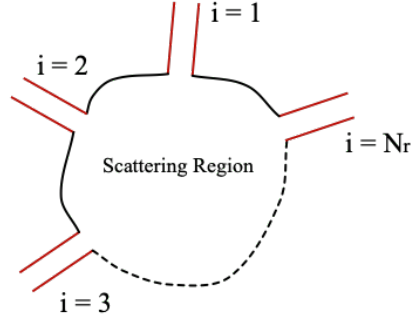
Figure 2.2: Example of a scattering region connected to the reservoirs via leads (red), i refers to the lead number where the total number of leads is N_r.

Landauer-Büttiker formalism [25] generalizes the Landauer formula above to an arbitrary scattering region with multiple contacts.We assume the electron can travel within the leads as plane waves along the longitudinal direction without backscattering. Macroscopic contacts serve as electron reservoirs. These reservoirs are in thermal equilibrium and are characterized by their chemical potential and temperature. Chemical potential differences between those contacts produce flowing electrons which are scattered by the mesoscopic system. Electron scattering from one lead to another gives the transmission amplitude, which describes the quantum properties of the system and is strongly affected by the system's geometry. Below we give a brief description of the scattering matrix in quantum mechanics.

2.4.1 Scattering Matrix Formalism

The scattering matrix relates incoming amplitudes to outgoing amplitudes in a matrix form. We neglect the electron-electron interaction, and treat the scattering problem in the single-electron approximation. The quantum state of a scattered electron is related to the state of the incident one by the scattering matrix as

$$|\psi_{out}\rangle = S|\psi_{in}\rangle,$$ (2.14)

we denote the wave functions of the incident (scattered) electrons by ψ_{in} (ψ_{out}). Consider the system in Fig. 2.2, which shows the scattering region connected to the leads labeled by $i = 1, 2, ...N_r$. At given energy E, each lead has a certain number of transverse channels labeled by m. Spin states of electrons are denoted by s. The size of the scattering matrix is $2M_T \times 2M_T$ where M_T is the total number of transverse channels summed over all of the leads, and the factor 2 comes from the up/down spin states. The element $S_{im,jm'}^{s,s'}(E)$ gives the transmission amplitude for an electron at energy E where the incident electron coming from lead j in the transverse channel m' and with spin s', is scattered into the lead i in channel m and spin s. The absolute square of the amplitude $|S_{im,jm'}^{s,s'}(E)|^2$ gives the probability of transmission. To avoid cluttering of indices, first, we present the scattering matrix showing the lead indices only as

$$
S = \begin{bmatrix}
\mathbf{r}_{1,1}(E) & \mathbf{t}_{1,2}(E) & \dots & \mathbf{t}_{1,N_r}(E) \\
\mathbf{t}_{2,1}(E) & \mathbf{r}_{2,2}(E) & \dots & \mathbf{t}_{2,N_r}(E) \\
\vdots & \vdots & \ddots & \vdots \\
\mathbf{t}_{N_r,1}(E) & \mathbf{t}_{N_r,2}(E) & \dots & \mathbf{r}_{N_r,N_r}(E)
\end{bmatrix}
\tag{2.15}
$$

where each element is a matrix labeled by the transverse channel and the spin indices. The submatrices $\mathbf{r}$ and $\mathbf{t}$ denote the reflection and transmission amplitudes as

$$
\mathbf{t}_{i,j}(E) = \begin{bmatrix}
t_{m_1,m_1}(E) & t_{m_1,m_2}(E) & \dots & t_{m_1,m_j}(E) \\
t_{m_2,m_1}(E) & t_{m_2,m_2}(E) & \dots & t_{m_2,m_j}(E) \\
\vdots & \vdots & \ddots & \vdots \\
t_{m_i,1}(E) & t_{m_2,2}(E) & \dots & t_{m_i,m_j}(E)
\end{bmatrix}
\tag{2.16}
$$

where m_i and m_j are the maximum number of the transverse channel in lead i and j, respectively. Furthermore, each element of the submatrices $\mathbf{t}_{i,j}(E)$ are 2×2 with spin indices $s = \uparrow, \downarrow$.

$$
t_{m_1,m_2}(E) = \begin{bmatrix}
t^{\uparrow\uparrow}(E) & t^{\uparrow\downarrow}(E) \\
t^{\downarrow\uparrow}(E) & t^{\downarrow\downarrow}(E)
\end{bmatrix}
\tag{2.17}
$$

Since the particle number is conserved during the process, the scattering matrix must obey the unitarity condition [26].

$$
\sum_{i,m} \sum_{s''} (S_{im,jm'}^{s',s''})^{\dagger} S_{im,km''}^{s'',s} = \delta_{j,k}\delta_{m',m''}\delta_{s,s'}
\tag{2.18}
$$

Another essential property of the scattering matrix is micro reversibility [26]. That means if the scattering processes are invariant under time reversal $t \to -t$, as both the Hamiltonian and the basis functions are left invariant under this operation. This condition imposes

$S^T = S$ in the presence of spin rotation invariance,

$$S_{im,jm'}^{s,s'} = S_{jm',im}^{s',s} . \tag{2.19}$$

One can modify micro reversibility when there is a magnetic field as

$$S(H) = S^T(-H) , \tag{2.20}$$

taking into account the sign flip of the magnetic field H under time reversal, provided that spin rotation invariance is not broken.

2.4.2 Electron Wave Function in the Leads

We do not need to follow what individual electrons do inside the scattering region to calculate a current. We need only the incident and the scattered wave functions in the leads. We represent the incident and the scattered wave functions ψ_{in} and ψ_{out} in the basis given by the product of longitudinal and transverse parts and the spin eigenfunctions:

$$\psi_{m,s}^{in}(E, \mathbf{r}) = \frac{1}{\sqrt{k_x(E)}} e^{+ik_x(E)x} \chi_m(y) \Sigma(s) , \tag{2.21}$$

$$\psi_{m,s}^{out}(E, \mathbf{r}) = \frac{1}{\sqrt{k_x(E)}} e^{-ik_x(E)x} \chi_m(y) \Sigma(s) , \tag{2.22}$$

for the incoming and outgoing electrons inside a lead, each with mode m with spin s. Here, we consider a plane waveform for the longitudinal part, properly normalized, and $\chi_m(y)$ denotes the transverse wave function, which we take as

$$\chi_m(y) = \sqrt{\frac{2}{W}} \sin\left(\frac{m\pi y}{W}\right) \tag{2.23}$$

where W is the width of the lead. It satisfies the orthogonality condition

$$\int dy\, \chi_m(y) \cdot \chi_{m'}(y)^\dagger = \delta_{mm'} . \tag{2.24}$$

Finally, $\Sigma(s)$ denotes spin eigenfunctions. We will use second quantized formalism for the total wave function in the lead i and write

$$\hat{\Psi}_i(t, \mathbf{r}) = \int_0^\infty dE\, e^{-i\frac{E}{\hbar}t} \left(\hat{a}_{i,m}^s(E)\psi_{m,s}^{in}(E, \mathbf{r}) + \hat{b}_{i,m}^s(E)\psi_{m,s}^{out}(E, \mathbf{r})\right) , \tag{2.25}$$

where $\hat{a}_{i,m}^{s,\dagger}(E)$, $\hat{a}_{i,m}^s(E)$ are creation and annihilation operators for the incident electrons in the lead i with the channel m and spin s. Similarly $\hat{b}_{i,m}^{s,\dagger}(E)$, $\hat{b}_{i,m}^s(E)$ are creation and an-

nihilation operators for scattered electrons. These operators satisfy the anticommutation relations:

$$\hat{a}_{i,m}^{s,\dagger}(E)\hat{a}_{j,m'}^{s'}(E') + \hat{a}_{j,m'}^{s'}(E')\hat{a}_{i,m}^{s,\dagger}(E) = \delta_{ij}\delta_{mm'}\delta_{ss'}\delta(E - E') \tag{2.26}$$

$$\hat{b}_{i,m}^{s,\dagger}(E)\hat{b}_{j,m'}^{s'}(E') + \hat{b}_{j,m'}^{s'}(E')\hat{b}_{i,m}^{s,\dagger}(E) = \delta_{ij}\delta_{mm'}\delta_{ss'}\delta(E - E'). \tag{2.27}$$

2.4.3 Spin and charge current calculation

The section above explains how to derive the total wave function in the lead i. We use the current operator expressed as the wave function (2.25) to obtain the current, and we then integrate the spin/charge current operator over energy as follows:

$$\hat{I}_i^s(t,x) = \int dy\, \hat{\Psi}_i^\dagger(t,\mathbf{r})\, \hat{J}_x^s\, \hat{\Psi}_i(t,\mathbf{r})\,, \tag{2.28}$$

$$\hat{I}_i(t,x) = e\int dy\, \hat{\Psi}_i^\dagger(t,\mathbf{r})\, \hat{J}_x\, \hat{\Psi}_i(t,\mathbf{r})\,, \tag{2.29}$$

where $\hat{J}_x^s$ denotes the spin current operator [27], in the absence of SOI:

$$\hat{J}_x^s = \frac{\hbar}{2}\frac{\hbar}{2mi}(\vec{\sigma}\cdot\hat{u})\left(\frac{\overrightarrow{\partial}}{\partial x} - \frac{\overleftarrow{\partial}}{\partial x}\right) \tag{2.30}$$

with $\hat{u}$ denoting the spin direction and $\hat{J}^x$ denotes the particle current operator,

$$\hat{J}_x = \frac{\hbar}{2mi}\left(\frac{\overrightarrow{\partial}}{\partial x} - \frac{\overleftarrow{\partial}}{\partial x}\right). \tag{2.31}$$

From now on, we will combine the definition of the spin and charge currents and denote them in a unified manner by $\hat{I}^a$ where $a = 0$ corresponds to the charge current, and $a = x, y, z$ corresponds to the spin current where a indicates the spin direction. For simplicity, we will show the derivation of only the spin current. The same derivation applies to the charge current with the replacement of the σ matrix with σ^0, which is the unit matrix. Note that spin and charge currents have different units. To account for this difference in the combined formula, we define an overall constant C_a with $C_{x,y,z} = \frac{1}{\hbar}\frac{\hbar}{2}$ for the spin, and $C_0 = \frac{e}{\hbar}$ for the charge current.

We substitute (2.25) in this equation for the spin current, and we use the small bias approximation [6]. Only the electrons nearby the Fermi energy $E \sim E' \sim E_F$ participate in the current. This approximation will allow us to simplify the y integral in Eq.(2.29) using Eq.(2.24) and also keep the longitudinal momenta $k(E') \sim k(E)$. Spin current in the a

direction is then,

$$\hat{I}_i^a(t) = C_a \int dE dE' e^{i(E-E')/\hbar} \times \tag{2.32}$$
$$\sum_{m \in i} \sum_{s,s'=\pm 1} \hat{b}_{im}^{\dagger,s}(E) \sigma_a^{ss'} \hat{b}_{im}^{s'}(E') - \hat{a}_{im}^{\dagger,s}(E) \sigma_a^{ss'} \hat{a}_{im}^{s'}(E')],$$

where m denotes sum over the channels in lead i.

The quantum mechanical average of the product of creation/annihilation operators gives the number operator, which is characterized by the Fermi function $f_i(E)$ in the lead i.

$$\langle \hat{a}_{i,m}^{\dagger,s}(E) \sigma_a^{ss'} \hat{a}_{j,m'}^{s'}(E') \rangle = \delta_{ij} \delta_{mm'} \sigma_a^{ss'} \delta(E - E') f_i(E) \tag{2.33}$$
$$\langle \hat{a}_{i,m}^{s}(E) \sigma_a^{ss'} \hat{a}_{j,m'}^{\dagger,s'}(E') \rangle = \delta_{ij} \delta_{mm'} \sigma_a^{ss'} \delta(E - E')(1 - f_i(E))$$

where the Fermi distribution function is

$$f_i(E) = \frac{1}{1 + e^{[(E-\mu_i)/k_B T]}} \tag{2.34}$$

where k_B is the Boltzmann constant, T is temperature and μ_i is the chemical potential in lead i. The creation/annihilation operators for scattering electrons $\hat{b}^\dagger(E)$, $\hat{b}(E)$ are written in terms of the creation/annihilation operators for incident electrons $\hat{a}^\dagger(E)$, $\hat{a}(E)$. This relation is given by the scattering matrix shown as

$$\hat{b}_{im}^s(E) = \sum_{j=1}^{N_r} \sum_{m' \epsilon j} \sum_{s'=\pm 1} S_{im,jm'}^{ss'}(E) \, \hat{a}_{jm'}^{s'}(E), \tag{2.35}$$

$$\hat{b}_{im}^{\dagger,s}(E) = \sum_{j=1}^{N_r} \sum_{m' \epsilon j} \sum_{s'=\pm 1} S_{im,jm'}^{*,ss'}(E) \, \hat{a}_{jm'}^{\dagger,s'}(E). \tag{2.36}$$

The current can be obtained after quantum statistical averaging over states of the electron, $I_i^a = \langle \hat{I}_i^a \rangle$. Using the relation Eqs. (2.33) and (2.36), in terms of the Fermi functions and scattering matrix, we obtain:

$$I_i^a = C_a \int dE \sum_{j}^{N_r} \sum_{m,m'} Tr[S_{im,jm'}^\dagger(E) \sigma_a S_{im,jm'}(E)](f_i(E) - f_j(E)). \tag{2.37}$$

2.4.4 Linear response

The current for a system with an applied bias voltage can be calculated in linear response if the bias voltage is small. We consider reservoirs with different electrochemical poten-

tials but kept at the same temperature T_0

$$\mu_i = \mu_0 + eV_i, \qquad eV_i \ll \mu_0 \tag{2.38}$$

In the linear response approximation, one can replace the difference of the Fermi functions as

$$f_i(E) - f_j(E) \rightarrow (eV_i - eV_j)\frac{\partial f(E)}{\partial E} \tag{2.39}$$

Furthermore, the Fermi distribution can be approximated by a step function at low temperatures,

$$f(E) \approx \theta(E - E_F), \tag{2.40}$$

which implies that only the electrons around E_F induce the current. Then the spin currents in the Landauer-Büttiker formalism [25] is

$$I_i^a = -\frac{e}{h}\sum_j T_{ij}^a(E_F)(\mu_i - \mu_j). \tag{2.41}$$

Here $a = x, y, z$ indicates the spin direction and T_{ij}^a are spin-dependent transmission probabilities [28].

$$T_{ij}^a = \sum_{m \in i, m' \in j} Tr[t_{mm'}^\dagger \sigma^a t_{mm'}] \tag{2.42}$$

where $t_{mm'}$ is a 2×2 matrix which gives the spin-dependent transmission amplitude (see 2.17) from channel m in the lead i to channel m' in lead j. The charge current becomes

$$I_i = \sum_j G_{ij}(E_F)(V_i - V_j). \tag{2.43}$$

where the voltage is $V_i = \mu_i/e$ and the conductance is $G_{ij} = -\frac{e^2}{h}\sum_j T_{ij}^0(E_F)$ with σ^0 defined as a unit matrix.

Chapter 3

SPIN TRANSPORT IN TIME DEPENDENT SYSTEMS

This chapter considers periodic time dependency and generalizes time-dependent formulas for spin and charge current calculations. We explain how to compute these currents in a time-dependent system using the scattering matrix formalism.

Time dependence can generically arise from two separate sources, which we will focus on in this section: (i) application of an external time-dependent voltage to generate an AC current [29]. (ii) a time-dependent potential inside the scattering region created by an applied AC gate voltage. These two settings are demonstrated in Fig. 3.1. In the latter case, charge and spin currents can be generated with or without an applied bias voltage. In order to examine the dynamics of a system with a time-dependent potential or voltage,
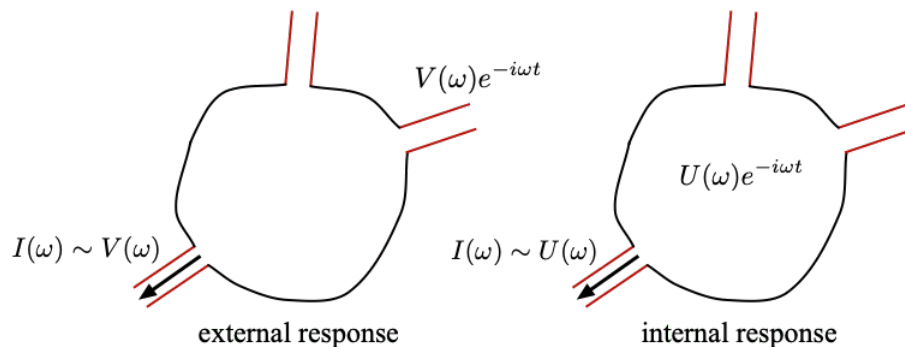
Figure 3.1: Demonstration of two cases of time-dependent response. (i) Response generated by a time-dependent voltage applied externally. (ii) Response created by a dynamical potential inside the cavity.

we need to solve the time-dependent Schrödinger equation,

$$i\hbar\frac{\partial\Psi(\vec{r},t)}{\partial t} = H(\vec{r},t)\Psi(\vec{r},t)\,. \tag{3.1}$$

The current computation using scattering matrix formalism that we outlined in the previous section should be adjusted to this time-dependent setting. If time dependency is periodic in time, the Floquet formalism [30] provides the right set of tools to obtain the wavefunctions numerically. Below, we first explain the Floquet scattering matrix formalism [6–8, 31, 32] in detail and review the formulas for charge and spin currents resulting from this formalism. Low-frequency limit of time-dependent response gives adiabatic transport. Adiabatic approximation applies when the frequency of the time-dependent potential is much smaller than the inverse time of flight of an electron in the scattering region. This approximation provides an alternative method to calculate the Floquet scattering matrix. To determine the adiabatic regime, we calculate the dwell time of an electron, which refers to the traveling time of an electron inside the scattering region, using the Wigner-Smith time-delay matrix [9, 10]. We end with a short explanation of how we numerically compute spin/charge currents.

3.1 Floquet Theory

The Floquet theory, based on the work of mathematician G. Floquet, introduced a solution for a linear differential equation with time-periodic coefficients [33]. Since the Schrödinger equation is linear, Floquet theory is instrumental to understanding the behavior of quantum mechanical systems with a Hamiltonian that is periodic in time:

$$H(\vec{r},t+\mathcal{T}) = H(\vec{r},t) \tag{3.2}$$

where the oscillation period is $\mathcal{T} = 2\pi/\Omega$ and Ω is typically the frequency of the periodically driven potential. Floquet wave functions are solutions to the time-dependent Schrödinger equation.

We now consider a 2D quantum mechanical system with a time-periodic Hamiltonian. The Hamiltonian can be separated into static and time-dependent parts as

$$H(\vec{r},t) = H_0(\vec{r}) + H_1(\vec{r},t)\,, \tag{3.3}$$

where the kinetic term is $H_0(\vec{r}) = -\frac{\hbar^2}{2m}(\partial_x^2 + \partial_y^2)$. It is easy to see that this Schrödinger

equation can be rewritten as:

$$H_F(\vec{r},t)|\Psi(\vec{r},t)\rangle = 0\,, \tag{3.4}$$

the Hermitian operator $H_F(\vec{r},t)$, which is called the Floquet Hamiltonian, is related to the original Hamiltonian by including a time derivative term

$$H_F(\vec{r},t) = H(\vec{r},t) - i\hbar\frac{\partial}{\partial t}\,. \tag{3.5}$$

The solution to (3.4) is formally given by the following Floquet states

$$|\Psi_\alpha(\vec{r},t)\rangle = e^{-iE_\alpha t/\hbar}|\phi_\alpha(\vec{r},t)\rangle\,, \tag{3.6}$$

where $|\phi_\alpha(\vec{r},t)\rangle$ is called a Floquet mode. Floquet modes are eigenfunctions of the Floquet Hamiltonian $H_F(\vec{r},t)$ with the eigenvalues E_α called quasienergies.

$$\left(H(t) - i\hbar\frac{\partial}{\partial t}\right)|\phi_\alpha(\vec{r},t)\rangle = H_F(\vec{r},t)|\phi_\alpha(\vec{r},t)\rangle = E_\alpha|\phi_\alpha(\vec{r},t)\rangle\,. \tag{3.7}$$

Let us now discuss the basic properties of these eigenfunctions. First, just as the Hamiltonian in Eq. (3.3) is symmetric under a discrete-time translation, $t \to t + \mathcal{T}$, its solutions exhibit the same property

$$|\phi_\alpha(\vec{r},t+\mathcal{T})\rangle = |\phi_\alpha(\vec{r},t)\rangle\,. \tag{3.8}$$

Time periodicity allows expanding Floquet modes in a Fourier series

$$|\phi_\alpha(\vec{r},t)\rangle = \sum_n e^{-in\Omega t}|n\rangle, \tag{3.9}$$

Here $|n\rangle$ are basis vectors of the eigenfunctions of the Floquet Hamiltonian and refer to the Floquet states. Substituting this in Eq. (3.6), one obtains

$$|\Psi_\alpha(\vec{r},t)\rangle = e^{-iE_\alpha t/\hbar}\sum_n e^{-in\Omega t}|n\rangle\,. \tag{3.10}$$

We can, then, rewrite the same wavefunction $|\Psi_\alpha(\vec{r},t)\rangle$ in an alternative way in terms of a shifted energy eigenvalue:

$$|\Psi_\alpha(\vec{r},t)\rangle = e^{-iE_\alpha t/\hbar}e^{in\Omega t}e^{-in\Omega t}|\phi_\alpha(\vec{r},t)\rangle \tag{3.11}$$
$$|\Psi_\alpha(\vec{r},t)\rangle = e^{-iE_{\alpha,n}t/\hbar}|\phi_{\alpha,n}(\vec{r},t)\rangle$$

where the shifted Floquet modes are $|\phi_{\alpha,n}(\vec{r},t)\rangle = e^{in\Omega t}|\phi_\alpha(\vec{r},t)\rangle$ and $E_{\alpha,n}$ denotes the

Floquet energy
$$E_{\alpha,n} = E_\alpha + n\hbar\Omega, \ \ n = 0, \pm 1, \pm 2, \ldots$$

These Floquet energies will be central to the spin and electric current calculation in time-dependent quantum systems, which we detail below. As a second fundamental property, the Floquet modes satisfy the following orthonormality and completeness conditions [6]:

$$\langle\langle\phi_{\alpha,n}(\vec{r},t)|\phi_{\beta,m}(\vec{r},t)\rangle\rangle \equiv \frac{1}{\mathcal{T}}\int_0^{\mathcal{T}} dt \int_{-\infty}^{\infty} d^2r\, \phi_{\alpha,n}(\vec{r},t)\phi_{\beta,m}(\vec{r},t) = \delta_{\alpha\beta}\delta_{nm}$$

$$\sum_\alpha \sum_n |\phi_{\alpha,n}(\vec{r},t)\rangle\langle\phi_{\alpha,n}(\vec{r}',t')| = \delta(\vec{r}-\vec{r}')\delta(t-t')\,.$$

3.1.1 Floquet Hamiltonian

In Fourier space, the time-dependent Hamiltonian in Eq. (3.7) becomes a static matrix Hamiltonian

$$H_F = \sum_{n=-\infty}^{\infty}\left((H_0 - n\hbar\Omega)|n\rangle\langle n| + \frac{iH_1}{2}(|n\rangle\langle n+1| - |n\rangle\langle n-1|)\right). \tag{3.12}$$

Here, we consider a general periodic-in-time Hamiltonian with a sinusoidal potential with frequency Ω and phases θ. With no loss of generality the Hamiltonian $H(\vec{r},t)$ is chosen as

$$H(\vec{r},t) = H_0 + H_1 \sin(\Omega t + \theta_1) + H_2 \cos(\Omega t + \theta_2)\,. \tag{3.13}$$

We can obtain the quantum expectation values of the separate contributions to the Floquet Hamiltonian. First, the time-independent component H_0 has the expectation value

$$\langle\phi_\alpha(\vec{r},t)|H_0|\phi_\alpha(\vec{r},t)\rangle = \sum_n \sum_m e^{in\Omega t}\langle n|(H_0)e^{-im\Omega t}|m\rangle = H_0\delta_{n,m}\,.$$

The following computation shows the quantum expectation value of the time derivative

$$\langle\phi_\alpha(\vec{r},t)|i\hbar\frac{\partial}{\partial t}|\phi_\alpha(\vec{r},t)\rangle = \sum_n \sum_m e^{in\Omega t}\langle n|\left(-i\hbar\frac{\partial}{\partial t}\right)e^{-im\Omega t}|m\rangle \tag{3.14}$$

$$= \sum_n \sum_m (-i\hbar)(-im\Omega)e^{i(n-m)\Omega t}\langle n|m\rangle = -m\hbar\Omega\delta_{n,m}\,.$$

Finally, the expectation values of the time-dependent sinusoidal terms can be computed by expanding the cosine and sin functions in terms of exponentials and shifting the summation index as follows

$$\langle\phi_\alpha(\vec{r},t)|H_1 sin(\Omega t + \theta_1)|\phi_\alpha(\vec{r},t)\rangle$$

$$= \sum_n \sum_m e^{in\Omega t} \langle n| \left(H_1 \frac{i}{2} \left(e^{-i\Omega t - i\theta_1} - e^{i\Omega t + i\theta_1} \right) \right) e^{-im\Omega t} |m\rangle$$

$$= H_1 \frac{i}{2} \sum_n \sum_m \left(e^{i(n-(m+1))\Omega t} e^{-i\theta_1} - e^{i(n-(m-1))\Omega t} e^{i\theta_1} \right) \langle n|m\rangle$$

$$= H_1 \frac{i}{2} (\delta_{n,m+1} e^{-i\theta_1} - \delta_{n,m-1} e^{i\theta_1}) \tag{3.15}$$

$$\langle \phi_\alpha(\vec{r}, t)| H_2 cos(\Omega t + \theta_2)|\phi_\alpha(\vec{r}, t)\rangle$$

$$= \sum_n \sum_m e^{in\Omega t} \langle n| \left(\frac{H_1}{2} \left(e^{-i\Omega t - i\theta_2} + e^{i\Omega t + i\theta_2} \right) \right) e^{-im\Omega t} |m\rangle$$

$$= \frac{H_2}{2} \sum_n \sum_m \left(e^{i(n-(m+1))\Omega t} e^{-i\theta_2} + e^{i(n-(m-1))\Omega t} e^{i\theta_2} \right) \langle n|m\rangle$$

$$= \frac{H_2}{2} (\delta_{n,m+1} e^{-i\theta_2} + \delta_{n,m-1} e^{i\theta_2}) . \tag{3.16}$$

Using the expressions above, one can convert the time-dependent Floquet Hamiltonian into a static matrix as [30]

$$H_F \approx \sum_{n=-N}^{N} \left((H_0 - n\hbar\Omega)|n\rangle\langle n| + \frac{iH_1}{2} (e^{-i\theta_1}|n\rangle\langle n-1| - e^{i\theta_1}|n\rangle\langle n+1|) \right. \tag{3.17}$$

$$\left. + \frac{H_2}{2} (e^{-i\theta_2}|n\rangle\langle n-1| + e^{i\theta_2}|n\rangle\langle n+1|) \right),$$

We truncated the infinite sums above level N for computational efficiency. This approximation becomes better as N is taken large. We should determine the optimal value of N for each particular system by analyzing the dependence of the amplitude and the frequency of the driving potential and balancing the error that results from keeping N finite with computation efficiency. As a result of this analysis, we convert the original periodically time-dependent system into a multi-channel stationary system expanded in the Floquet states.

3.1.2 Floquet scattering matrix

The Floquet scattering theory [6–8, 31, 32] describes how to calculate the current in a system with periodically driven parameters. While in the stationary case, components of the scattering matrix give quantum transmission amplitudes. These amplitudes depend on a single energy E in the stationary case. On the other hand, in the periodically driven case, with frequency Ω, an electron with initial energy E can interact with an oscillating scatterer. As a result, it can absorb/emit energy quanta $n\hbar\Omega$. Then the scattered electron leaves the system generally with a different energy $E_n = E + n\hbar\Omega$ where

$n = 0, \pm1, \pm2, \ldots$. Therefore, the scattering matrix is a function of initial and final energies. This matrix is called the Floquet scattering matrix and is denoted by $S_F(E_n, E)$, where index F represents the Floquet scattering matrix, and n denotes the Floquet channel. A generic transmission amplitude in the Floquet scattering matrix for a spin $\frac{1}{2}$ particle system is given by $S_{F,ij}^{ss'}(E_n, E)$, which describes the transmission amplitude of an electron scattered from lead j with spin polarization s' and energy E, and transmitted to lead i with spin polarization s and the final energy E_n (for simplicity, consider a single-channel scattering matrix). As a result of the conservation of the particle current during the scattering process, Floquet scattering matrix obeys the unitary condition [34]

$$\sum_{i=1}^{N_r} \sum_{s,s'=\uparrow,\downarrow} \sum_{n=-\infty}^{\infty} S_{F,ij}^{ss',*}(E_n, E) S_{F,ik}^{ss'}(E_n, E_m) = \delta_{m0}\delta_{jk} \qquad (3.18)$$

$$\sum_{j=1}^{N_r} \sum_{s,s'=\uparrow,\downarrow} \sum_{n=-\infty}^{\infty} S_{F,ij}^{ss',*}(E, E_n) S_{F,kj}^{ss'}(E_m, E_n) = \delta_{m0}\delta_{ik}.$$

The states with energies $E_n = E + n\hbar\Omega < 0$ do not contribute to the current and are called localized states. Thus, only values of n for $E_n > 0$ are kept while taking the sum over n. In a dynamical system, the microreversibility condition of the scattering matrix differs from the stationary systems. Generally, consider a time-dependent Hamiltonian with parameters p_α changing periodically in time with angular frequency Ω and phase shifts θ_a

$$p_\alpha(t) = p_{\alpha,0} + p_\alpha(cos(\Omega t + \theta_\alpha)). \qquad (3.19)$$

The Hamiltonian is then invariant under the time reversal, $t \to -t$, together with changing the sign of the phase shifts $-\theta$ where θ is set of all θ_α. Then, if there is a magnetic field, the Floquet scattering matrix obeys the following symmetry [35]:

$$S_{F,ij}^{ss'}(E, E_n; H, \theta) = S_{F,ji}^{s's}(E_n, E; -H, -\theta). \qquad (3.20)$$

In addition to incoming/outgoing channels in the leads, their corresponding energies E and E_n interchange as well.

To calculate elements of the Floquet scattering matrix, one can substitute the Floquet Hamiltonian in the time-dependent Schrödinger equation and obtain the Floquet wavefunction for each Floquet channel. The linear relation between the creation/annihilation operators $\hat{a}^\dagger(E)/\hat{a}(E)$ for incidents electrons and $\hat{b}^\dagger(E)/\hat{b}(E)$ for scattered electrons gives the Floquet scattering matrix elements as

$$\hat{b}_i^s(E) = \sum_{n=-\infty}^{\infty} \sum_{s'=\uparrow,\downarrow} \sum_{j=1}^{N_r} S_{F,ij}^{ss'}(E, E_n) \hat{a}_j^{s'}(E_n), \qquad (3.21)$$

$$\hat{b}_i^{s,\dagger}(E) = \sum_{n=-\infty}^{\infty} \sum_{s'=\uparrow,\downarrow} \sum_{j=1}^{N_r} S_{F,ij}^{ss',*}(E, E_n)\, \hat{a}_j^{s',\dagger}(E_n). \tag{3.22}$$

3.1.3 Adiabatic approximation to Floquet scattering matrix

Components of the Floquet scattering matrix increase proportional to the number of total Floquet states $2N + 1$ where N gives the maximum amount of energy $N\hbar\omega$ an electron loses or gains during the scattering process. The value of N, which depends on both the frequency and the amplitude and of the time-dependent potential, is restricted by numerical efficiency, hence determined by optimizing the calculation time vs. numerical accuracy. The larger the Floquet scattering matrix is, the heavier the numerical calculations will be.

In the adiabatic limit, there is a practical way to obtain the Floquet scattering matrix [6, 32, 34]. The condition of the adiabatic limit $\Omega\tau \ll 1$ where $\Omega/2\pi$ is the driving frequency, and τ is the typical dwell time that an electron spends on the scattering region during scattering. We will explain the calculation of the dwell time in a ballistic system in Section 3.2.3. Considering a set of time-dependent parameters $p_\alpha(t)$, one calculates a stationary scattering matrix with these parameters at a given time t. This scattering matrix is called the frozen scattering matrix:

$$S(E, t) = S(E, \{p_\alpha(t)\}). \tag{3.23}$$

In case these time-dependent parameters $p_\alpha(t)$ are periodic in time with period $\mathcal{T} = 2\pi/\Omega$ the full Floquet scattering matrix in the adiabatic limit approximates as

$$S_F(E_n, E) \simeq \frac{1}{\mathcal{T}} \int_0^{\mathcal{T}} S(E, t) e^{in\Omega t} dt. \tag{3.24}$$

That is named the frozen scattering matrix approximation.

3.2 Spin and Charge Current Calculation

We outline how to derive the current formula in time-dependent systems [6] using Landauer-Büttiker formalism, including spin degrees of freedom [36]. We start with the charge/spin current operator in Chapter 2.4.3, Eq. (3.25). Recall that $a = x, y, z$ denotes components

of the spin current with the a direction and $a = 0$ term denotes the charge current.

$$\hat{I}_i^a(t) = C_a \int dE dE' e^{i(E-E')t/\hbar} [\hat{b}_{im}^{\dagger,s}(E)\sigma_a^{ss'}\hat{b}_{im}^{s'}(E') - \hat{a}_{im}^{\dagger,s}(E)\sigma_a^{ss'}\hat{a}_{im}^{s'}(E')] \,, \quad (3.25)$$

where the overall constant C_a defines the unit of charge and spin, $C_{x,y,z} = \frac{1}{h}\frac{\hbar}{2}$ and $C_0 = \frac{e}{h}$. $\hat{b}_{im}^{(\dagger)\,s}$ / $\hat{a}_{im}^{(\dagger)\,s}$ are the creation/annihilation operators for scattered and incident electrons respectively in channel m in the lead i with spin s. Note that this equation is derived from the assumption $E - E' \ll E_F$. In a periodically driven system, one can express the spin current operator on the frequency basis

$$\hat{I}_i^a(\omega) = \int_{-\infty}^{\infty} dt\, e^{i\omega t}\hat{I}_i^a(t).$$

Using Eq. (3.25), the spin current operator becomes [6, 37]

$$\hat{I}_i^a(\omega) = C_a 2\pi\hbar \int dE \,\{\hat{b}_{im}^{\dagger,s}(E)\sigma_a^{ss'}\hat{b}_{im}^{\dagger,s'}(E+\hbar\omega) - \hat{a}_{im}^{\dagger,s}(E)\sigma_a^{ss'}\hat{a}_{im}^{\dagger,s'}(E+\hbar\omega)\} \,. \quad (3.26)$$

As a result, the electron can acquire or lose energy quanta after the scattering in the periodically driven case. The Floquet scattering matrix gives the relation between the operators $\hat{a}$ and $\hat{b}$ for scattered and incident electrons are given by :

$$\hat{b}_{im}^s(E) = \sum_{n=-\infty}^{\infty} \sum_{j=1}^{N_r} \sum_{m\epsilon j} \sum_{s=\pm 1} S_{F,im,jm'}^{ss'}(E, E_n)\, \hat{a}_{jm'}^{s'}(E_n) \,, \quad (3.27)$$

$$\hat{b}_{im}^{\dagger,s}(E) = \sum_{n=-\infty}^{\infty} \sum_{j=1}^{N_r} \sum_{m\epsilon j} \sum_{s=\pm 1} S_{F,im,jm'}^{*,ss'}(E, E_n)\, \hat{a}_{jm'}^{\dagger,s'}(E_n) \,. \quad (3.28)$$

The product of $\hat{a}_{jm'}^{s'}$ and $\hat{a}_{jm'}^{\dagger,s'}$ gives the number operator, and after taking the quantum statistical average one obtains the Fermi function $f_i(E)$ where i denotes the lead index

$$\langle \hat{a}_{ims}^{\dagger}(E)\hat{a}_{jm's'}(E')\rangle = \delta_{ij}\delta_{mm'}\delta_{ss'}\delta(E-E')f_i(E) \quad (3.29)$$
$$\langle \hat{a}_{ims}(E)\hat{a}_{jm's'}^{\dagger}(E')\rangle = \delta_{ij}\delta_{mm'}\delta_{ss'}\delta(E-E')(1-f_i(E)) \,.$$

Substituting Eq. (3.27) and (3.28) into Eq. (3.26), and taking the quantum statistical average using the Eq. (3.29), one can find the current spectrum [38] $I_i^a(\omega) = \langle \hat{I}_i^a(\omega)\rangle$ as follows.

$$I_i^a(\omega) = \sum_{l=-\infty}^{\infty} 2\pi\delta(\omega - l\Omega)I_{i,l}^a \quad (3.30)$$

with $I_{i,l}^a = \langle \hat{I}_i^a(l\Omega) \rangle$ given by

$$
\begin{aligned}
I_{i,l}^a =& C_a \int_0^\infty dE \sum_{n=-\infty}^{\infty} \sum_{j=1}^{N_r} \sum_{m \epsilon j} Tr[S_{F,im,jm'}^\dagger(E_n, E)\sigma^a S_{F,im,jm'}(E_{l+n}, E)] \times \\
& \{ f_j(E) - f_i(E_n) \} \,.
\end{aligned}
\tag{3.31}
$$

The expectation value of the current in the time domain can then be written as the inverse Fourier series,

$$
I_i^a(t) \equiv \langle \hat{I}_i^a(t) \rangle = \sum_{l=-\infty}^{\infty} e^{-il\Omega t} I_{i,l}^a,
\tag{3.32}
$$

Using Eqs. (3.31) and (3.32), we can then calculate the time-dependent current in the presence of the periodic in-time potential.

3.2.1   AC and DC current generated by a dynamic scatterer

A dynamical scatterer, which changes periodically, always generates an AC current even without a bias voltage. On the other hand, a dynamical scatterer generates a DC current only under certain conditions; see Chapter 6. The previous section showed how to calculate the time-dependent spin current for the general case. Here, we concentrate on the AC and DC with no applied bias voltage. In general, the spin current formula is

$$
I_i^a(t) = \sum_{l=-\infty}^{\infty} e^{-il\Omega t} I_{i,l}^a \,,
\tag{3.33}
$$

together with

$$
\begin{aligned}
I_{i,l}^a =& C_a \int_0^\infty dE \sum_{n=-\infty}^{\infty} \sum_{j=1}^{N_r} \sum_{m \epsilon j} Tr[S_{F,im,jm'}^\dagger(E_n, E)\sigma^a S_{F,im,jm'}(E_{l+n}, E)] \times \\
& \{ f_j(E) - f_i(E_n) \}, \,.
\end{aligned}
\tag{3.34}
$$

If the leads have the same chemical potential, the Fermi functions become equal, $f_i(E) = f_j(E) = f_0(E)$. Furthermore, when $\hbar\Omega$ is small compared to the Fermi energy, $E_n = E + n\hbar\Omega$, the difference between the Fermi functions becomes

$$
\frac{\partial f_0}{\partial E} \approx \frac{f_0(E + n\hbar\Omega) - f_0(E)}{n\hbar\Omega} \,.
\tag{3.35}
$$

23

Substituting this in Eq. (3.34), we obtain

$$
\begin{aligned}
I_{i,l}^a =& C_a \int_0^\infty dE \left(-\frac{\partial f_0}{\partial E} \right) \sum_{n=-\infty}^{\infty} \sum_{j=1}^{N_r} \sum_{m\epsilon j} \\
& \times (n\hbar\Omega) Tr[S_{F,im,jm'}^\dagger(E_n, E)\sigma^a S_{F,im,jm'}(E_{l+n}, E)].
\end{aligned}
\tag{3.36}
$$

Since in the zero temperature limit, only electrons at E_F participate to the current, one has $\frac{\partial f_0}{\partial E} = \delta(E - E_F)$. We can then evaluate the integral above,

$$
I_{i,l}^a = C_a \hbar\Omega \sum_{n=-\infty}^{\infty} \sum_{j=1}^{N_r} \sum_{m'\epsilon j, m\epsilon i} n\, Tr[S_{F,im,jm'}^\dagger(E_{F,n}, E_F)\sigma^a S_{F,im,jm'}(E_{F,l+n}, E_F)].
\tag{3.37}
$$

Eqs. (3.33) and (3.34) when $l = 0$ gives the DC component. Then the DC charge/spin currents due to the dynamical scatterer become

$$
I_{i,DC}^a = I_{i,0}^a.
\tag{3.38}
$$

Non-vanishing l contributions give the AC current. In practice, we use only $l = \pm 1$ terms, and the AC charge/spin current in the linear order frequency becomes

$$
I_{i,AC}^a(t) = e^{-i\Omega t} I_{i,1}^a + e^{i\Omega t} I_{i,-1}^a.
$$

3.2.2 External AC voltage

In this part, we study a system with an AC bias voltage [6, 34, 39, 40] without any time-dependent potential inside the scattering region. We will consider the response only for non-interacting electrons. Then the internal potential due to the Coulomb interaction is neglected at low temperatures.

We assume a periodic in-time voltage on the reservoirs but none in the leads. In the transition region between the reservoir and the leads, the effect of the AC voltage is assumed to slow compared with the Fermi energy, in such a way that electrons are regarded as fixed energy eigenstates. Therefore the chemical potential in the leads is not dependent on time-dependent voltage. Let us assume that potentials in the reservoirs are in phase with the same frequency,

$$
V_i(t) = V_i \cos(\Omega t), \; i = 1, ..., N_r
\tag{3.39}
$$

24

Schrödinger equation with a spatially uniform potential is

$$i\hbar\frac{\partial\Psi_i}{\partial t} = (H_{0,i} + eV_i(t))\Psi_i \tag{3.40}$$

which leads to an electron wave function in the lead i

$$\Psi_i(x,t;E) = \phi_i(x;E)e^{-iEt/\hbar}\sum_{l=-\infty}^{\infty}J_l\left(\frac{eV_i}{\hbar\Omega}\right)e^{-il\Omega t} \tag{3.41}$$

where $\phi_i(x;E)$ is the solution of the Eq. (3.40) when $eV_i(t) = 0$ and J_l is the lth order Bessel function. Here l denotes the Floquet eigenstate.

We begin with the spin/charge current operator in the lead in Eq. (3.25)

$$\hat{I}_i^a(t) = C_a\int dEdE' e^{i(E-E')/\hbar}[\hat{a}_{im}^{\dagger,s}(E)\sigma_a^{ss'}\hat{a}_{im}^{s'}(E') - \hat{b}_{im}^{\dagger,s}(E)\sigma_a^{ss'}\hat{b}_{im}^{s'}(E')] \tag{3.42}$$

where creation and annihilation operators for an electron in the leads are given by these operators $\hat{a}'$ for an electron in the reservoir up to order $\hbar\omega/E_F$

$$\hat{a}_{ims}(E) = \sum_{l=-\infty}^{\infty}J_l\left(\frac{eV_i}{\hbar\Omega}\right)\hat{a}'_{ims}(E - l\hbar\omega). \tag{3.43}$$

They satisfy

$$\{\hat{a}_i(E), \hat{a}_j^{\dagger}(E')\} = \delta_{ij}\delta(E - E'). \tag{3.44}$$

Substituting the creation/ annihilation operators above in Eq. (3.25) and taking its average, we obtain,

$$I_i^a(t) = C_a\int dE\sum_{j,mm'}\sum_{kl}Tr\{\delta_{ij}\mathbb{1}_i - S_{im',jm}^{\dagger}(E)\sigma^a S_{im',jm}(E + (k-l)\hbar\Omega)\}\times \tag{3.45}$$

$$J_l\left(\frac{eV_j}{\hbar\Omega}\right)J_k\left(\frac{eV_j}{\hbar\Omega}\right)e^{-i(k-l)\Omega t}f_j(E - l\hbar\Omega).$$

For $k = l$ this gives the DC component of the current

$$I_i^a = C_a\int dE\sum_{j,mm'}\sum_{l}Tr\{\delta_{ij}\mathbb{1}_i - S_{im',jm}^{\dagger}(E)\sigma^a S_{im',jm}(E)\}\times \tag{3.46}$$

$$J_l^2\left(\frac{eV_j}{\hbar\Omega}\right)f_j(E - l\hbar\Omega).$$

Moreover, Eq. (3.45) with $k - l = \pm 1$ gives the AC current in the linear order frequency.

One can write this current in frequency as

$$I_i^a(\omega) = C_a \int dE \sum_{j,mm'} \sum_l Tr\{\delta_{ij}\mathbb{1}_i - S_{im',jm}^\dagger(E)\sigma^a S_{im',jm}(E+\hbar\omega)\} \times \quad (3.47)$$

$$J_l\left(\frac{eV_j}{\hbar\omega}\right) J_{l+1}\left(\frac{eV_j}{\hbar\omega}\right) f_j(E-l\hbar\omega).$$

Using the linear response expression $G_{ij}^a(\omega) \equiv \langle \delta I_i^a(\omega)\rangle / \delta V_j(\omega)$, the AC conductance can be obtained as [29, 40, 41]

$$G_{ij}^a(\omega) = C_a e \int dE \quad Tr\{\delta_{ij}\mathbb{1}_i - S_{ij}^\dagger(E)\sigma^a S_{ij}(E+\hbar\omega)\} \times \quad (3.48)$$

$$\frac{f_j(E) - f_j(E+\hbar\omega)}{\hbar\omega}.$$

In the time domain, the current is obtained by Fourier transforming as

$$I^a(t) = \int \frac{d\omega}{2\pi} e^{i\omega t} I^a(\omega). \quad (3.49)$$

3.2.3 Calculation of the dwell time

We investigate the dwell time of electrons with a time-dependent potential. We will take the Wigner-Smith time delay, presented below in (3.52), as the time of flight of an electron during the scattering process.

Eisenbud and Wigner [9] introduced the time delay concept and formulated it in terms of derivatives of the scattering phase shifts with respect to energy in quantum-mechanical scattering processes. Smith [10] generalized the time delay formulation and defined the dwell time for an $N \times N$ scattering matrix $S(E)$ in a given spatial region. Because the scattering matrix is unitary, it is diagonalized as

$$S(E) = U(E)e^{i\Theta(E)}U^\dagger(E) \quad (3.50)$$

where U is a unitary matrix and Θ is a diagonal matrix consisting of scattering phase shifts, $\Theta(E) = diag(\theta_1, ..., \theta_N)$. The lifetime matrix, also called the Wigner-Smith time-delay matrix, $Q(E)$ is obtained as

$$Q(E) = -i\hbar S^\dagger(E)\frac{\partial S(E)}{\partial E}. \quad (3.51)$$

Diagonal elements of the Wigner-Smith time-delay matrix $Q(E)$ are real and yield the proper time delays $\tau_1, ..., \tau_N$ in each transport channel. Taking the average over all chan-

nels, one obtains the Wigner-Smith time delay as

$$\tau_W(E) = \frac{1}{N}Tr\{Q\} \tag{3.52}$$
$$= -\frac{i\hbar}{N}\frac{\partial}{\partial E}detS(E) = \frac{\hbar}{N}\frac{\partial}{\partial E}Tr\Theta(E)$$

where N is the total number of transverse channels over all leads.

One can also obtain partial time delays using the energy derivatives of the phase shifts for each transverse channel, spin polarization, etc.

$$\tau_{a,\sigma} = \hbar\frac{\partial\theta_{a,\sigma}}{\partial E} \tag{3.53}$$

where $\theta_{a,\sigma} = arg|t_{a,\sigma}|$ and $t_{a,\sigma}$ is the transmission amplitude with spin polarization $\sigma = \uparrow\downarrow$ and the transverse channel $a = 1, ..., N$.

For our simulations, we calculate the Wigner-Smith time delay for the time-dependent case. We can convert the time-dependent transmission amplitudes to stationary transmission amplitude in Floquet channels. Using Eqs. (3.51) and (3.52) with the Floquet scattering matrix, we obtain the dwell time for the sum of all Floquet channels

$$\tau_W(E) = -\frac{i\hbar}{N'}Tr\left\{\sum_{n=-n'}^{n'} S_F^\dagger(E, E_n)\frac{\partial S_F(E, E_n)}{\partial E}\right\}, \tag{3.54}$$

where the Floquet energy $E_n = E + n\hbar\Omega$ and $N' = 2N(2n' + 1)$ is the total number of the scattering channels that results from the total number of Floquet bands n' and spin polarizations. Eq. (3.54) gives the average time of flight overall channel for a given energy E. We also obtain energy average time of flight and denote it as τ. We first choose the energy values where the number of the open transverse channel is held constant, then taking the average over these energy values gives the averaged time of flight for a chosen open transverse channel. Finally, we use this parameter τ to determine the low-frequency and high-frequency regime where $\Omega < 1/\tau$ and $\Omega > 1/\tau$ respectively.

3.3   Numerical Methods for Simulations

We perform our numerical simulations in Python with the quantum transport library Kwant [42]. We start by placing our Hamiltonian on a square lattice using the finite difference method, which is called the tight-binding approach [22]. In the time-dependent case, we consider the Floquet Hamiltonian for a 2DEG with Rashba SOI as the input in

Kwant. After defining the geometry of the 2-dimensional material and connecting the leads to the scattering region, we input in Kwant the tight-binding Floquet Hamiltonian for the scattering region and the leads separately. Using Kwant, we then compute all scattering matrix elements for a chosen Fermi energy and the other parameters of the system. We extract the transmission amplitudes from the $n = 0$ to all Floquet channels from these matrix elements. Using these amplitudes, we calculate spin/charge conductances and currents.

3.4 Conclusion

In this chapter, we explained how to obtain the spin/charge current for two cases: a system with periodic in-time potential and a periodic in-time bias voltage applied to the system. Floquet theory allows us to convert a time-dependent Hamiltonian into a static Hamiltonian with Floquet channels. From this, we can obtain the Floquet scattering matrix that depends on an electron's initial and final energy. Moreover, we can compute the adiabatic approximation of the Floquet scattering matrix obtained in the adiabatic limit by using the frozen scattering matrix. Using the Floquet scattering matrix, we then generalized the Landauer-Büttiker formalism to calculate the time-dependent currents. Moreover, we showed how to compute the AC and DC currents in the presence of a time-dependent potential and the absence of a bias voltage. Finally, we explained how to determine the frequency range for the adiabatic and the high-frequency regimes using the Wigner-Smith time-delay matrix.

Chapter 4

AC SPIN CURRENT GENERATION

Spin current manipulated by tuning the Rashba spin-orbit interaction can be essential for spin-based devices, eventually, for the future of information technology. This chapter demonstrates how to create spin currents in mesoscale conductors by time-dependent Rashba SOI. We focus on a 2DEG with time-dependent Rashba SOI, which can be engineered via an AC top gate and follow a mixed analytical-numerical approach to compute the AC spin and charge currents in a periodically driven system in both low and high-frequency regimes.

First, we study both linear in-frequency response and high harmonic generation of spin and charge currents generated by the Rashba coupling. We compare the Floquet formalism and its adiabatic approximation after defining the range of low and high frequencies. Second, we show that one can write the spin-orbit coupling in 2DEGs in terms of appropriate $SU(2)$ gauge fields. After an $SU(2)$ gauge transformation, the current generated by the time-dependent Rashba SOI in the absence of the bias voltage can be expressed approximately via charge conductance and spin-dependent voltage $V^\uparrow - V^\downarrow$. As a result, the dynamical Rashba SOI generates spin electric force. We show that the spin currents after this gauge transformation and in the original system with Rashba coupling agree to good accuracy. Last, we apply the net spin-dependent voltage as a bias in the spinless system. We implement the frequency dependence of the conductance and verify that this becomes significant in the high-frequency regime.

4.1   AC Spin Current Generation via Time Dependent Rashba SOI

We investigate the charge and spin currents in response to time-dependent Rashba coupling on a 2DEG cavity shown in Fig. 4.1. We use the Floquet scattering formalism, re-

viewed in the previous chapter, to calculate the currents in the periodically time-dependent system. We first determine the cut-off value for number of Floquet channels, which depends on the Rashba SOI strength and the driving frequency. We also calculate the dwell time to specify the low-frequency range where the adiabatic limit holds. We then compare the AC currents calculated with the Floquet scattering matrix and its adiabatic approximation. The main outcome of this calculation of the spin current generated by a dynamical scatterer with the time-dependent Rashba coupling.
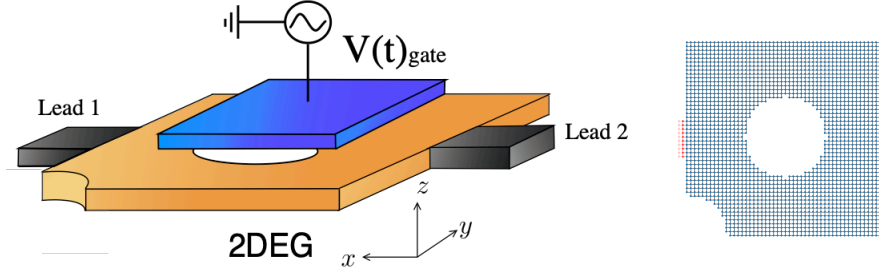
Figure 4.1: (Left) Sketch of the spin current source. An AC top gate voltage is applied in a chaotic ballistic cavity connected to two leads, which controls the Rashba coupling and thus creates a spin electric force. (Right) The shape of the scattering region.

4.1.1 Numerics: Spin current calculation

To obtain the time-dependent currents arising from time-periodic Rashba SOI, we use the Floquet scattering matrix. We follow two approaches as reviewed in Chapter 3. First, we numerically solve the Schrödinger equation using the Floquet Hamiltonian. The Floquet Hamiltonian with the Rashba coupling with $\alpha(t) = k_{so} \sin(\Omega t)$ is

$$H_F = \sum_{n=-\infty}^{\infty} \left((H_0 - n\hbar\Omega)|n\rangle\langle n| + \frac{iH_1}{2}(|n\rangle\langle n+1| - |n\rangle\langle n-1|) \right), \qquad (4.1)$$

where $H_0 = -\frac{\hbar^2}{2m}(\partial_x^2 + \partial_y^2)$ and $H_1 = ik_{so}(\sigma_y\partial_x - \sigma_x\partial_y)$ are the kinetic and the Rashba contributions. Floquet states $|n\rangle$ form basis vectors of time-periodic eigenfunctions $|\phi_\alpha(\vec{r}, t)\rangle$ of the Floquet Hamiltonian (see Eq. (3.9)). After obtaining elements of the Floquet scattering matrix, we calculate the AC spin currents induced by the Rashba SOI without a bias voltage. As stated before, the current is

$$I_i^a(t) = \sum_{l=-\infty}^{\infty} e^{-il\Omega t} I_{i,l}^a = I_{i,+}^a \cos(\Omega t) + I_{i,-}^a \sin(\Omega t) + \cdots \qquad (4.2)$$

where $a = 0$ corresponds to the electric current, $a = x, y, z$ corresponds to the spin current with spin direction a. This section considers only the leading term $l = \pm 1$ to obtain the linear frequency response. We will examine high harmonic generation $l > 1$ in Section 4.4. The Fourier components are determined in terms of the Floquet scattering

matrices $S_F(E_n, E)$ as

$$I^a_{i,l} = C_a \int dE \sum_{n=-\infty}^{\infty} \sum_{j=1}^{N_r} \sum_{m \in i, m' \in j} Tr[S^\dagger_{F,im,jm'}(E_n, E)\sigma^a S_{F,im,jm'}(E_{l+n}, E)], \quad (4.3)$$

where N_r denotes the number of leads, σ^a is the Pauli matrix with the spin direction a and σ^0 defined as a unit matrix. C_a specifies the unit of spin and charge current with $C_{x,y,z} = \frac{1}{h}\frac{\hbar}{2}$ and $C_0 = \frac{e}{h}$. We consider the system shown in Fig. 4.1 for numerical calculations. We set the Rashba SOI as $\alpha(t) = k_{so}\sin(\Omega t)$, and it is non-vanishing only in the scattering region and vanishes in the leads. The precise shape of the system is depicted on the right of Fig. 4.1. L is the system size, which we take as $L = 50a$ where a is the lattice constant and the width of the leads for this system is $10a$. We choose parameters appropriate for an InAs $2DEG$ material, where the effective mass $m = 0.023\,m_0$ and lattice spacing is fixed at $a = 2$ nm. Then the magnitude of the Rashba coupling is $0.8 \cdot 10^{-11}\,eVm$ in InAs systems, which is experimentally achievable [5]. We perform
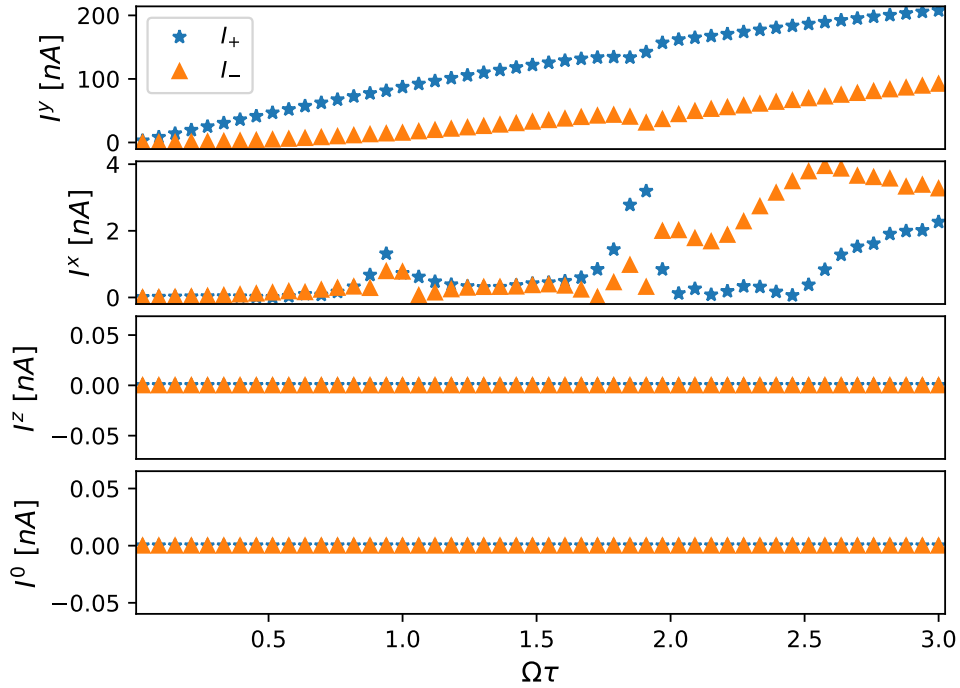
Figure 4.2: Charge and spin currents in x, y, z direction with the time-dependent Rashba SOI where $I^a(t) = I^a_+ \cos(\Omega t) + I^a_- \sin(\Omega t)$. The currents are calculated by the Floquet scattering matrix where $k_{so}L = 1$ and $E_F = 0.2$ eV.

our numerical calculations in Python using the quantum transport library Kwant [42]. To obtain time-dependent scattering amplitudes from which we determine spin and the charge currents, we implement the Floquet Hamiltonian Eq. (4.1) in tight-binding form (see Chapter 2.3.2). In practice, we use only $l = \pm 1$ in Eq. (4.2), and we must also limit the sum over the Floquet bands n in Eq. (4.3). We show that, for our purposes, including

up to 21 bands ($|n| \leq 10$) will be sufficiently good depending on the Rashba coupling constant. Also, we calculate the adiabatic approximation of the Floquet scattering matrix for the system with the time-dependent Hamiltonian, using Kwant to check its validity.

A typical energy scale associated with the problem specifies the energy dependence of the scattering matrix and determines the borderline between adiabatic and high-frequency regimes. For a few open ballistic channel transport, this energy scale is related to the inverse time of flight ($\hbar/\tau$) of an electron between two leads which is calculated using the Wigner-Smith time-delay matrix [9, 10]. If the frequency is much smaller than the inverse of the time of flight and the Fermi energy, $\Omega\tau \ll 1$ and $\hbar\Omega \ll E_F$, the scattering process is in the adiabatic regime. We use frequencies $\Omega/2\pi$ of the time-dependent potential between approximately 100 GHz and 330 GHz for calculations in this low-frequency limit. We choose frequencies up to 1 THz for calculations in the high-frequency limit.

First, to see whether a dynamical Rashba SOI induces any current without applied bias voltage, we compute the charge current and the x, y, z component of the spin current where the AC current is approximated as in Eq. (4.2). We plot the spin and charge current versus $\Omega\tau$ in Fig. 4.2, where the Fermi energy $E_F = 0.2\ eV$ and $k_{so}L = 1$. We find that the periodic Rashba SOI generates a spin current, with a magnitude of a few hundred nanoamperes in spin direction y, and a few nano amperes in x, while we do not find a charge current and spin current in z.

4.1.2 Role of the number of Floquet bands for the numerical results

Here we present our procedure to determine the number of Floquet channels for numerical convergence. In the calculation of the spin current using Eq.(4.1) we need to choose a cut-off value n_{max} in the sum over the Floquet channels n. This cut-off value n_{max} will depend on the ratio between the amplitude of the oscillating potential and the driving frequency. As discussed in Ref.[6] (see chapter 3), if the amplitude of the oscillating potential is much smaller than $\hbar\Omega$, then $n_{max} = 1$ turns out to be sufficient for numerical calculations. On the other hand, if the amplitude of the oscillating potential is comparable to the driving frequency, then one typically needs $n_{max} > 1$ for numerical calculations. It is crucial to know the number of channels prior to numerical calculations as the time cost of a calculation heavily depends on this number. To determine this number, we compute the spin current for a selected number of Floquet states $2n + 1$ and change n to calculate the precision defined by $\Delta I_n = (I_n - I_{n-1})/I_n$. We plot this quantity, shown in Fig. 4.3, for the system in Fig. 4.1 where $k_{so}L = 0.2$ and 2 and $\Omega\tau \approx 0.1$ and 1.

Generally, we observe that smaller cut-off values n_{max} suffice for smaller choices of k_{so}, independent of frequency, as expected. At moderate values of k_{so}, while smaller n_{max} suffice for smaller frequencies, higher n_{max} is needed at higher frequencies. We find that
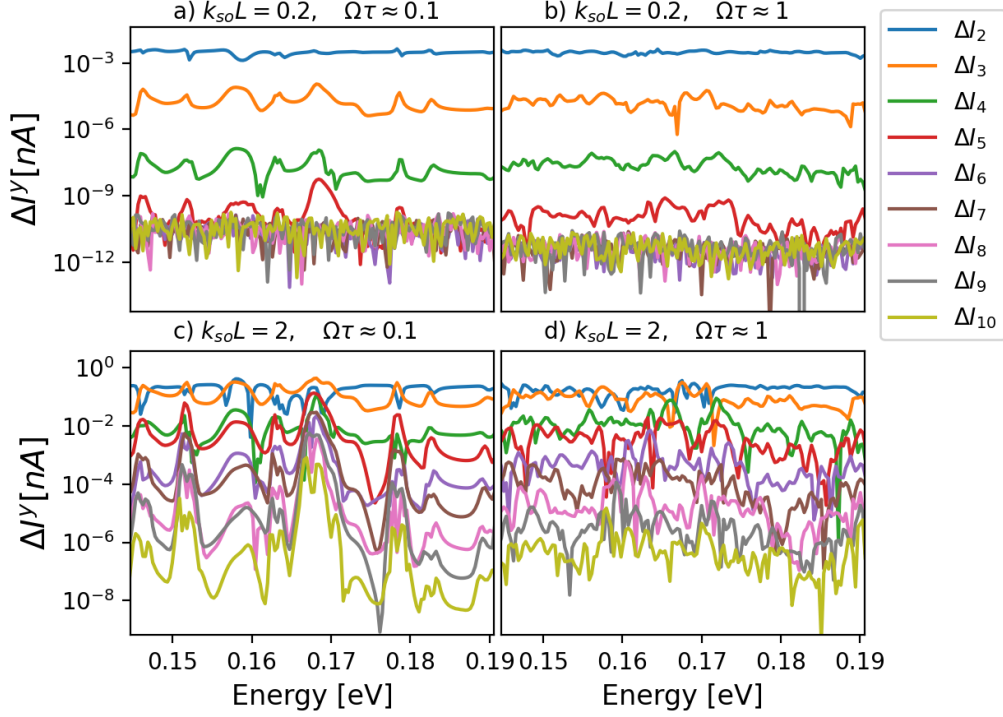
Figure 4.3: Convergence in n of AC spin currents generated by time-dependent Rashba SOI, where $\Delta I_n = (I_n - I_{n-1})/I_n$ and I_n is the current calculated with maximum Floquet states $n_{max} = n$. Parameters correspond to $\Omega\tau \approx 0.1$ and 1, and $k_{so}L = 0.2$ and 2.

our chosen cut-off value $n_{max} = 10$ provides a sufficiently good approximation to the time-dependent currents for the range of parameters considered in this thesis.

4.1.3 Comparison of the Floquet scattering matrix with its adiabatic approximation

As a second approach, we determine elements of the Floquet scattering matrix using the frozen scattering matrix $S(t, E)$ in the adiabatic limit (see Section 3.1.3),

$$S_F(E_n, E) \simeq \frac{1}{\mathcal{T}} \int_0^{\mathcal{T}} S(E, t) e^{in\Omega t} dt. \tag{4.4}$$

Here we compare our results for the spin currents following the Floquet scattering matrix and its adiabatic approximation for low and high frequencies. Our purpose is to determine the maximum frequency value up to which the adiabatic approximation is valid in our system. In Fig. 4.4, we compare the adiabatic and full Floquet spin currents for the chaotic ballistic system of Fig. 4.1 for frequency ranges between $\Omega\tau \approx 0.1$ and $\Omega\tau \approx 3$ where $k_{so}L = 1$. We plot our results as a function of the Fermi energy. The results agree with the adiabatic regime $\Omega\tau \approx 0.1$ as expected and show semi-quantitative agreement up to the frequency of $\Omega\tau \approx 1$.
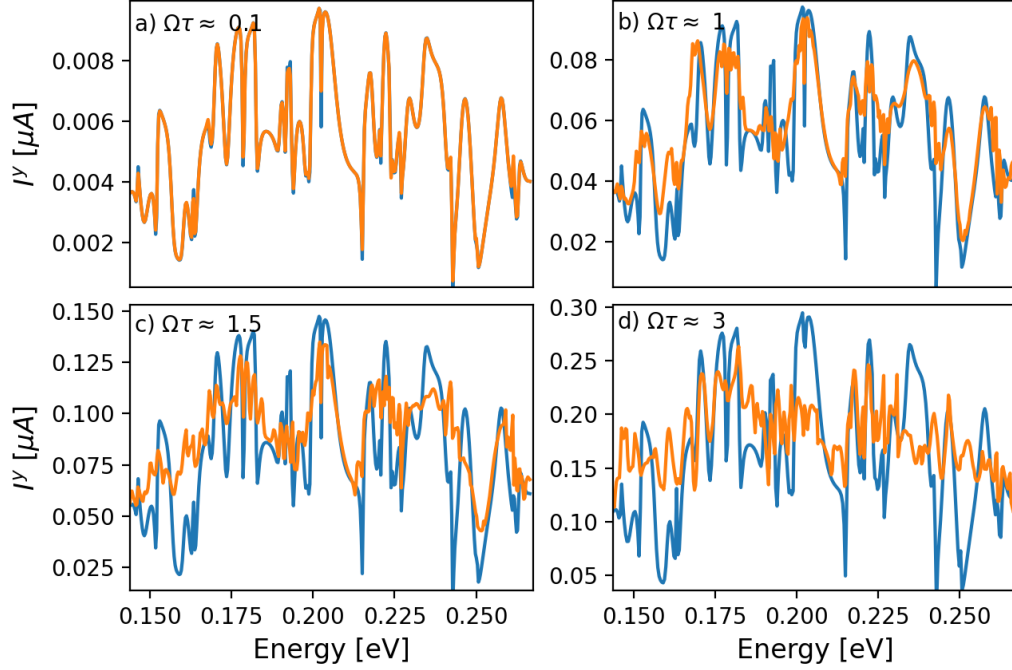
Figure 4.4: Spin currents for the chaotic ballistic system in Fig. 4.1, calculated by using the full Floquet scattering matrix (orange) and by the adiabatic approximation (blue) for $k_{so}L = 1$ and $\Omega\tau \approx 0.1$ (a), 1 (b), 1.5 (c) and 3 (d).

4.1.4 Calculation of the dwell time

The energy derivative of the phase shift, written in terms of the scattering matrix (see Chapter 3.2.3), gives the average time that an electron spends in a scattering region. The Wigner-Smith time-delay matrix is real and give the proper time delays for each transport channel. We calculate the average time of flight τ for an electron by taking the average over all energies while keeping the number of open channels. To obtain the time delay matrix of an electron for the chaotic cavity in Fig. 4.1 with the time-dependent Rashba SOI, we calculate the time delay with the Floquet scattering matrix using Eq. (3.54),

$$\tau_W(E_F) = -\frac{i\hbar}{N'}Tr\left\{ \sum_n S_F^\dagger(E_F, E_{F,n})\frac{\partial S_F(E_F, E_{F,n})}{\partial E} \right\},$$

where $N' = 2N(2n + 1)$ is the total number of the scattering channels with the Floquet bands n, the transverse channels N including spin polarization. We then check the time delay using the frozen scattering matrix

$$\tau_W(E_F) = -\frac{i\hbar}{N}Tr\left\{ \frac{1}{\mathcal{T}}\int_0^{\mathcal{T}} dt\, S^\dagger(E_F, t)\frac{\partial S(E_F, t)}{\partial E} \right\}$$

where $\mathcal{T}$ is the period. Fig. 4.5 shows that both scattering matrices give the same time of flight as expected in the adiabatic limit. This agreement breaks down around $\Omega\tau \approx 1$.

Fermi energy are chosen when only 2 transport channels are open. We also examined
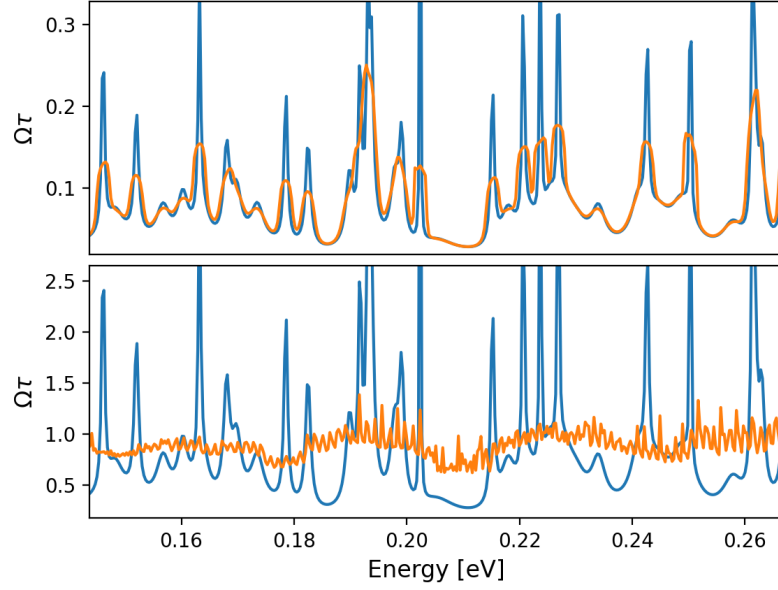
Figure 4.5: Average time of flight calculations using Wigner-Smith time delay matrix obtained by Floquet scattering matrix (orange) and frozen scattering matrix (blue) where $\Omega\tau \approx 0.1$ (above) and $\Omega\tau \approx 1$ (below).

how the driving frequency and the Rashba SOI strength k_{so} affect the energy average of the time of flight. In the range of driving frequencies and the Rashba SOI strength we consider, the energy average of the time of flight stays approximately the same.

4.2 AC Spin Current Generated by Spin Electric Fields

In this section, we employ a different method to carry out the same computation. We first perform a gauge transformation to rewrite the time-dependent Rashba SOI as a spin-dependent potential. We then verify this method by numerically calculating the spin current and comparing it with the previous result.

4.2.1 Model and its non-Abelian gauge structure

4.2.1.1 General case

Our starting point is the standard low-energy model for a spin-orbit coupled electron or hole gas in 2D [43]. The Hamiltonian reads

$$H = \frac{p^2}{2m} + \mathbf{b}(\mathbf{p}) \cdot \sigma + \mathbf{W}(\mathbf{x}). \tag{4.5}$$

Here $W(\mathbf{x})$ is the electrostatic potential specifying the static environment, which might originate from gates, applied bias, impurities, *etc.*, m is the effective electron mass, and

$\mathbf{b}(\mathbf{p})$ is a spin-orbit field that couples spin to momentum. We assume that the strength of this SOI can be controlled externally and more generally, both in a position- and time-dependent way: $\mathbf{b}(\mathbf{p}) \to \mathbf{b}(\mathbf{p}; \mathbf{x}, t)$. For the rest of this section, we specialize to electrons and light holes for which this field is linear in momentum. Then the Hamiltonian can be rewritten introducing non-Abelian gauge fields. Following the Ref.[44], the Hamiltonian reads

$$H = -\frac{D_\mu D_\mu}{2m} + V(\mathbf{x}). \tag{4.6}$$

Here $D_\mu = \partial_\mu - (ik_{so}/2)\sigma^a A_\mu^a$ is the $SU(2)$ covariant derivative along $\mu = x, y$, with σ^a the Pauli matrices ($a = x, y, z$), $A_\mu^a(\mathbf{x}, t)$ a dimensionless $SU(2)$ vector potential and $V = W - k_{so}^2(A_\mu^a A_\mu^a)/(8m)$. Unless specified otherwise, in this section, we assume that the repeated indices are summed over. The SOI strength is controlled by the parameter k_{so}, typically much smaller than the Fermi momentum k_F. In terms of this spin-orbit parameter, the accuracy of Eq. (4.6) is $\mathcal{O}(k_{so}/k_F)^2$. We now make our central assumption that $L \ll l_{so}$, where $l_{so} = \pi/|k_{so}|$ is the spin-orbit length and L is the system size. That is usually fulfilled for experimental realizations using systems at nano- to mesoscales. We also assume that time-dependence of $A_\mu^a(t)$ is slow, then $x_\mu k_{so}\partial_t A_\mu^a \ll E_F$, where E_F is the Fermi energy. $SU(2)$ gauge transformations are unitary transformations of the form

$$U = \exp(i\Lambda_a(\mathbf{x}, t)\sigma_a/2). \tag{4.7}$$

It is then straightforward to show that this transformation maps $A_\mu^a(\mathbf{x}, t) \to (A')_\mu^a(\mathbf{x}, t)$ and $V(\mathbf{x}, t) \to V'(\mathbf{x}, t)$, where

$$(A')_\mu^a = A_\mu^a - \epsilon^{abc}\Lambda^b A_\mu^c + \frac{1}{k_{so}}\partial_\mu\Lambda^a \quad, \tag{4.8}$$

$$V' = V - \sigma^a\frac{1}{2}\frac{\partial\Lambda^a}{\partial t} \quad. \tag{4.9}$$

These transformations allow us, among other advantages, to gauge away the homogeneous and time-independent components of the spin-orbit field up to quadratic order in the coupling constant [45, 46]. For a concrete example, we now specialize to a 2D electron gas with a Rashba spin-orbit interaction

$$H = \frac{p^2}{2m} + \frac{1}{2}\{\alpha_R, (\sigma^x p_y - \sigma^y p_x)\} + V(\mathbf{x}), \tag{4.10}$$

where the Rashba coupling constant α_R can be a function of both position and time. However, for simplicity, we concentrate on regions of either time- or position dependent Rashba coupling, *i.e.* $\alpha_R(t), \alpha_R(\mathbf{x})$, and combine them later using rules for the combination of the respective scattering matrices. In this chapter, we identify and study the effects of time-dependent Rashba coupling and the generation of spin electric fields. We will

discuss the generation of spin magnetic fields via position dependent Rashba coupling in Chapter 5.

4.2.1.2 Spin electric field from time-dependent SOI

A time-dependent Rashba SOI constant $\alpha(t) = k_{so} \sin(\Omega t)$ with $T = 2\pi/\Omega$, the AC modulation period from a top gate [5], will generate the spin electric forces, see Fig. 4.1. In this case $A_\mu^a(t) = \epsilon_\mu^a \sin(\Omega t)$, and the $SU(2)$ gauge transformation (4.7) becomes

$$U = \exp\left(-ix_\mu k_{so} A_\mu^a \sigma^a / 2\right).$$
(4.11)

To order $(k_{so}L)^2$ one obtains a vanishing vector potential, while $\partial_t A_\mu^a(t)$ generates a non-zero $SU(2)$ scalar potential

$$(A')_\mu^a = 0\,,$$
(4.12)

$$(V')^a = x_\mu k_{so} \partial_t A_\mu^a \sigma^a / 2\,,$$
(4.13)

yielding the transformed Hamiltonian

$$H' = -\frac{1}{2m}\partial_\mu\partial_\mu + (x_\mu k_{so}\partial_t A_\mu^a)\frac{\sigma^a}{2} + V(\mathbf{x}).$$
(4.14)

A further global spin rotation [47] $\sigma^a \to \sigma^z$ then leads to the diagonal Hamiltonian

$$H_d = \frac{p^2}{2m} + V(\mathbf{x}) + \frac{V^s(t)}{2}\sigma^z,$$
(4.15)

$$V^s \equiv \epsilon_\mu^s x_\mu k_{so}\partial_t \sin(\Omega t)\quad,$$
(4.16)

i.e. opposite-spin electrons feel a different electric field

$$\mathcal{E}_\mu^{\uparrow\downarrow} = -\partial_\mu\left[V(\mathbf{x}) \pm V^s(t)/2\right] \equiv E_\mu \pm \mathcal{E}_\mu^s.$$
(4.17)

The component $\mathcal{E}_\mu^s$ is a spin-electric field accelerating opposite spin species in opposite directions.

4.2.2 Numerical calculations

In this subsection, we perform numerical simulations to confirm that one obtains the same spin current before and after the gauge transformation in subsection 4.2.1. The gauge transformation results in a spin potential in the spin z direction that enables to write potentials for up and down separately. The spin potential is linear both in x and y inside the scattering region and stays constant in the x-direction in the leads because the Rashba

SOI is absent there. We consider a system in Fig 4.1, where we position lead 1 at $x = 0$
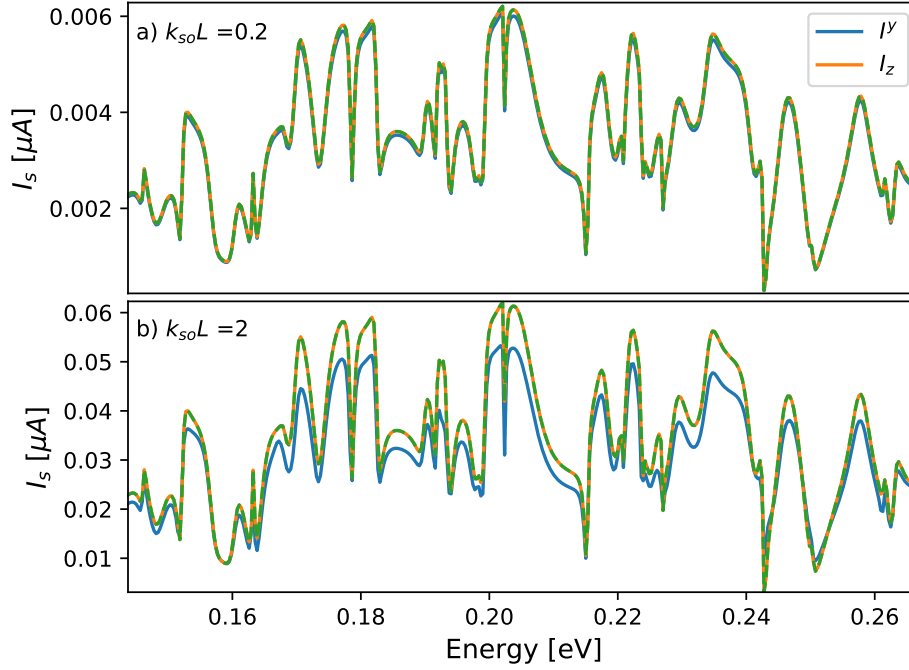
Figure 4.6: Spin current in y direction generated by the Rashba SOI (blue), spin current in z direction generated by the spin electric field, which is obtained after the gauge transformation, calculated by Floquet scattering matrix (green) and its adiabatic approximation (orange) where $k_{so}L = 0.2$ (a) and 2 (b) with $\Omega\tau \approx 0.3$..

and lead 2 at $x = L$ and choose the system size and width as $L = 50a$ and $W = 10a$. The spin potentials for this configuration are

$$V_s^{\uparrow(\downarrow)} = \pm x\, k_{so} \cos\left(\Omega t\right) \mp y\, k_{so} \cos\left(\Omega t\right) \tag{4.18}$$

$$V_1^{\uparrow(\downarrow)} = \mp y\, k_{so} \cos\left(\Omega t\right) \tag{4.19}$$

$$V_2^{\uparrow(\downarrow)} = \pm L\, k_{so} \cos\left(\Omega t\right) \mp y\, k_{so} \cos\left(\Omega t\right) \tag{4.20}$$

where we used Eq. (4.14). V_s and $V_{1(2)}$ denote spin potentials for up and down spins inside the scattering region and on the lead 1(2), respectively. It is important to note that the wave functions also transform under the gauge transformations as $\psi(x) \rightarrow e^{i \int dx\, \alpha(t) \frac{\sigma^z}{2}} \psi(x)$ [48]. In the full Floquet scattering matrix calculation, this is already implemented in the Floquet Hamiltonian. On the other hand, we have to explicitly include this effect in the scattering matrix when we use the adiabatic approximation. That is because the effect that would normally arrive from the time derivative in the Schrödinger equation is absent in this approximation. That yields a phase in the frozen scattering matrix [48]. Then the
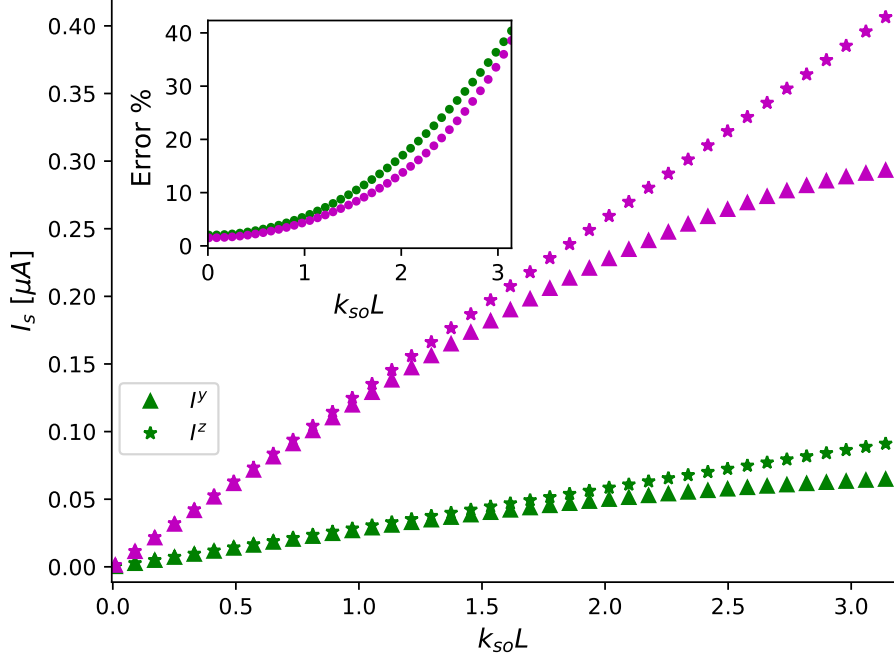
Figure 4.7: Comparison of the spin current in y direction generated by the Rashba SOI (triangle) and the spin current in z direction generated by the spin electric field, obtained after the gauge transformation (star). We choose $\Omega\tau \approx 0.3$ (green), 1.5 (magenta) and $E_F = 0.2$ eV. The inset shows the percentage error between two currents.

Fourier transform is calculated including the phase factor as

$$S_n(E) = \frac{1}{2\pi}\int_0^{2\pi} e^{-in\Omega t}e^{i\int dx\,\alpha(t)\frac{\sigma^z}{2}}S(E,t).$$

We first calculate the spin current in the z direction for the system in Fig. 4.1 with spin electric fields in Eq. (4.18) using the Hamiltonian in Eq. (4.6). We then compare this current with the spin current generated by the time-dependent Rashba SOI where $\alpha(t) = k_{so}\sin(\Omega t)$. The parameters are chosen as $L = 50a$, $k_{so}L = 0.2$ with $\Omega\tau \approx 0.1$ and 1 for the adiabatic and the full Floquet calculations respectively. These are shown in the top and bottom Figs. 4.6, respectively. We observe very good numerical agreement between the two methods. Furthermore, as shown in Fig. 4.7, our approximation, which is expected to work theoretically when $k_{so}L \ll \pi$, in practice, works even for $k_{so}L \approx 1$. This choice corresponds to a good optimal value for a sufficiently large current and relatively small errors.

4.3   AC Spin Current in the Presence of Spin Voltage

In this section, we will represent the spin-dependent potentials obtained after the gauge transformation in terms of an applied bias on the leads. This bias is given by the difference between spin voltages generated by up and down spins, $V^\uparrow - V^\downarrow$. We first provide the formulas for the current in the presence of the spin voltage both in the adiabatic and

the high-frequency regimes. We consider the same 2D chaotic cavity with only time-dependent Rashba coupling, which is applied via AC gate voltage on the top of the system as shown in Fig. 4.1. It generates a spin voltage on both leads in the opposite direction. Then, the voltage difference between the two leads results in a spin current in the y-direction. We compare our prediction of the spin current induced by the spin voltage with the spin currents generated by the time-periodic Rashba SOI.

4.3.1 Linear response currents :
Basic expressions for charge and spin conductance

We consider a mesoscopic sample attached to leads labeled by i, j. The leads are in contact with different metallic reservoirs used to apply spin voltages. The linear response Landauer-Büttiker formula for the a-polarized spin current flowing into/out of contact i is generalized as follows [28, 49]

$$I_i^\alpha = \sum_\beta (2\frac{e^2}{h} N_i \delta_{\alpha\beta} - G_{ii}^{\alpha\beta}) V_i^\beta - \sum_\beta \sum_{j \neq i} G_{ij}^{\alpha\beta} V_j^\beta, \tag{4.21}$$

where N_i is the number of channels in lead i. In this section, we use Latin letters (a=x,y,z) to denote spin components of the current while Greek letters commonly describe electric (0) and spin components (a). Note that this is different from the previous sections, where we used a for both charge and spin, and makes our presentation clear. We also take charge and spin current to have the same units, which is achieved by multiplying the spin current in the previous sections by the factor $\frac{2e}{\hbar}$, which is called charge per unit time (The other method is the angular momentum per unit time, obtained without the factor $\frac{2e}{\hbar}$).

The spin voltage $V_j^b = \mu_j^b/e$ physically represents an imbalance of spins polarized along a b-axis in reservoir j, with spin accumulation $\mu_j^b = \mu_j^{(\uparrow)} - \mu_j^{(\downarrow)}$. The conductance is a (4×4)-matrix in the combined spin-charge space:

$$G_{ij} = \begin{pmatrix} G_{ij}^{00} & G_{ij}^{0b} \\ G_{ij}^{a0} & G_{ij}^{ab} \end{pmatrix}, \tag{4.22}$$

where the superscript "0" indicates the charge component. Here $G \equiv G^{00}, G^{0b}, G^{b0}$ and G^{ab} are, respectively, the charge, charge-spin, spin-charge, and spin-spin conductances.

$$G_{ij}^{00} = \frac{e^2}{h} \sum_{m,n} \text{Tr}[t_{mn}^\dagger t_{mn}], \tag{4.23}$$

$$G_{ij}^{0b} = \frac{e^2}{h} \sum_{m,n} \text{Tr}[t_{mn}^\dagger t_{mn} \sigma^b], \tag{4.24}$$

$$G_{ij}^{b0} = \frac{e^2}{h} \sum_{m,n} \text{Tr}[t_{mn}^\dagger \sigma^b t_{mn}], \tag{4.25}$$

$$G_{ij}^{ab} = \frac{e^2}{h} \sum_{m,n} \text{Tr}[t_{mn}^\dagger \sigma^a t_{mn} \sigma^b]. \tag{4.26}$$

Here, t_{mn} is the (2×2)-matrix of spin-dependent transmission amplitudes connecting channel n in lead j to channel m in lead i, and σ^a are the Pauli spin matrices. Even in the absence of any charge bias, the system can feature a charge response given by

$$I_i^0 = -\sum_b G_{ii}^{0b} V_i^b - \sum_b \sum_{j \neq i} G_{ij}^{0b} V_j^b, \tag{4.27}$$

in addition to the spin response

$$I_i^a = \sum_b (2\frac{e^2}{h} N_i \delta_{ab} - G_{ii}^{ab}) V_i^b - \sum_b \sum_{j \neq i} G_{ij}^{ab} V_j^b. \tag{4.28}$$

Under the assumption $L \ll l_{so}$, *i.e.* a moderate Rashba constant k_{so}, the spin precession conductance G^{ab} is equivalent to the charge conductance, $G^{ab} \propto \delta^{ab} G^{00}$. Hence all spin conductances in Eqs. (4.27) and (4.28) are expressed in terms of the charge conductance to linear order in k_{so}. Besides, after the gauge transformation, the time-dependent Rashba SOI is converted to spin-dependent fields, then we can consider these fields as a spin-dependent voltage $V^a = V^\uparrow - V^\downarrow$.

4.3.2 Spin current generation

We first calculate spin current generation by a spin-dependent voltage using Eq. (4.28) in both the adiabatic and high-frequency regimes. We consider a 2D chaotic cavity with only time-dependent Rashba coupling, induced by an AC top gate voltage, see Fig. 4.1. The Rashba SOI strength has a time dependence given by $\alpha_R(t) = k_{so} \sin(\Omega t)$, with $\Omega/2\pi$ the driving frequency. As discussed above, this time-dependent coupling induces a spin voltage on the leads, and the spin voltage difference between two leads results in a spin current polarized in the y-direction. Throughout this section, we will work in the linear response regime and ignore effects nonlinear in the spin-orbit coupling. We derive our general spin current formulae in low and high-frequency regimes. Next, we present our numerical results in Sec. 4.3.3, also including a comparison with our analytical results in Sec. 4.3.4.

4.3.2.1 AC spin current in the low-frequency regime

In the low-frequency regime, one can neglect the frequency dependence of the charge conductance. The spin current in Eq. (4.28) can thus be computed using the DC conductance. To leading order in the spin-orbit coupling, all spin effects are included in the spin voltage. Hence $G^{ab} = \delta^{ab}G$. We note that the case of a large Rashba coupling with a small time-dependent part can also be treated with our gauge transformation method. Then the results of this section need to be modified to account for spin precession. In the absence of a bias voltage ($V^0 = 0$), the spin current at lead 1 is the current generated by the spin voltage

$$I_1^a = \sum_j (2\frac{e^2}{h}N_1\delta_{1j} - G_{1j})V_j^a. \tag{4.29}$$

The spin voltage from the time-dependent Rashba SOI reads

$$V^{a,\uparrow(\downarrow)} = \pm\partial_t\alpha_R(t)\epsilon_\mu^a l_\mu. \tag{4.30}$$

Here l_μ is the system size in the direction $\mu = x, y$. For the system shown in Fig. 4.1, Rashba SOI generates a spin voltage with spin direction y along the x axis. Up and down spins feel opposite voltage biases, hence the total spin voltage bias is

$$V_{1(2)}^y = V_{1(2)}^\uparrow - V_{1(2)}^\downarrow = \pm\partial_t\alpha_R(t)L_{12} \tag{4.31}$$

with L_{ij} the distance between lead i and lead j According to Eq. (4.29), this spin voltage then drives a spin current

$$I_1^y(t) = \left(2\frac{e^2}{h}N_1 - G_{11} + G_{12}\right)\partial_t\alpha_R(t)L_{12}. \tag{4.32}$$

To summarize, we expressed the spin current in terms of the DC charge conductance and time-dependent α_R in the small-Ω limit. This is our first prediction for the spin current in the low-frequency regime.

4.3.2.2 AC spin current in the general frequency regime

In a system driven by a time-dependent voltage, both particle and displacement currents will appear. In order to take these into account, we no longer neglect the frequency-dependence of the AC conductance, which in Fourier space is given by the admittance $G_{ij}(\omega)$. In linear response, we have

$$G_{ij}(\omega) = \langle \delta I_i(\omega)/\delta V_j(\omega)\rangle. \tag{4.33}$$

In the presence of a bias voltage $V(t) = V(\omega)e^{i\omega t}$, the current $I_i(\omega)$ is calculated via the Floquet formalism. Using linear response theory, one can obtain the AC conductance as [29, 40, 50]

$$G_{ij}(\omega) = \frac{e^2}{h} \int dE\, Tr\{\delta_{ij}\mathbf{1}_i - S_{ij}^\dagger(E)S_{ij}(E + \hbar\omega)\}\frac{f_j(E) - f_j(E + \hbar\omega)}{\hbar\omega}. \quad (4.34)$$

The AC charge current driven by $V(\omega)$ is then given by

$$I_i(\omega) = \sum_j G_{ij}(\omega)V_j(\omega). \quad (4.35)$$

In our case, a time-dependent SOI $\alpha_R(t) = \alpha_R(\omega)e^{i\omega t}$ leads to a (spin) voltage in the frequency domain:

$$V^y(\omega) = \pm i\omega\alpha_R(\omega)L, \quad (4.36)$$

which in turn drives a spin current

$$I_1^y(\omega) = (2\frac{e^2}{h}N_1 - G(\omega)_{11} + G(\omega)_{12})i\omega\alpha_R(\omega)L_{12}. \quad (4.37)$$

Equation (4.37) is our main result for the spin (generation) conductance. It generalizes Eq. (4.32) to high frequencies and applies beyond the range of validity of the adiabatic approximation. For general time-dependent α_R, we can obtain the time-dependent spin current via the inverse Fourier transform of $I(\omega)$:

$$I_1^y(t) = \int \frac{d\omega}{2\pi}e^{i\omega t}I_1^y(\omega). \quad (4.38)$$

4.3.3 AC spin current generation: Comparison with numerics

We now perform numerical simulations to check our predictions summarized in Eqs. (4.32) and (4.37) for spin current. The Rashba SOI has an AC-form $\alpha_R(t) = k_{so}\sin(\Omega t)$, with $k_{so} \sim 1/L$. The system size is $L = 50a$, with a being the lattice constant of our discretized model. The width of the leads is $10a$. We choose parameters appropriate for an InAs 2DEG material with effective mass $m = 0.023\, m_0$, lattice spacing $a = 2$ nm. The magnitude of the Rashba coupling is $0.8 \cdot 10^{-11}$ eVm, which is in the experimental range of InAs systems [5]. We calculate the AC spin current polarized in the y direction, $I^y(t) = I^y\cos(\Omega t)$, induced by the time-dependent Rashba SOI $\alpha_R(t) = k_{so}\sin(\Omega t)$. The spin current given in Eq. (4.2) is computed using the Floquet scattering matrix and then compared with our analytical results in Eqs. (4.32) and (4.37). We first check the validity of our approximation (4.32) in the low-frequency regime. We choose $\Omega/2\pi \approx 100$ GHz, corresponding to $\Omega\tau \approx 0.3$. In Fig. 4.8, we perform the comparison for varying values of
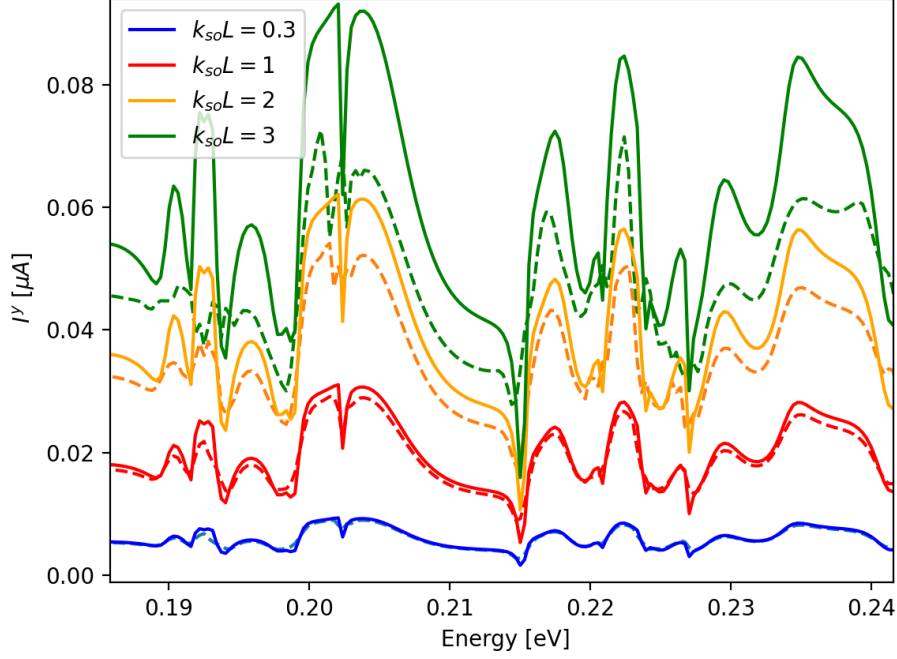
Figure 4.8: Comparison of the AC spin currents generated by the spin-dependent voltage, Eq. (4.32), (solid line) and numerically (dashed) directly for the time-dependent Rashba SOI $\alpha_R(t) = k_{so}\sin(\Omega t)$ with $\Omega\tau \approx 0.3$ for varying values of $k_{so}L = 0.3$ (blue), 1 (red), 2 (orange), 3 (green).

k_{so}: $k_{so}L = 0.3$, 1, 2 and 3. We deliberately show a small energy value range to clarify the differences. Even though our approximation, in principle, requires $k_{so}L \ll \pi$, we see that up to $k_{so}L = 1$, our theory still gives quantitative agreement with the full numerical results, as can be seen in Fig. 4.8 (red curve). Secondly, we calculate the AC spin current by incorporating the effect of the AC bias voltage in the system in Eq. (4.28). First, we check the admittance for particular frequencies to see when the dynamic properties of the conductance become nonnegligible. We choose the same cavity in Fig. 4.1 for a spinless system (only kinetic term) and calculate the DC conductance ($\Omega = 0$) and AC conductance using Eq. (4.34) where $\Omega\tau \approx 0.1, 0.3, 0.6$ and 1. As shown in Fig. 4.9, our adiabatic assumption for calculating the time-dependent current with DC conductance holds where $\Omega\tau \ll 1$. However, as $\Omega\tau$ approaches 1, the frequency dependency of the conductance becomes significant. Therefore we should obtain the current from Eqs. (4.37) and (4.34). We compare our analytical prediction with the numerical Floquet results (4.2) and (4.3) for a range of frequencies. We can neglect the frequency dependence of the conductance in Eq. (4.34) in the low-frequency regime where $\Omega\tau < 1$. We then use Eq. (4.32) to obtain our prediction and show that the result agrees well with the Floquet result as shown in Fig. 4.10 in panels a) and b). We note that the spin current is in the nano-Ampere range where the corresponding frequencies $\Omega/2\pi$ are approximately between 10 and 100 GHz. In the high-frequency regime where $\Omega\tau > 1$, AC spin current is calculated by incorporating the effect of the AC bias voltage and the admittance in Eq. (4.34). That is, we use
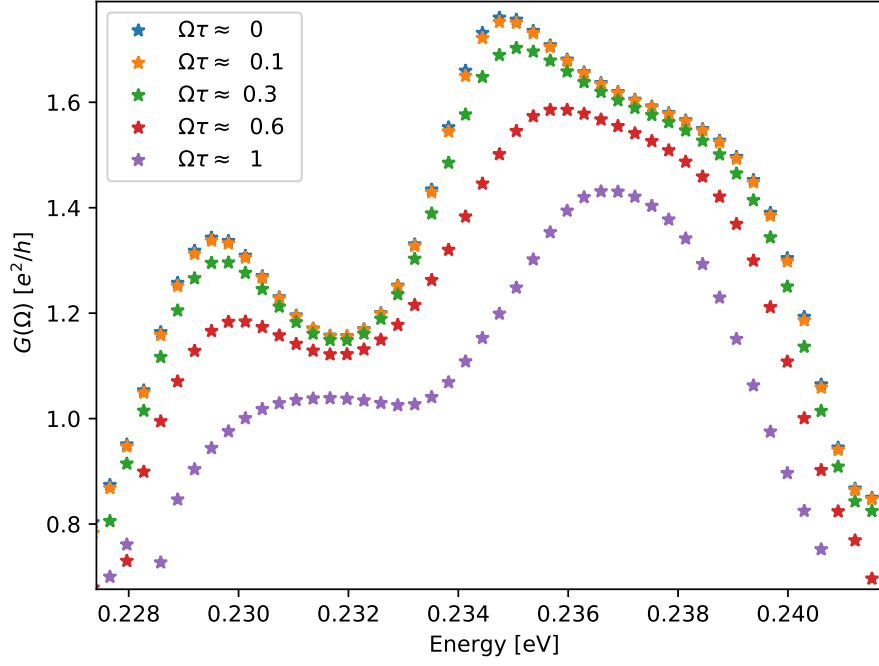
Figure 4.9: AC conductance for frequencies $\Omega\tau \approx 0.1(a), 0.3(b), 0.6(c)$ and $1(d)$. We consider a small range of energies to make the differences visible.

Eqs. (4.37) and (4.38). We find reasonable agreement for the higher frequencies up to $\Omega\tau \approx 3$; see Fig. 4.10. The frequencies $\Omega/2\pi$ corresponding to those in panels c),d) and e) of Fig. 4.10 are 330, 700 GHz and 1 THz, respectively. These numbers are within experimental reach. Notably, in this high-frequency regime, we can generate spin currents up to 250 nano-Amperes using geometry with a length scale of about 100 nm.
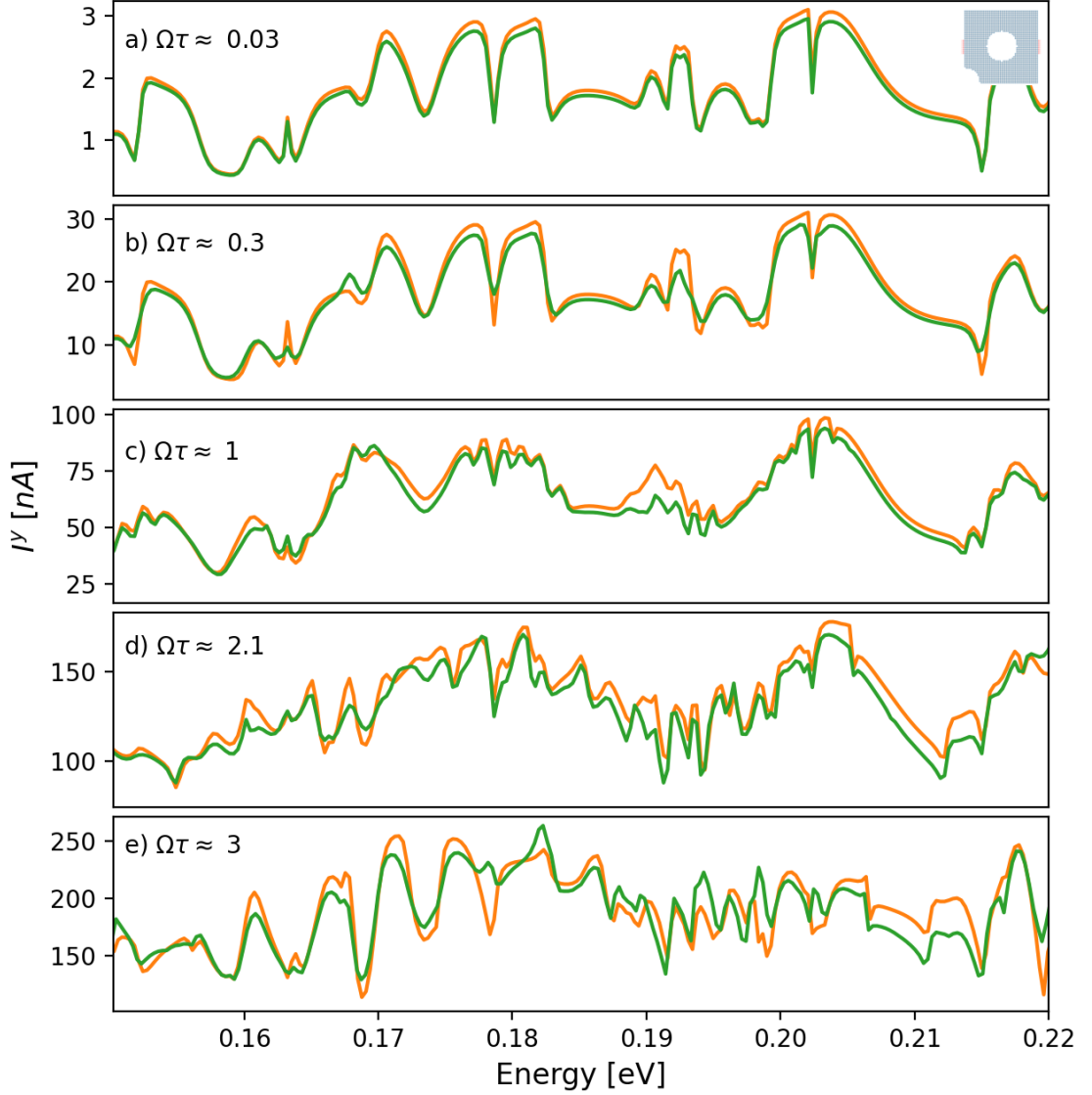
Figure 4.10: AC spin currents induced by the time-dependent Rashba SOI without a bias voltage. The numerical Floquet results (green) are compared to the spin current in the y direction with the time-dependent spin voltage (orange), which are calculated using Eq. (4.32) in the low-frequency regime in panels a) and b) and by Eq. (4.38) in the high-frequency regime in panels c), d) and e). The system size is $L = 50a$ and the Rashba SOI is $\alpha_R(t) = k_{so}\sin(\Omega t)$ with $k_{so}L = 1$. The frequency values are indicated at the top left corner of each panel, $\Omega\tau \approx 0.03, 0.3, 1, 2.1$ and 3 in panels a) and b), etc., respectively. The system geometry is shown in the top right inset.

4.3.4 Adiabatic approximation versus analytical results

This section compares our analytical results with the adiabatic approximation of the Floquet scattering matrix. We use the frozen scattering matrix in Eq. (4.4) to obtain the adiabatic approximation. In Fig. 4.11, we choose the Rashba coupling constant $k_{so}L = 0.01$ to obtain better agreement for our analytical result, and the driving frequency in the high-frequency regime, *i.e.*, $\Omega\tau \approx 1.5$ corresponding to a driving frequency $\Omega/2\pi$ of approximately 500 GHz. The adiabatic approximation is expected to fail beyond frequencies
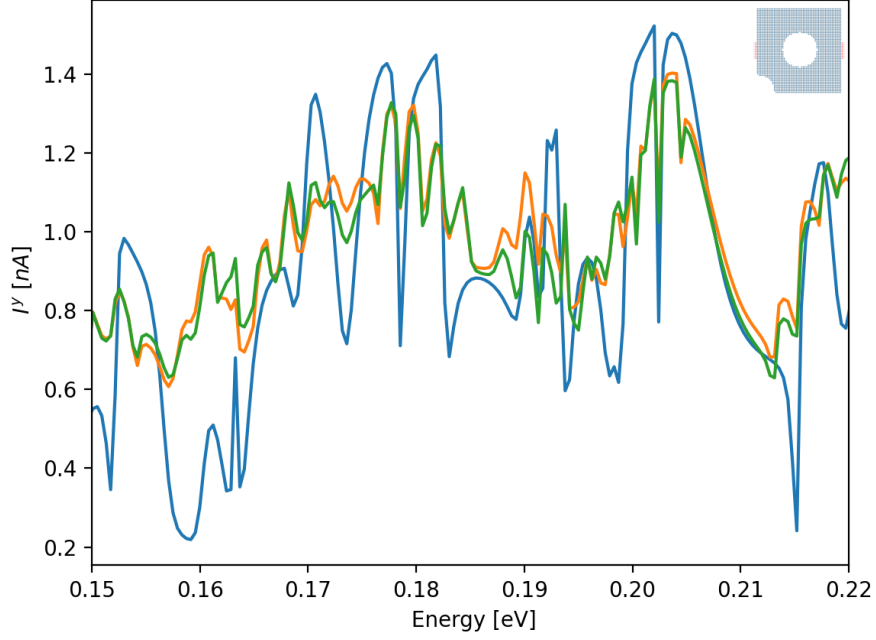
Figure 4.11: AC spin currents induced by the time-dependent Rashba SOI without a bias voltage. In the high-frequency regime, the numerical Floquet results (green) are compared to the adiabatic approximation (blue), and the spin current in the y-direction calculated from the time-dependent spin voltage, Eq. (4.38) (orange). The system size is $L = 50a$, and the Rashba SOI is $\alpha_R(t) = k_{so}\sin(\Omega t)$ with $k_{so}L = 0.01$ and $\Omega\tau \approx 1.5$.

around $\Omega\tau \approx 1$. Indeed, Fig. 4.11 shows that the adiabatic approximation breaks down at high frequencies while our prediction (4.38) still shows good agreement with the numerical Floquet result. We note that in addition to having a much wider range of validity, the computation of our analytical result is much easier and takes much less computing time compared to the frozen scattering matrix approximation.

4.4 High Harmonic Generation via Time Dependent Rashba SOI

This section investigates the high harmonic generation (HHG) of spin and charge current generated by the time-dependent Rashba SOI. First, we analyze how the symmetry prop-

erties of the system affect the generation of high harmonics spin and charge currents. Then we show that our numerical results conform with the theory based on these symmetries.

4.4.1 Symmetry Properties Of the System For HHG

Symmetry properties of the system determine which higher harmonics yield a non-vanishing contribution to spin and charge currents. In particular, one can show that if the system possesses a particular discrete symmetry, that is, if the Hamiltonian is invariant under a discrete symmetry that involves the translation of time by half-period, then either odd or even harmonics will yield a non-vanishing contribution to a given current. We follow the references [51, 52] to investigate the implications of symmetries in our system, which will be obtained from the selection rules of a higher harmonic contribution [53]. Suppose that the Hamiltonian is invariant under the transformation,

$$\hat{h} H(\mathbf{k}, t) \hat{h}^{-1} \equiv H(\mathbf{k}, t)$$

Then the selection rule for the n-harmonic contribution to an operator $O(\mathbf{k}, t)$ is

$$\hat{h} O(\mathbf{k}, t) e^{in\Omega t} \hat{h}^{-1} \equiv O(\mathbf{k}, t) e^{in\Omega t} \,. \tag{4.39}$$

This operator can be for instance the velocity operator $v_j(k, t) = \frac{\partial}{\partial k_j} H(k, t)$ or the spin current operator [54]

$$\mathcal{V}_{ij}(\mathbf{k}, t) = \frac{1}{2}[\sigma_i v_j(\mathbf{k}, t) - v_j(\mathbf{k}, t)\sigma_i] \,. \tag{4.40}$$

Here i refers to the direction of the electron's spin which moves along the j direction. The Hamiltonian of our system in Eq. 6.1 is invariant under the transformation:

$$(\sigma_x, \sigma_y) \to (-\sigma_x, -\sigma_y), \qquad t \to t + T/2 \,. \tag{4.41}$$

On the other hand, using the relations above, components of the spin current operators are

$$\mathcal{V}_{xx}(\mathbf{k}, t) = \sigma^x (k_x/m + k_{so}\sin(\Omega t)\sigma^y) - (k_x/m + k_{so}\sin(\Omega t)\sigma^y)\sigma^x \tag{4.42}$$

$$\mathcal{V}_{yx}(\mathbf{k}, t) = \sigma^y (k_x/m + k_{so}\sin(\Omega t)\sigma^y) - (k_x/m + k_{so}\sin(\Omega t)\sigma^y)\sigma^y \tag{4.43}$$

$$\mathcal{V}_{zx}(\mathbf{k}, t) = \sigma^z (k_x/m + k_{so}\sin(\Omega t)\sigma^y) - (k_x/m + k_{so}\sin(\Omega t)\sigma^y)\sigma^z \,, \tag{4.44}$$

where we used

$$v_x(k, t) = k_x/m + k_{so}\sin(\Omega t)\sigma^y \,. \tag{4.45}$$

Clearly $\mathcal{V}_{xx}(\mathbf{k}, t)$ and $\mathcal{V}_{yx}(\mathbf{k}, t)$ are odd under the symmetry (4.41) above, whereas $v_x(k, t)$ and $\mathcal{V}_{zx}(\mathbf{k}, t)$ is even. Then (4.39) implies that

$$- \mathcal{V}_{xx}(\mathbf{k}, t)e^{in\Omega(t+\frac{T}{2})} = \mathcal{V}_{xx}(\mathbf{k}, t)e^{in\Omega t} \qquad - \mathcal{V}_{yx}(\mathbf{k}, t)e^{in\Omega(t+\frac{T}{2})} = \mathcal{V}_{yx}(\mathbf{k}, t)e^{in\Omega t},$$
(4.46)

which can only hold for n odd and

$$\mathcal{V}_{zx}(\mathbf{k}, t)e^{in\Omega(t+\frac{T}{2})} = \mathcal{V}_{zx}(\mathbf{k}, t)e^{in\Omega t}, \qquad v_x(k, t)e^{in\Omega(t+\frac{T}{2})} = v_x(k, t)e^{in\Omega t}, \quad (4.47)$$

which can only hold for n even. Therefore we conclude that only odd harmonics contribute to the spin currents in the x and y direction, and only even harmonics contribute to the spin in the z-direction and charge current.

4.4.2 Numerical results for HHG of spin and charge currents

We also numerically calculate the HHG of the spin and charge current by the time-dependent Rashba SOI. We consider the chaotic ballistic system connected to the two leads as in the section 4.1.1 with the parameters Rashba SOI $\alpha(t) = k_{so} \sin(\Omega t)$, $k_{so}L = 1$ and $\Omega \tau \approx 1$. We calculate high harmonic currents up to $l = 5$ using Eq. 4.3. We find that spin currents in the x and y directions receive contributions from odd harmonics and spin current in the z-direction and charge current receive contributions from the even ones, as expected from theory. We show the spin current in the y and z directions as a function of the Fermi energy. As shown in Fig.4.12, the first harmonic term is the order of magnitude higher than higher harmonics contributions.

4.5 Conclusion

In this chapter, we investigated the AC spin current generated by periodically time-dependent Rashba SOI in the absence of bias voltage. Furthermore, we showed that time-dependent Rashba coupling could be formulated as spin electric fields with opposite directions for up and down spins. Then, we obtain the AC spin current directly from the net spin voltage using charge conductance. This conversion of the spin current into an electric field renders spin currents experimentally measurable. To check the accuracy of this conversion, we obtain numerical results in both adiabatic and high-frequency regimes. We show a good agreement between two currents with the range of the experimentally relevant parameters. In conclusion, we find that the Rashba coupling can create a spin current and that the vivid picture of a spin-dependent potential (with the charge conduction G) works well in the right parameter regime compared to calculating the AC spin current directly.
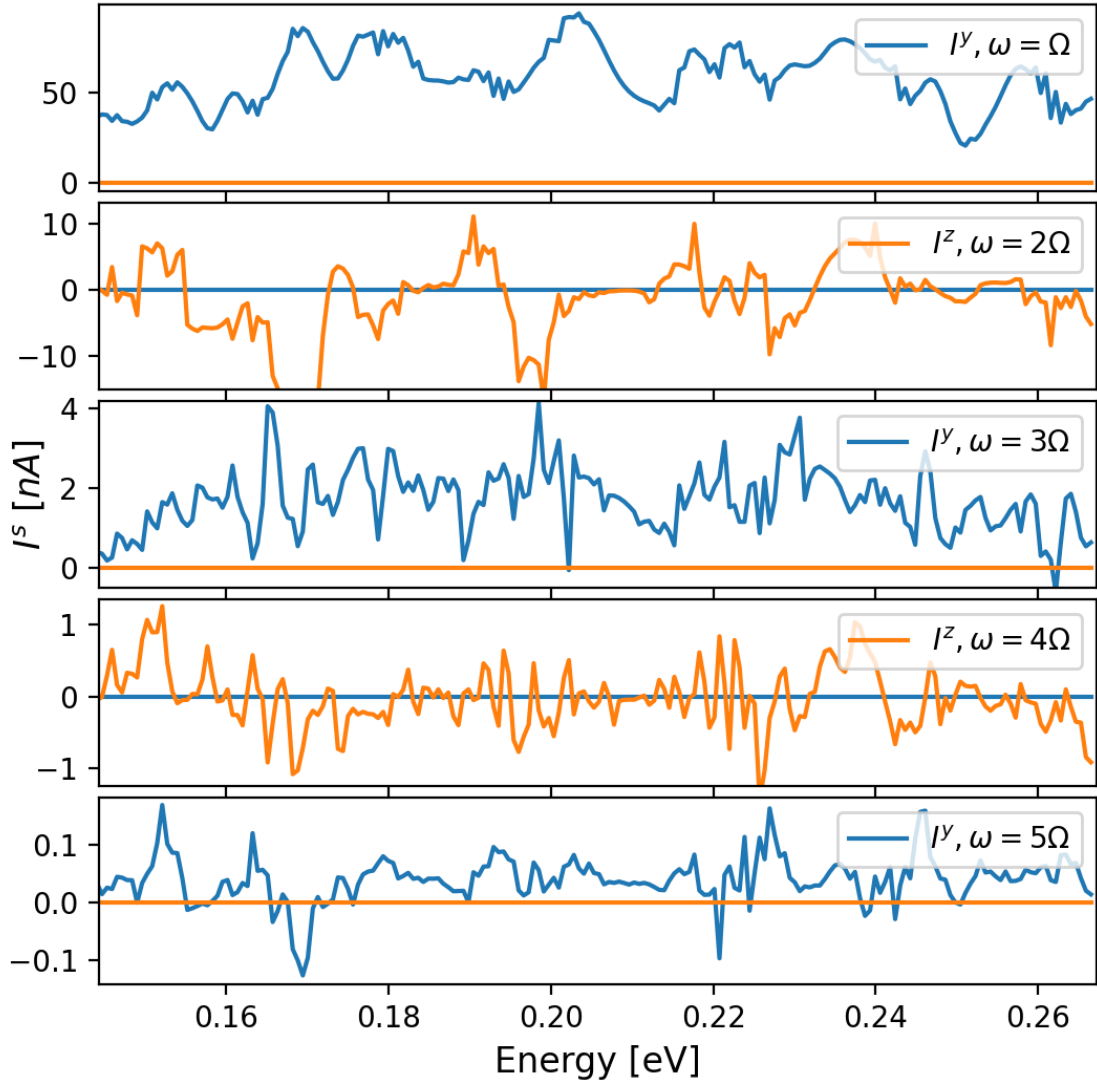
Figure 4.12: Higher harmonics of the induced spin currents in y (blue) and z (orange) direction due to the Rashba SOI ($\alpha(t) = k_{so}\sin(\Omega t)$). The currents for $k_{so} = 1/L$ and, where L is the system size in the x-direction. The frequency is chosen so that $\Omega\tau \approx 1$, where τ is the time of flight.

Chapter 5

DYNAMICAL SPIN TRANSISTOR

Following the theoretical proposal for a spin field-effect transistor by Datta and Das in 1990. [55], much research has focused on the realization of spin-based transistors that might eventually be more efficient and faster compared to the present transistors based on charge transport. The central issue for spin-based transistors is a realization of efficient generation, manipulation, and detection schemes for spin currents and spin accumulations. While conventional means of doing this involve ferromagnetic structures [2], these steps could also be achieved via all-electrical means, hence bypassing the need for magnetic components, using the spin-orbit interaction (SOI). The proposals that are based on exploiting phenomena of current-induced spin accumulation [56] and spin Hall effect – the generation of spin currents transverse to an applied electric field [57] – have become the most commonly employed lines of study to achieve this goal.

The SOI can be induced by electric fields of either charge impurities or the crystal lattice. In the latter case, one speaks of an "intrinsic" SOI. Prominent examples are Rashba- and Dresselhaus-type SOI in semiconductor quantum wells [43]. While Dresselhaus SOI arises from a crystal's lack of inversion center, the Rashba term arises in low-dimensional systems, and it is induced by inversion symmetry breaking generated by the confining electric field of a quantum well. Because this electric field can be tuned by top or back gates, as established in two-dimensional electron gases (2DEGs) over 20 years ago [5], it is possible to modulate the Rashba SOI both spatially and, in principle, temporally. A spatial variation can generate a spin-dependent force [58], and a temporally oscillating SOI may be capable of inducing charge and spin currents in the absence of any bias voltage [59–61]. Such physics is most conveniently handled by rewriting the SOI in terms of non-Abelian gauge fields [45, 62, 63].

Among other things, such an approach allows one to directly identify spin-electric and

spin-magnetic fields [44, 59, 64–66]. These fields accelerate electrons longitudinally or sideways à la Lorentz, respectively, but their sign depends on the electronic spin – opposite spin species are accelerated and bent in opposite directions. While these fields may exist in the presence of time-independent and homogeneous spin-orbit (and Zeeman) interaction, additional components appear when the SOI is time- and space-dependent [44, 64, 65].

In this chapter, we exploit time- and space-tunability of Rashba SOI to explore how the non-Abelian (spin) gauge fields induce spin transport. We note from the outset that the effect of driven or position dependent Rashba SOI has been studied in different contexts ranging from diffusive systems [65, 67] to ballistic quantum rings [68], to 1D electron gases [69, 70] and graphene [71–73]. However, usual Onsager reciprocal relations valid for spin transport [66, 74, 75] become more restrictive in the presence of a non-Abelian gauge structure such as induced by the space- and time-dependent Rashba interaction. Here we will explore the consequences of these "hidden" Onsager relations recently established for spin and charge transport in 2DEGs [44]. As a demonstration, we will devise a multiterminal mesoscopic spin transistor, whose working principle builds upon the "hidden" Onsager relations [44]. While the transistor operates on pure spin currents, the output signal is a charge signal which can be detected by simple experimental procedures. The spin transistor setting, combining time-dependent and spatially-inhomogeneous SOI, is shown schematically in Fig. 5.1: The AC-modulated Rashba SOI on the right injects a pure spin current into the left region. The latter is then converted into a charge signal by a spin magnetic field, induced by a static but non-homogeneous Rashba SOI, and read out as a voltage V_{out} between contacts 1 and 3.
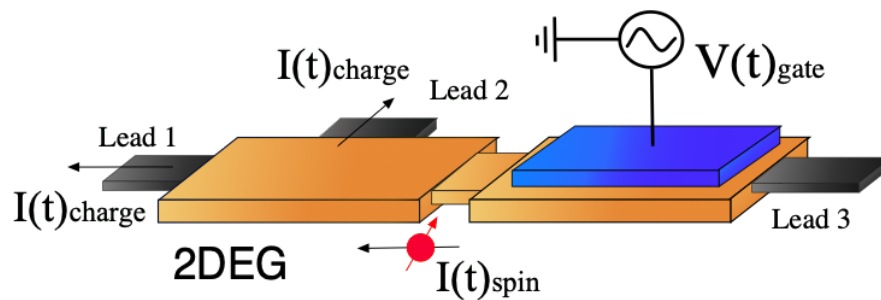
Figure 5.1: Sketch of a dynamical spin transistor. The on/off state of the spin transistor can be controlled by connecting a third terminal (Lead 2). An AC top gate voltage generates spin current on the right part of the device and injects it through the middle bridge. It is converted to nonzero charge current on the left part in the multiterminal system via spatially inhomogeneous Rashba interaction. Owing to the hidden Onsager relations, the spin to charge conversion vanishes to leading order in the spin-orbit coupling in a two-terminal system.

Our gauge field analytics based on Ref.[44] allows us to approximately express the desired

spin-dependent quantities (such as time-dependent spin currents, AC spin conductances) in terms of conventional charge transport quantities (such as time-dependent charge currents, impedances), and to make general predictions for expected output signals, by making use of the Onsager relations.

This chapter is organized as follows. We first rewrite the gauge transformation in the presence of the spatially inhomogeneous Rashba coupling. We then show how such spin signals can be non-locally converted into charge by the non-homogeneous but static Rashba SOI within a second mesoscopic cavity. This combined functionality is integrated and tested for a dynamical SOI-based spin transistor. Finally, we present our results in both adiabatic and high-frequency regimes.

5.1 Spin Magnetic Field from Spatially Inhomogeneous SOI

5.1.1 Gauge transformation for spatially inhomogeneous SOI

A spatially inhomogeneous Rashba SOI constant $\alpha_R(\mathbf{x}) = k_{so}\bar{\alpha}_R(\mathbf{x})$, with $\bar{\alpha}_R$ being a dimensionless function, can create or convert spin currents into charge currents; see Fig. 5.1. This interconversion is achieved by the spin-dependent Lorentz force due to a "spin" magnetic field [44, 46]

$$\mathcal{B}^a = \partial_x A_y^a(\mathbf{x}) - \partial_y A_x^a(\mathbf{x}) \tag{5.1}$$

where $A_\mu^a(\mathbf{x}) = \bar{\alpha}_R(\mathbf{x})\epsilon_\mu^a$. Below we specialize in the case

$$A_\mu^a = k_{so}\alpha_0(\mathbf{x} \cdot \mathbf{f})\epsilon_\mu^a, \tag{5.2}$$

where $\mathbf{f}$ is a unit vector determining the fixed direction of the gradient of $\bar{\alpha}_R$. We now use the following generic decomposition for each spin component

$$A_\mu^a = -(\partial_\mu \chi^a + \epsilon_{\mu\nu}\partial_\nu \phi^a) \tag{5.3}$$

and perform an $SU(2)$ gauge transformation

$$U = \exp\left(ik_{so}\,\chi^a\sigma^a/2\right), \tag{5.4}$$

taking into account terms up to linear order in k_{so}. The vector potential then becomes

$$(A')_\mu^a = \epsilon_{\mu\nu}\,\partial_\nu\,\phi^a, \tag{5.5}$$

$$(V')^a = V. \tag{5.6}$$

The transformed Hamiltonian becomes, up to linear order in the spin-orbit coupling,

$$H' = -\frac{1}{2m}[\partial_\mu + i\frac{k_{so}}{2}\epsilon_{\mu\nu}\partial_\nu\varphi(\mathbf{x})\sigma\cdot\mathbf{f}]^2 + V(\mathbf{x}) \tag{5.7}$$

where $\phi^a = \varphi(\mathbf{x})f^a$. We now perform a global spin rotation $\sigma\cdot\mathbf{f} \to \sigma^z$ to obtain

$$H_d = \frac{1}{2m}(\mathbf{p} + ik_{so}\mathbf{a}\,\sigma^z)^2 + V(\mathbf{x}), \tag{5.8}$$

where $\mathbf{a} = \alpha_0(\hat{\mathbf{z}} \times \mathbf{x})/2$. Hence the Hamiltonian structure implies that the two spin species decouple, where each one subject to a homogeneous magnetic field (as well as Lorentz force) of opposite sign. The strength of this magnetic field is given by $\sum_a \mathcal{B}^a f^a$, in agreement with Eq. (5.2).

5.1.2 Link between spin and charge conductance via gauge transformation

We now use the gauge transformations discussed in Sec. 5.1 to get the spin conductances in an alternative way. After the gauge transformation and working up to linear order in k_{so}, the full Hamiltonian is block-diagonalized into spin blocks. The time-dependent part of the SOI transforms into spin-dependent electric fields, which we treat as spin-dependent voltages $V^a = V^\uparrow - V^\downarrow$ (see Section 4.3.1). The spatially inhomogeneous part of the SOI enters as a spin-dependent magnetic field, as shown in Eq. (5.8). Owing to the block diagonal structure, the spin conductance in the transformed basis is simply

$$G_{ij}^a = G_{ij}^\uparrow - G_{ij}^\downarrow. \tag{5.9}$$

We now transform back to the initial gauge to obtain the spin-conductances in the original spin basis:

$$G_{ij}^a \approx [G_{ij}(\mathcal{B}_z^a) - G_{ij}(-\mathcal{B}_z^a)]\,f^a. \tag{5.10}$$

Here $G_{ij}(\mathcal{B}_z^a)$ is the charge conductance of a spinless electron moving in the same scalar potential V (including confinement and disorder) as the original electron, but in the presence of an additional induced magnetic field $\mathcal{B}_z^a$ given in Eq. (5.2). Thus the gauge transformation allows us to express the mesoscopic spin conductances in terms of charge con-

ductances. Recall that under the assumption $L \ll l_{so}$ where $l_{so} = \pi/|k_{so}|$, the spin precession conductance $G^{ab} \propto \delta^{ab} G^{00}$.

Using Onsager relations [76] $G_{ij}(\mathcal{B}_z^a) = G_{ji}(-\mathcal{B}_z^a)$ and current conservation, one can show that G_{ij}^a in Eq. (5.10) vanishes in a system with two connected leads in the presence of time-reversal symmetry. On the other hand, breaking the time-reversal symmetry, e.g., via an applied magnetic field or connecting the third terminal to the system [44] results in nonzero conductance.

We compute below the driven charge and spin currents without resorting to the approximate $SU(2)$ manipulations described here and in Sec. 4.2.1. Using these numerics as reference calculations, we will be able to show that the description in terms of spin-electric and spin-magnetic fields acting on effectively decoupled ↑↓-electrons is very accurate up to $L \sim l_{so}$ although Eq.(5.10) is valid formally for small k_{so}.

5.2 Charge Signal from a Spin Current

5.2.1 Dynamical SOI-based spin transistor setting

This section discusses detecting the AC spin current generated by the spin potential induced through a time-dependent SOI. Usually, this can be achieved with a device with nonzero spin (detection) conductance. While the conventional means of detecting spin currents are based on ferromagnetic leads, here we will exploit the SU(2) gauge structure of the Rashba SOI to further design a device with a nonzero spin magnetic field. The latter can then convert spin currents into charge signals.

Spin (detection) conductance in Eq. (4.27) is converted into the difference of two charge magneto-conductances according to Eq. (5.10). Then an Onsager relation implies that the total charge conductance vanishes in the presence of time-reversal symmetry. On the other hand, breaking time-reversal symmetry, e.g. via an applied magnetic field or connecting the third terminal to the system [44] results in a nonzero charge conductance and an AC charge current. As a result, we can obtain the on/off states of this dynamical spin transistor by controlling the symmetry properties of the system. Below we will take the latter route, connecting to the third terminal..

To explore how this conversion works in detail, we consider a system that consists of two subsystems containing a spatially inhomogeneous and a time-dependent Rashba SOI, respectively, as shown in Fig. 5.2. The right subsystem consists of a 2D quantum wire
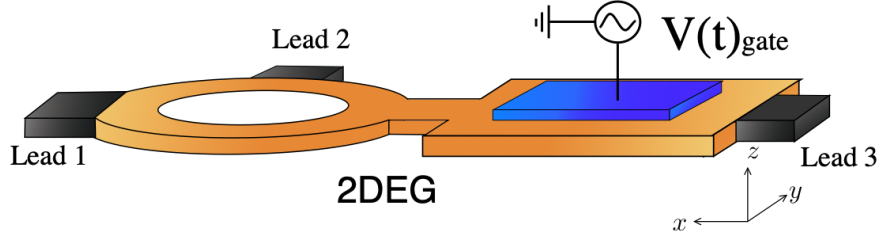
Figure 5.2: Setup of the dynamical spin-orbit based spin transistor with the top terminal (Lead 2) controlled electrostatically. The AC gate voltage in the right cavity induces a dynamical Rashba SOI, which creates an AC spin current that flows into the left cavity. Due to a spatially inhomogeneous Rashba SOI, the spin current is transformed into a nonzero charge current in the multiterminal system. The charge current vanishes in the two-terminal system.

(with length L and width W) with a time-dependent SOI $\alpha_R(t) = k_{so}\sin(\Omega t)$ engineered by an AC gate voltage. The left subsystem contains a ballistic ring (with diameter L) with a spatially inhomogeneous SOI $\alpha_R(\mathbf{x}) = k_{so}(L-y)/L$. This way, spin currents generated in the right subsystem via a spin electric field are converted into charge currents via a spin magnetic field in the left subsystem.

5.2.2   AC charge signal in the low-frequency regime

The charge current without a bias voltage V follows from Eq. (4.27) as

$$I_1 = -\sum_{j,b} G_{1j}^{0b} V_j^b, \tag{5.11}$$

where 1 indicates the lead number and $b = x, y, z$ is the spin direction. We express the spin conductance in terms of the charge magneto-conductance (5.10). In the low-frequency regime, we again neglect the frequency dependence of the conductance. Then the charge current in the lead i reads

$$I_1 \approx -\sum_b \sum_j (G_{1j}(\mathcal{B}^b) - G_{1j}(-\mathcal{B}^b)) f^b V_j^b. \tag{5.12}$$

For spatially inhomogeneous SOI $\alpha_R(\mathbf{x}) = k_{so}(L-y)/L$ we obtain from Eq. (5.2) the spin magnetic field components $\mathcal{B}_z^a$ in the x- and y-directions as

$$\mathcal{B}^x = -\partial_x \alpha_R(\mathbf{x}) f^x,$$
$$\mathcal{B}^y = -\partial_y \alpha_R(\mathbf{x}) f^y. \tag{5.13}$$

The spin voltages generated by the time-dependent SOI $\alpha_R(t) = k_{so}\sin(\Omega t)$ are obtained from Eq. (4.16) as

$$V^y_{1(3)} = V^\uparrow_{1(3)} - V^\downarrow_{1(3)} = \pm\partial_t\alpha_R(t)L\,. \tag{5.14}$$

We now have all the ingredients to calculate the charge current in the lead 1. We obtain

$$I_1(t) = G_s\partial_t\alpha_R(t)L\,, \tag{5.15}$$

where

$$G_s = -G_{11}(\mathcal{B}^y) + G_{11}(-\mathcal{B}^y) + G_{13}(\mathcal{B}^y) - G_{13}(-\mathcal{B}^y)\,. \tag{5.16}$$

This equation formulates our further prediction that the spin current can be converted into a charge current in a spatially inhomogeneous system through a spin magnetic field.

5.2.3 AC charge signal in the high-frequency regime

As explained in Section 4.3.2.2, we should retain the AC conductance's frequency dependence at high frequency. We follow the same steps as in Section 4.3.2.2 and rewrite the AC charge current expression (5.12), but retaining the frequency dependence given in Eq. (4.34), as

$$I_1(\omega) \approx -\sum_b\sum_j[G_{1j}(\omega,\mathcal{B}^b) - G_{1j}(\omega,-\mathcal{B}^b)]f^bV(\omega)^b_j\,, \tag{5.17}$$

where the spin-dependent magnetic field is $\mathcal{B}^y = k_{so}L^{-1}f^y$ and the spin voltage is $V^{\uparrow(\downarrow)}(\omega) = \pm i\omega\alpha(\omega)\,L$. This equation constitutes our main result for the spin (detection) conductance, which applies to both high- and low-frequency regimes.

5.2.4 Numerical calculations for conductance and admittance

Before using Eq. (5.10) for the numerical calculations of current in our actual model, we first show its validity in a chaotic ballistic system, shown on the right part of Fig. 5.3. In the presence of time-reversal symmetry, the conductance vanishes in a two-lead system, as shown in the top figure in Fig. 5.3.

$$G_{ij}(\mathcal{B}^a_z) - G_{ij}(-\mathcal{B}^a_z) \approx 0 \tag{5.18}$$

When we break this symmetry by applying an external magnetic field, the conductance
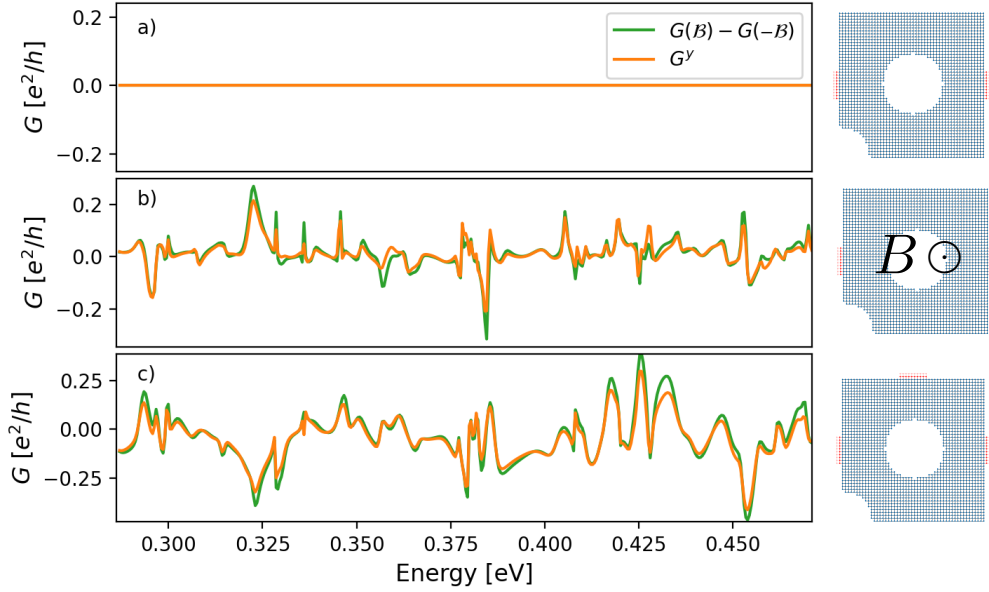
Figure 5.3: Numerical check of Eq. (5.10) for the conductance. a) Vanishing conductance in a two-lead system with time-reversal symmetry, b) two-lead system with an applied magnetic field, c) three-lead system.

becomes

$$G_{ij}(B + \mathcal{B}^a_z) - G_{ij}(B - \mathcal{B}^a_z) \neq 0 \,. \tag{5.19}$$

Another way to make the right-hand side of (5.18) is to connect a third terminal to the system. The current conservation between the first two leads is broken in this case. Hence one has $G_{ij} \neq G_{ji}$. That again leads to a non-vanishing result for the conductance. We showed that Eq. (5.10) is valid in all these cases, for $k_{so}L = 1$ with $L = 50a$. We then explore the frequency dependence of Eq. (5.10) by checking its validity for $\omega\tau = 0$ and $\omega\tau = 1$ on the chaotic system with the third terminal (shown on the right part of Fig. 5.3 c)) where position dependent Rashba coupling is $\alpha_R(\mathbf{x}) = k_{so}(L - y)/L$ with $k_{so}L = 1$, as seen in Fig. 5.4.

5.2.5 Simulating the dynamical spin-transistor functionality

We performed numerical transport simulations of the spin transistor in Fig. 5.2 and explored the range of validity of our analytical result (5.17). We choose time-dependent Rashba SOI to be $\alpha_R(t) = k_{so}\sin(\Omega t)$ and the spatially inhomogeneous Rashba SOI to be $\alpha_R(\mathbf{x}) = k_{so}(L - y)/L$, where the Rashba SOI constant is selected such that $k_{so}L = 1$, where L is the system size along the x direction for the right subsystem. The shape of the system is shown in the top right corner of Fig. 5.2. The right part is a 2D wire with length $L = 50a$, width $W = 30a$, and one connected lead of width $10a$. The left part is a ballistic ring with an inner radius of $10a$, an outer radius of $25a$, and two connected leads
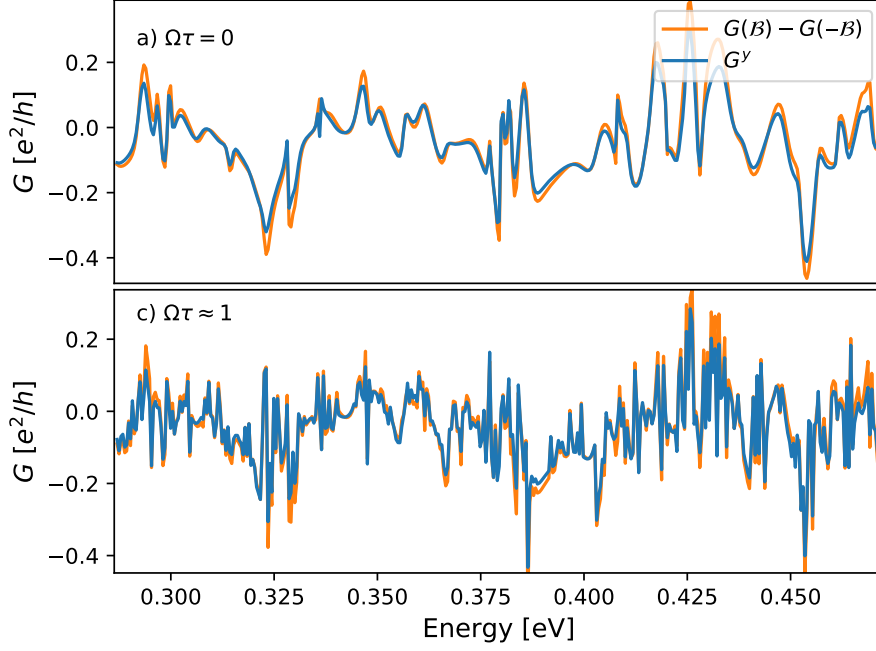
Figure 5.4: Comparison of the two sides of Eq. (5.10) for two different frequency choices a) $\Omega\tau = 0$ and b) $\Omega\tau \approx 1$

of width $10a$. The two parts are connected via a bridge of width $10a$ made of the same material.

We consider 3 open channels and choose the Fermi energy between 0.29 and 0.47 eV. After computing the dwell time to specify the range of the frequency, we calculate the AC charge currents $I(t) = I\cos(\Omega t)$ in the absence of the bias voltage on the left using the Floquet scattering matrix given in Eq. (4.2) and Eq. (4.3). Finally, we compare the Floquet result for AC charge current with our analytical prediction both in the low and the high-frequency regimes. Our analytical results are obtained from Eq. (5.16) for $\Omega\tau \approx 0.1$, 0.3 and shown in Fig. 5.5 $a)$ and $b)$. Here, the frequencies $\Omega/2\pi$ are approximately 40 and 120 GHz. We find excellent agreement between our analytical results and the numerically obtained AC charge current. Moreover, even in the low-frequency regime, we see that the mechanism produces few-nA charge currents that are experimentally observable.

For higher frequencies where $\Omega > 1/\tau$, we compare our prediction based on Eq. (5.17) with the numerical dynamical conductance using driving frequencies $\Omega\tau \approx 1$, 1.5, and 2.1. These values correspond to $\Omega/2\pi$ being approximately 400, 600, and 840 GHz. In Fig. 5.5 $c)$, $d)$, $e)$, we also observe on the whole a fairly good match between the two currents in the high-frequency regime up to $\Omega\tau \approx 2.1$.

In Fig. 5.6, we show the on/off signals of the dynamical spin transistor. We compute the AC charge currents in these plots using the Floquet scattering matrix. Hidden Onsager relations for the two terminal devices ensure that the spin/charge conversion is suppressed.
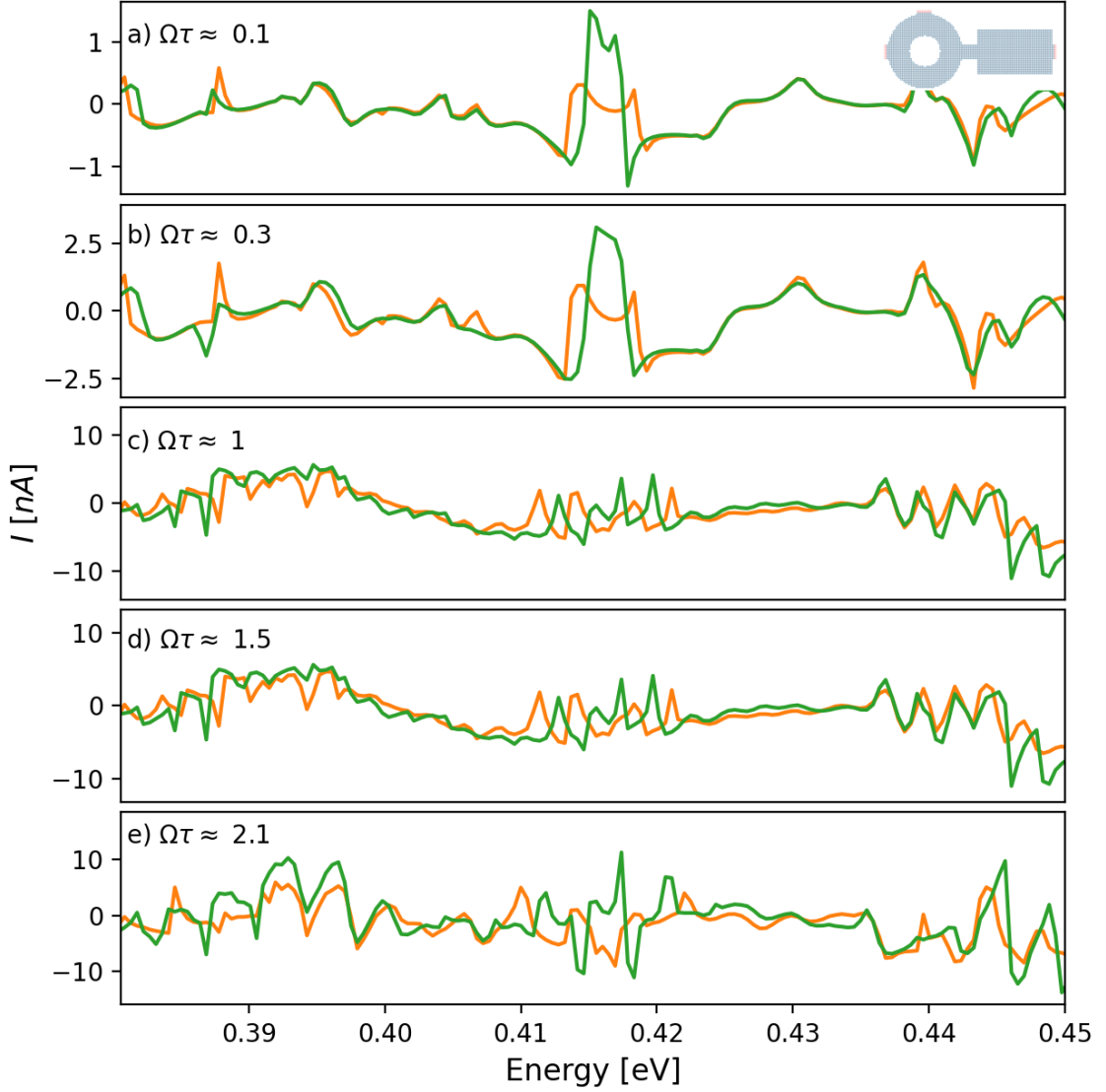
Figure 5.5: Dynamical spin transistor function: AC charge current in Lead 1, see Fig. 5.2, generated by the time-dependent and spatially inhomogeneous Rashba SOI. Numerical results based on the Floquet formalism (green) are compared to the current generated by the spin-dependent voltage and pseudo-magnetic field (orange) in the low- and high-frequency regime. The analytical results in a) and b) are calculated based on Eq. (5.16) and in panels c) to e) using Eq. (5.17). The dynamical Rashba SOI in the right half system is $\alpha_R(t) = k_{so}\sin(\Omega t)$ with $k_{so}L = 1$ and the spatially inhomogeneous Rashba SOI in the left half system (the ring) is $\alpha_R(\mathbf{x}) = k_{so}(L - y)/L$. The size of each system part is $L = 50a$. The frequencies used are $\Omega\tau \approx 0.1, 0.3, 1, 1.5$ and 2.1 from top to bottom panel.

This is the off state of the spin transistor. Connecting to a third terminal to the system results in a non-zero charge current, as seen from Fig. 5.6. It is the on state of the spin transistor.
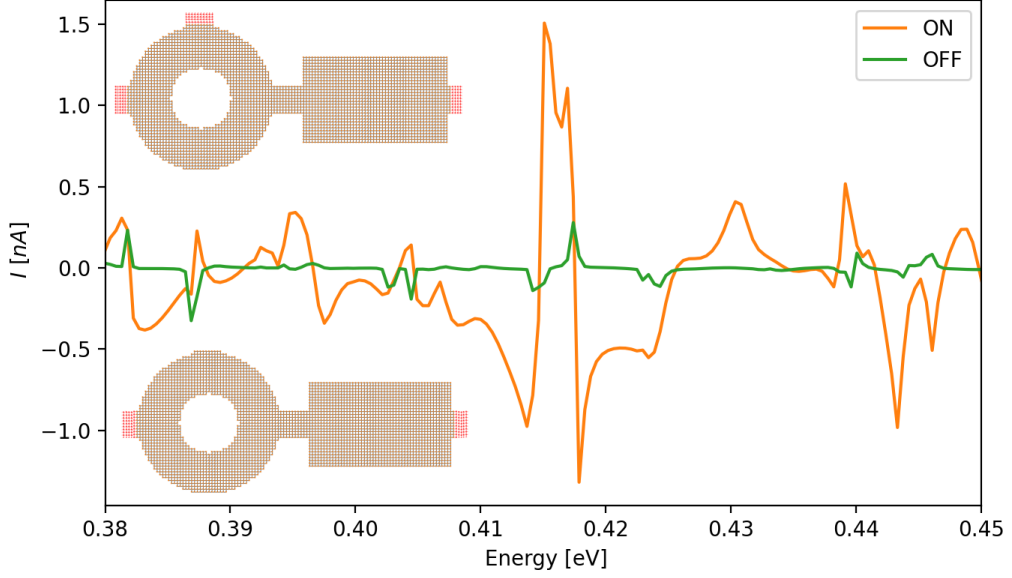
Figure 5.6: Demonstration of the on/off states of a dynamical spin transistor. AC charge currents in Lead 1 as a function of the Fermi energy, generated by time-dependent and spatially inhomogeneous Rashba SOI, are plotted. Numerical results based on the Floquet formalism. The charge current is calculated for both two-lead (inset below) and three-lead (inset above) systems. The dynamical Rashba SOI in the right half system is $\alpha_R(t) = k_{so} \sin(\Omega t)$ with $k_{so}L = 1$ and the spatially inhomogeneous Rashba SOI in the left half system (the ring) is $\alpha_R(\mathbf{x}) = k_{so}(L - y)/L$. The size of each system part is $L = 50a$ and the driving frequency is $\Omega\tau \approx 0.1$.

5.3 Conclusion

In this chapter, we investigated 2DEGs consisting of two parts, one with the time-dependent Rashba SOI and another with the spatially inhomogeneous Rashba SOI. After an appropriate gauge transformation, the time-dependent part of Rashba coupling transforms into a spin-dependent voltage, which generates a spin current without a bias voltage. Moreover, for the spatially inhomogeneous part of Rashba SOI, a similar gauge transformation converts the spin conductance to charge magnetoconductance that is measurable experimentally. Therefore the time-dependent Rashba SOI generates a spin current, which is then detected as a charge current in the company of inhomogeneous Rashba SOI. We also show that this charge current vanishes in the two-terminal system with time-reversal symmetry while it turns into a non-zero charge current via opening the third terminal or breaking time-reversal symmetry. Thus, we propose a spin transistor that is controllable by the Onsager relation for the system and readable purely by electric means. We compare the numerical results with our prediction and show a good agreement for both the adiabatic and the high-frequency regimes. We also obtain the AC charge current in the nano-Ampere range with experimentally relevant parameters.

Chapter 6

DC SPIN AND CHARGE CURRENT GENERATION

Pumping is a general dynamical quantum transport mechanism for DC current in the absence of bias voltage, generated when some system parameters change periodically. It was first theoretically proposed by Thouless [77], who showed that a quantized charge current could be transported in an adiabatically modulated potential. This mechanism was later confirmed experimentally by investigating electron pumping in a quantum dot [78]. Charge pumping has been extensively studied in the literature with various applications in adiabatic regimes [79–86] and non-adiabatic regimes [87–89]. In its original formulation, the adiabatic modulation of the system was crucial to generating a current. In particular, Brouwer [90] formulated pumping current in terms of the scattering matrix of the system and showed that there is a non-vanishing current when at least two of the system's parameters are modulated with the same frequency but with a phase difference. This way, the quantized pumping charge is expressed as an integral of derivatives of the scattering matrix with respect to the modulation parameters in an area in the parameter space. On the other hand, pumping in systems with a single modulation parameter is realized outside the adiabatic regime [78]. The general formulation of the pumping current is theoretically formulated by Moskalets and Buttiker [32]. They provide a formula for the pumping current using the Floquet scattering matrix, explained in Chapter 3. A comparison of the two methods is also studied in [91] for adiabatic pumping.

The idea of pumping an electric current can also be used to generate DC spin currents, which goes under the name of *spin pumping*. This method is promising in developing spin transport, especially for spin injection, and it will be the focus of attention in this chapter. Spin-polarized pumping has been realized in experiment [92] following a theoretical proposal by Mucciolo et al. [93] which suggested generating a spin current by pumping

electrons through a chaotic dot together with an in-plane magnetic field. Spin pumping utilizing a magnetic field has also been proposed in [94–96]. Zhang et al. suggested pumping spin using ferromagnetic leads [70].

We are interested in pumping spin degrees of freedom using electrical methods based on Rashba SOI. This method has attracted interest over the last decade [60, 61, 97–104]. Below, we focus on the DC spin and charge current in the presence of a time-dependent potential. First, we investigate the two-parameter charge and spin pumping in the adiabatic regime. We compare the adiabatic approximation result with the Floquet scattering matrix result on a 2D quantum wire in the presence of the two separate time-dependent Rashba couplings with a phase difference. Secondly, we investigate the single parameter pumping. Adiabatic approximation yields vanishing results in single-parameter systems for charge and spin currents because these currents go like Ω^2 in single-parameter systems [105, 106]. Therefore we investigate the single-parameter systems using the Floquet scattering matrix. We numerically compute charge and spin currents in the system with one-parameter time-dependent Rashba SOI and find non-vanishing results.

6.1 Model And Formulation

For our numerical simulations, we consider a quantum wire consisting of a 2DEG. Applying two separate AC gate voltages on the right and left part of the wire generates periodic Rashba SOI inside the scattering region, as shown in Fig. 6.1. The wire is connected to two leads as electron reservoirs, and the Rashba coupling is absent on the leads. We choose the geometry of the 2D quantum wire with cavities which breaks the spatial symmetry independent of the Hamiltonian as shown at the bottom in Fig 6.1. (We note that the spatial symmetry in our system would also be broken even in the absence of this cavity due to the Rashba coupling which breaks the reflection symmetry in the x direction).

The Hamiltonian of our model is

$$H = \frac{p^2}{2m} + \alpha(t)(\sigma^x p_y - \sigma^y p_x) + V(\mathbf{x}),\qquad(6.1)$$

where $V(\mathbf{x})$ is the electrostatic potential. We choose the Rashba SOI as

$$\alpha_i(t) = k_{so,0} + k_{so,1}\cos(\Omega t + \theta_i)\qquad(6.2)$$

where $k_{so,0}$ denotes the static part of the Rashba SOI strength and $k_{so,1}$ gives the amplitude of the time-dependent part of the Rashba SOI with driving frequency Ω and phase θ_i. We denote the Rashba couplings for the left and right part of the system in Fig 6.1 by $i = 1$ and
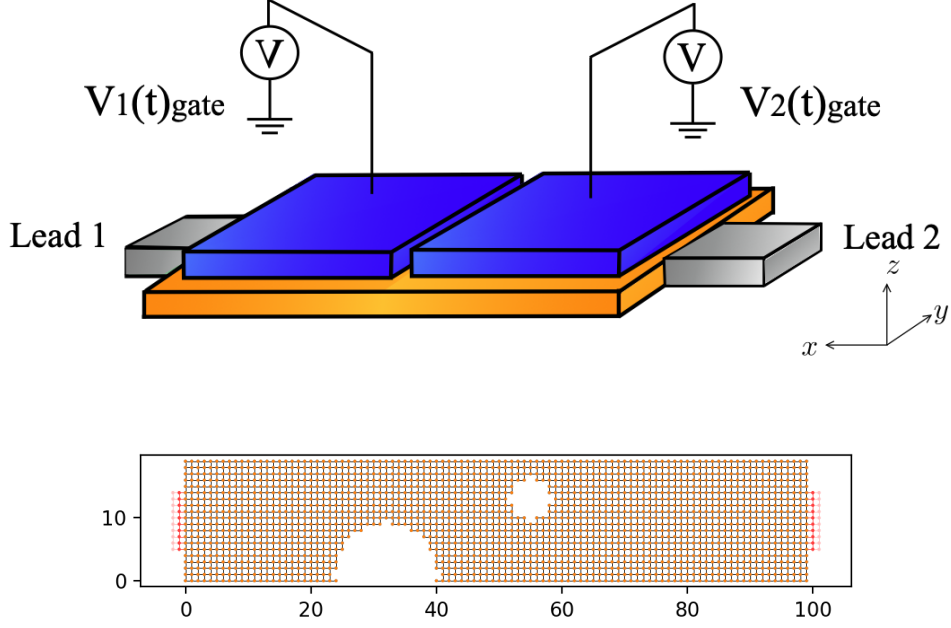
Figure 6.1: Setup for spin pumping connected to two leads. AC gate voltages, which generate a time-dependent Rashba SOI, are applied on top of the 2DEG with the same frequency but a different phase as shown in the top panel. The geometry of the 2D quantum wire is shown in the bottom panel.

$i = 2$, respectively, with a non-vanishing phase difference $\theta_2 - \theta_1 = \theta$ where $\theta_1 = 0$ and $\theta_2 = \theta$. In chapter 3, we outline the DC current calculations with the help of the Floquet scattering theory when there is a time-dependent potential. Using the unitarity condition of the Floquet scattering matrix in Eq. 3.18 and making the energy shift $E \rightarrow E - n\hbar\Omega$, the DC current which corresponds to the $l = 0$ term in Eq. 3.34 represents a difference of the two Floquet scattering matrices in the absence of the bias voltage, where the Fermi function on both leads are equal $f_1(E) = f_2(E) = f_0(E)$:

$$I_{i,0}^a = C_a \int dE f_0(E) \sum_{n=-\infty}^{\infty} \sum_{j}^{N_r} \times$$

$$\left\{ S_{F,ij}(E_n, E, \theta)^\dagger \sigma^a S_{F,ij}(E_n, E, \theta) - S_{F,ij}(E, E_n, \theta)^\dagger \sigma^a S_{F,ij}(E, E_n, \theta) \right\} \quad (6.3)$$

This expression helps us understand how the symmetry properties of the system affect the spin and charge pumping in both adiabatic and high-frequency regimes. We recall that the Floquet scattering matrix satisfies the following symmetry (see Chapter 3).

$$S_{F,ij}^{ss'}(E, E_n, \theta) = S_{F,ji}^{s's}(E_n, E, -\theta). \quad (6.4)$$

In general, to generate a non-vanishing pumping current in the equation above, one needs

to break the left-right symmetry, which can be achieved at least in two separate ways, namely, by breaking the time-reversal symmetry or the spatial symmetry [6]. However, in the adiabatic regime for $n\hbar\Omega \ll E$, the adiabatic approximation of the Floquet scattering matrix in Eq.(4.4) will depend on single energy E, and we will need breaking of both the time-reversal and the spatial symmetry to generate a non-trivial pumping. In the current setup, we maintain a phase difference on the system's left and right parts, hence breaking the time-reversal symmetry as well. Moreover, cavities in the quantum wire also break the spatial symmetry in the system.

6.2 Numerical Results: Adiabatic Spin And Charge Pumping

In this section, we investigate spin and charge pumping due to time-dependent Rashba SOI generated by the AC gate voltage. We consider the model shown in Fig. 6.1 by applying two gate voltages with phase difference θ. Rashba SOI on the left part of the system $\alpha(t) = k_{so,0} + k_{so,1}\cos(\Omega t)$ and on the right part of the system $\alpha(t) = k_{so,0} + k_{so,1}\cos(\Omega t + \theta)$ where $k_{so,0} = k_{so,1} = 1/L$ and the length of the system is given by $L = 100a$ and a the lattice constant is 2 nm. We chose the width of the system as $W = 20a$ and the leads as $10a$.

We first investigate how the phase difference between the two gate voltages (see Fig. 6.1) affects the pumping currents in the adiabatic approximation. For these calculations, we use the formula in Eq.(6.3)) with the adiabatic approximation of the Floquet scattering matrix in Eq.(4.4). The current is calculated with the Fermi energy $E_F = 0.2\ eV$, at which only two transverse channels are open. In this computation, first, we obtain the time of flight τ using the Wigner-Smith time delay matrix explained in Chapter 3.2.3. We then choose $\Omega\tau \approx 0.012$, here corresponding frequency $\Omega/2\pi$ is approximately 10 GHz. As expected, we obtain a vanishing current when the phase difference is $\theta = 0, \pi$, and 2π and the current attains its maximum value at the phase difference $\theta = \pi/2$ and $3\pi/2$. These results are shown in Fig. 6.2, where charge and spin pumping currents with the spin directions x, y, and z are plotted. We note that the direction of the current changes with $\theta \rightarrow -\theta$. In Fig. 6.3, we concentrate on the spin pumping current and analyze its dependence on the value of the Rashba coupling. This figure plots the spin current in the z-spin direction as a function of the Fermi energy. We observe that the current magnitude increases with the coupling strength. Finally, in Fig. 6.4, we compare the charge and spin pumping currents obtained by The Floquet scattering matrix and its adiabatic approximation. We see that, while the two agree remarkably well for small
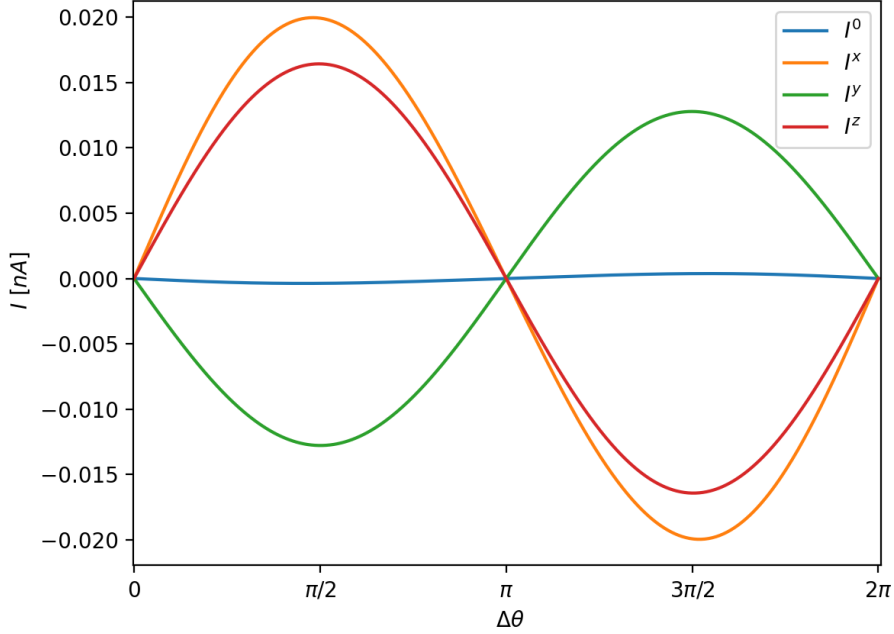
Figure 6.2: Spin and charge pumping currents versus the phase difference $\Delta\theta$ between left and right Rashba SOI in the system in the adiabatic approximation where the Fermi energy $E_F = 0.2\,\mathrm{eV}$, $\Omega\tau \approx 0.012$, Rashba SOI $\alpha(t) = k_{so,0} + k_{so,1}\cos(\Omega t + \theta)$, and $k_{so,0} = k_{so,1} = 1/L$. The charge current turns out to be non-vanishing yet much smaller than the spin currents in the adiabatic approximation.

frequencies, below $\Omega\tau < 0.012$, they start to show disagreement in the charge current for $\Omega\tau \approx 0.12$. This corresponds approximately to $\Omega/2\pi \approx 100\,\mathrm{GHz}$. We remark that the agreement holds for the spin currents in this frequency range.

6.3   Numerical Results : Spin and Charge Pumping beyond the Adiabatic Approximation

In this section, we investigate single-parameter pumping beyond the adiabatic approximation. First, we compare the two methods, the full Floquet formalism and its adiabatic approximation. We consider the same model as in Fig. 6.1 with the system length $L = 100a$, system width $W = 20a$, and width of the leads $10a$ where the lattice constant, $a = 2$ nm. To obtain one parameter pumping, we consider the vanishing phase difference between right and left gate voltages and the Rashba SOI inside the scattering region is then uniform as $\alpha(t) = k_{so,0} + k_{so,1}\cos(\Omega t)$ where we choose $k_{so,0}L = k_{so,1}L = 1$. Because we preserve the time-reversal symmetry, the adiabatic approximation gives vanishing currents in this case. On the other hand, Floquet formalism containing the higher order terms in the driving frequency yields non-vanishing results even in the one-parameter case.
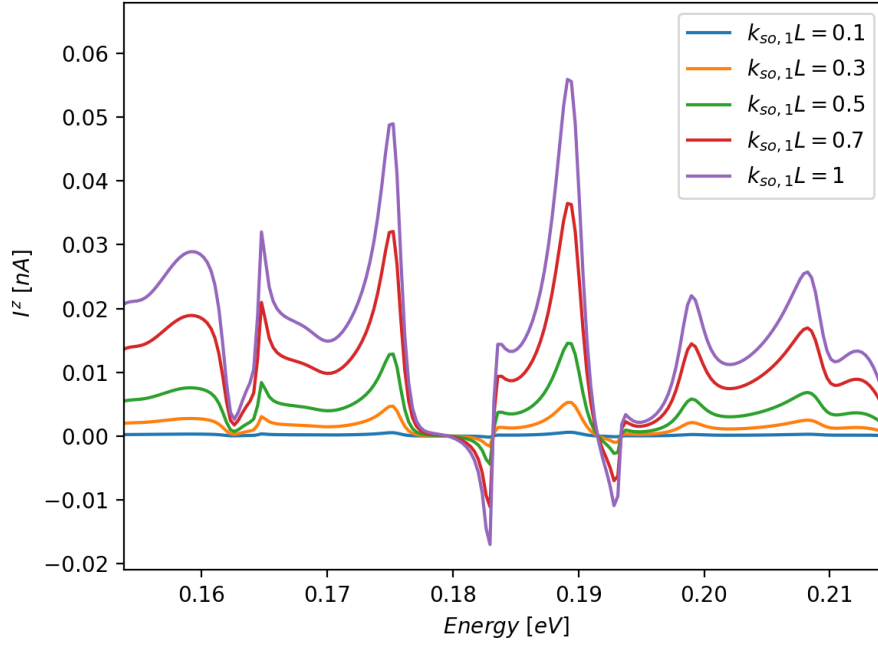
Figure 6.3: Spin pumping currents in z direction for values of the Rashba coupling $k_{so,1} = 0.1, 0.3, 0.5, 0.7$ and 1 where $\Omega\tau \approx 0.012$, Rashba SOI $\alpha(t) = k_{so,0} + k_{so,1}\cos(\Omega t + \theta)$ where $k_{so,0}L = k_{so,1}L = 1$, and on the right part $\theta = \pi/2$.

We plot the charge and spin pumping as a function of the Fermi energy, generated by one parameter driving Rashba SOI where $\Omega\tau \approx 1$ with 2 open transverse channel in Fig.6.5. This corresponds to $\Omega/2\pi \approx 800$ GHz. These results altogether show that we can acquire experimentally detectable pumping currents in the nA scale using the full Floquet scattering matrix for one parameter pumping. In Fig. 6.6, we also show how these currents are affected by the driving frequency up to $\Omega\tau \approx 1$ (left) and by the Rashba coupling constant up to $k_{so}L = 2$ (right). We observe in the left figure that the currents increase quadratically as a function of the frequency for small values of Ω. Finally, we observe in the right figure that the currents also increase as a function of k_{so} as expected.

6.4   Conclusion

In this chapter, we investigated pumping current both for charge and spin transport in the presence of the time-dependent Rashba coupling. In the adiabatic regime, we showed that DC spin and charge currents are present in the system with two-parameter pumping. We observed that the resulting pumping currents are directly proportional to the amplitude of the time-dependent Rashba coupling. We also compared adiabatic approximation with the full Floquet scattering matrix analysis and confirmed that they agree at low frequencies. Finally, we investigated one parameter pumping beyond the adiabatic approximation and demonstrated using the Floquet scattering matrix that non-vanishing pumping currents
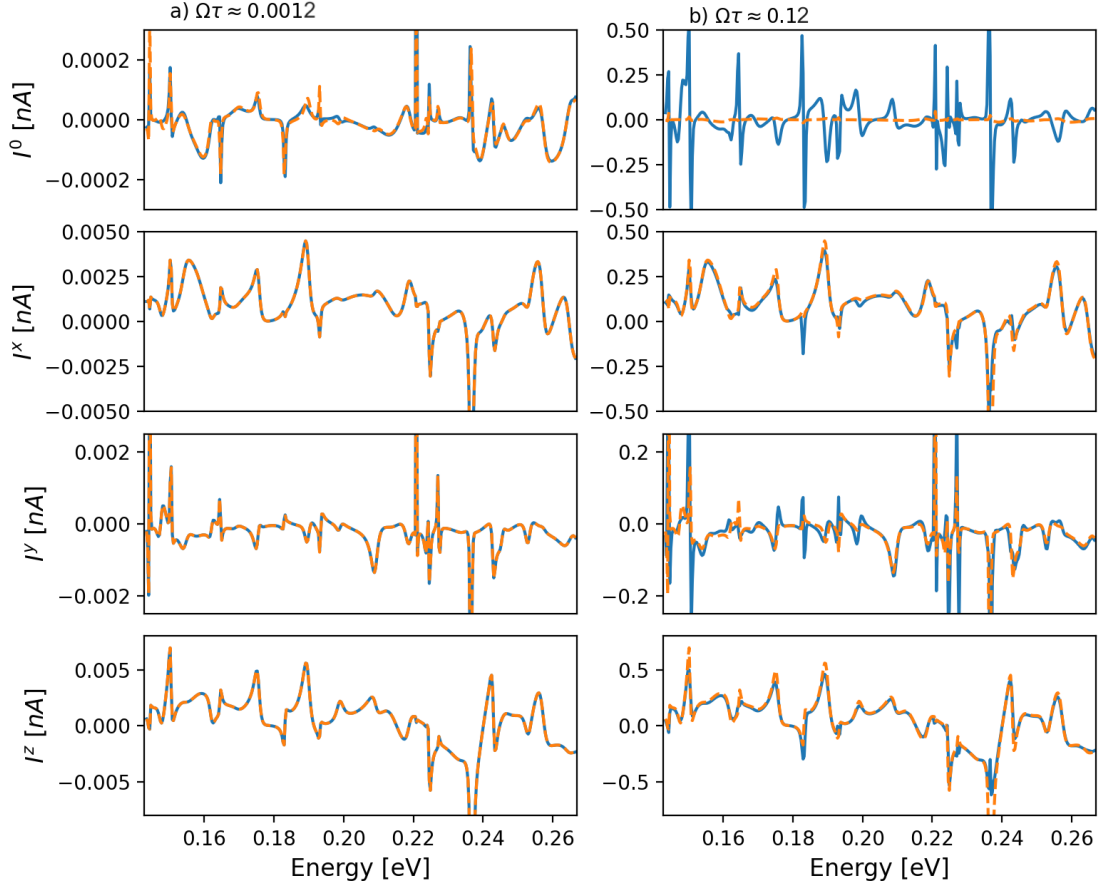
Figure 6.4: Comparing adiabatic approximation result (orange) with Floquet scattering matrix result (blue) in the adiabatic regime where $\Omega\tau \approx 0.0012$ and 0.12, Rashba SOI $\alpha(t) = k_{so,0} + k_{so,1}\cos(\Omega t + \theta)$ where $k_{so,0} = k_{so,1} = 1/L$ and on the right part of the system $\theta = \pi/2$.

can be obtained via the driving Rashba SOI while preserving the time-reversal symmetry. Our results show that we can acquire experimentally detectable pumping currents in the nA scale using the full Floquet scattering matrix formalism.
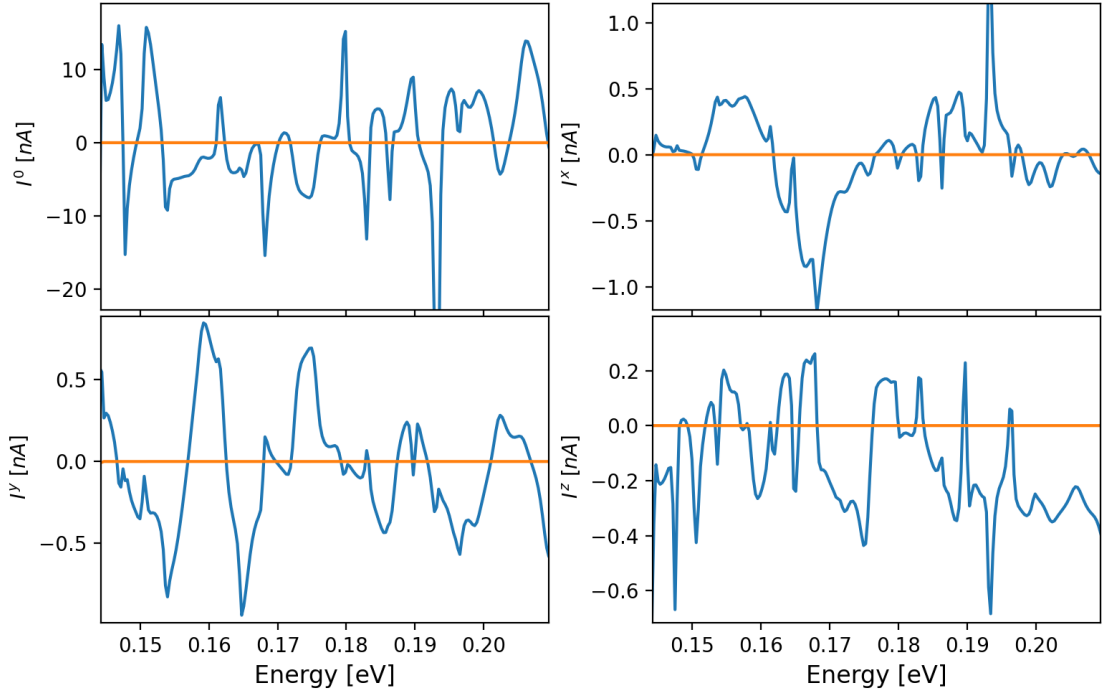
Figure 6.5: Single parameter spin and charge pumping calculated by adiabatic approximation (orange) and full Floquet scattering matrix (blue) where $\Omega\tau \approx 1$, Rashba SOI $\alpha(t) = k_{so,0} + k_{so,1}\cos(\Omega t)$, where $k_{so,0} = k_{so,1} = 1/L$.
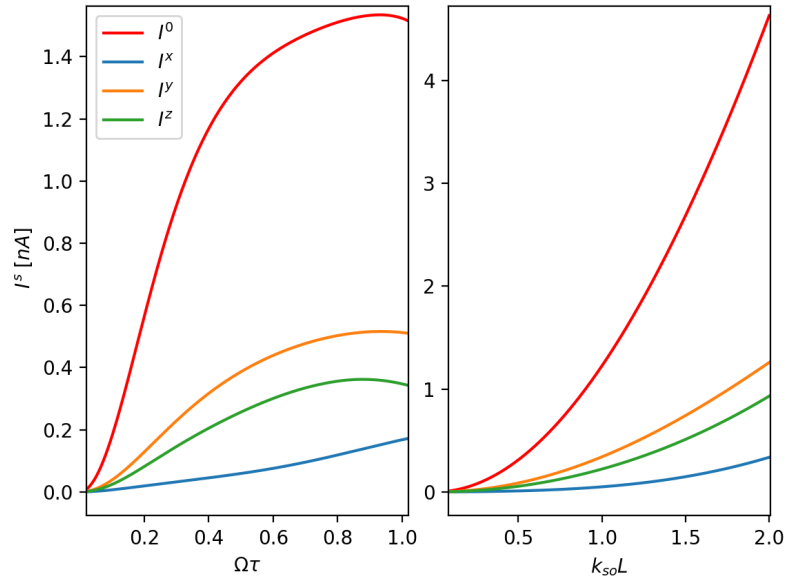
Figure 6.6: Single parameter spin and charge pumping as a function of $\Omega\tau$ up to $\Omega\tau \approx 1$ (left) and as a function of $k_{so}L$ up to 2 (right). The parameters are chosen as $E_F = 0.2$ eV, the Rashba SOI $\alpha(t) = k_{so,0} + k_{so,1}\cos(\Omega t)$. $k_{so,0} = k_{so,1} = 1/L$ (left) and $\Omega\tau \approx 0.5$ (right).

69

Chapter 7

CONCLUSION

The aim of this thesis was to study time-dependent charge/spin transport in ballistic 2DEGs. Time dependence of the current results either from a periodic in-time potential inside the scattering region or from an AC bias voltage. We focused on the effects of the Rashba SOI, modulated by an AC gate voltage. We used Floquet scattering theory to calculate time-dependent currents in these systems. We calculated Floquet scattering matrices with numerical tight-binding simulations. Results of Chapters 4 and 5 are published in Ref. [107].

In chapter 2, we briefly overview spin and charge transport in stationary systems to provide a background for time-dependent transport. We shortly introduced mesoscopic systems consisting of the 2DEGs with spin-orbit interaction and the relevant length scales. We outlined the calculation of spin and charge currents using scattering matrix and applying the Landauer-Büttiker formula in ballistic systems.

Chapter 3 explains how to formulate the time-dependent currents with a periodic in-time potential. We use the Floquet scattering theory. First, we showed how to convert the time-dependent Hamiltonian into a static matrix Hamiltonian with Floquet states which are eigenfunctions of the Floquet Hamiltonian. We can then obtain each transmission amplitude from one Floquet channel to another, which forms the elements of the Floquet scattering matrix. We also defined the adiabatic approximation to the Floquet scattering matrix in the low-frequency regime. We outlined the Dwell time calculation using the Wigner-Smith time-delay matrix to characterize the onset of the adiabatic regime. Finally, we explained how the Landauer-Büttiker formalism is adapted to two time-dependent situations: a dynamical potential in the scattering region and an AC bias voltage application.

In chapter 4, we investigated the generation of the AC spin current via tuning the Rashba SOI periodically in time. In particular, we used the Floquet scattering theory to show these

spin currents in a chaotic ballistic 2DEG without a bias voltage. We first determined the number of Floquet channels needed depending on our choice of system parameters and the low and high-frequency regimes. We demonstrated that the adiabatic approximation agrees with the full Floquet result up to a specific frequency value. We also studied higher harmonic generation of charge and spin currents and observed that either odd or even harmonics contribute non-trivially. We explained this finding based on discrete symmetries in our system. We then showed that formulation of the Rashba coupling in terms of an SU(2) gauge field allows us to express, by a gauge transformation, the time-dependent coupling as a spin-dependent electric field and demonstrated this numerically. We then considered these fields as spin-dependent voltage. We converted the AC spin current generated by periodic in-time Rashba SOI into an AC spin current obtained by this spin voltage and charge conductance.

In chapter 5, we explored the conversion of the AC spin current into an AC charge current utilizing spatially inhomogeneous Rashba SOI. We considered a two-terminal system consisting of two parts, one with dynamical Rashba SOI and another with spatially inhomogeneous Rashba SOI. In the latter case, a similar gauge transformation results in two spin magnetic fields in opposite directions. Then, spin conductance is approximated to the charge magnetoconductance. All in all, the spin current resulting from the time-dependent Rashba SOI is read out as a charge current using a spin-dependent voltage and a charge magnetoconductance. Using the Onsager relation, we propose our system as a spin transistor by opening the third terminal to control the on/off states. We demonstrate our results by numerical simulations in the low and high-frequency regimes with experimentally relevant parameters.

In chapter 6, we focused on the generation of DC current. First, we analyzed spin and charge pumping for a ballistic 2DEG quantum wire with periodically time-dependent Rashba SOI. In the case of two-parameter pumping, one obtains a non-trivial current in the adiabatic approximation due to a phase difference between two driving potentials. We show how this phase difference and the amplitude of the Rashba coupling affect pumping of the spin and charge currents. We also explore one parameter pumping beyond the adiabatic approximation. Using the Floquet scattering matrix, we obtained a non-vanishing spin and charge current, which are generated by the dynamical Rashba SOI even in this case.

Bibliography

[1] G. Moore, "Cramming more components onto integrated circuits," *Proceedings of the IEEE*, vol. 86, no. 1, pp. 82–85, 1998.

[2] I. Žutić, J. Fabian, and S. Das Sarma, "Spintronics: Fundamentals and applications," *Rev. Mod. Phys.*, vol. 76, pp. 323–410, Apr 2004.

[3] G. Schmidt, D. Ferrand, L. W. Molenkamp, A. T. Filip, and B. J. van Wees, "Fundamental obstacle for electrical spin injection from a ferromagnetic metal into a diffusive semiconductor," *Phys. Rev. B*, vol. 62, pp. R4790–R4793, Aug 2000.

[4] M. Johnson and R. H. Silsbee, "Coupling of electronic charge and spin at a ferromagnetic-paramagnetic metal interface," *Phys. Rev. B*, vol. 37, pp. 5312–5325, Apr 1988.

[5] J. Nitta, T. Akazaki, H. Takayanagi, and T. Enoki, "Gate control of spin-orbit interaction in an inverted $in_{0.53}ga_{0.47}as/in_{0.52}al_{0.48}as$ heterostructure," *Phys. Rev. Lett.*, vol. 78, pp. 1335–1338, Feb 1997.

[6] M. V. Moskalets, *Scattering Matrix Approach to Non-Stationary Quantum Transport*. World Scientific Publishing Co, Sept. 2012.

[7] G. Platero and R. Aguado, "Photon-assisted transport in semiconductor nanostructures," *Physics Reports*, vol. 395, p. 1–157, May 2004.

[8] M. Grifoni and P. Hänggi, "Driven quantum tunneling," *Physics Reports*, vol. 304, no. 5, pp. 229–354, 1998.

[9] E. P. Wigner, "Lower limit for the energy derivative of the scattering phase shift," *Phys. Rev.*, vol. 98, pp. 145–147, Apr 1955.

[10] F. T. Smith, "Lifetime matrix in collision theory," *Phys. Rev.*, vol. 118, pp. 349–356, Apr 1960.

[11] Y. Imry, *Introduction to Mesoscopic Physics*. Mesoscopic physics and nanotechnology, Oxford University Press, 2002.

[12] C. Beenakker and H. van Houten, "Quantum transport in semiconductor nanostructures," in *Semiconductor Heterostructures and Nanostructures* (H. Ehrenreich and D. Turnbull, eds.), vol. 44 of *Solid State Physics*, pp. 1 – 228, Academic Press, 1991.

[13] J. Fabian, A. Matos-Abiague, C. Ertler, P. Stano, and I. Zutic, "Semiconductor spintronics," *Acta Physica Slovaca*, vol. 57, 08 2007.

[14] G. Dresselhaus, "Spin-orbit coupling effects in zinc blende structures," *Phys. Rev.*, vol. 100, pp. 580–586, Oct 1955.

[15] E. Rashba, "Properties of semiconductors with an extremum loop.1. cyclotron and combinational resonance in a magnetic field perpendicular to the plane of the loop," *Soviet Physics-Solid State*, vol. 2, no. 6, pp. 1109–1122, 1960.

[16] D. Stein, K. v. Klitzing, and G. Weimann, "Electron spin resonance on $GaAs - al_xga_{1-x}As$ heterostructures," *Phys. Rev. Lett.*, vol. 51, pp. 130–133, Jul 1983.

[17] H. L. Stormer, Z. Schlesinger, A. Chang, D. C. Tsui, A. C. Gossard, and W. Wiegmann, "Energy structure and quantized hall effect of two-dimensional holes," *Phys. Rev. Lett.*, vol. 51, pp. 126–129, Jul 1983.

[18] Y. A. Bychkov and E. I. Rashba, "Oscillatory effects and the magnetic susceptibility of carriers in inversion layers," *Journal of Physics C: Solid State Physics*, vol. 17, pp. 6039–6045, nov 1984.

[19] S. Giglberger, L. E. Golub, V. V. Bel'kov, S. N. Danilov, D. Schuh, C. Gerl, F. Rohlfing, J. Stahl, W. Wegscheider, D. Weiss, W. Prettl, and S. D. Ganichev, "Rashba and dresselhaus spin splittings in semiconductor quantum wells measured by spin photocurrents," *Phys. Rev. B*, vol. 75, p. 035327, Jan 2007.

[20] T. Schäpers, G. Engels, J. Lange, T. Klocke, M. Hollfelder, and H. Lüth, "Effect of the heterointerface on the spin splitting in modulation doped inxga1xas/inp quantum wells for b0," *Journal of Applied Physics*, vol. 83, no. 8, pp. 4324–4333, 1998.

[21] D. Grundler, "Large rashba splitting in inas quantum wells due to electron wave function penetration into the barrier layers," *Phys. Rev. Lett.*, vol. 84, pp. 6074–6077, Jun 2000.

[22] G. E. Kimball and G. H. Shortley, "The numerical solution of schrödinger's equation," *Phys. Rev.*, vol. 45, pp. 815–820, Jun 1934.

[23] S. Datta, *Electronic Transport in Mesoscopic Systems*. Cambridge Studies in Semiconductor Physics and Microelectronic Engineering, Cambridge University Press, 1995.

[24] R. Landauer, "Spatial variation of currents and fields due to localized scatterers in metallic conduction," *IBM Journal of Research and Development*, vol. 1, no. 3, pp. 223–231, 1957.

[25] M. Büttiker, "Four-terminal phase-coherent conductance," *Phys. Rev. Lett.*, vol. 57, pp. 1761–1764, Oct 1986.

[26] Y. V. Nazarov and Y. M. Blanter, *Quantum Transport: Introduction to Nanoscience.* Cambridge University Press, 2009.

[27] E. I. Rashba, "Spin–orbit coupling and spin transport," *Physica E: Low-dimensional Systems and Nanostructures*, vol. 34, no. 1, pp. 31 – 35, 2006.

[28] İ. Adagideli, J. H. Bardarson, and P. Jacquod, "Electrical probing of the spin conductance of mesoscopic cavities," *Journal of Physics: Condensed Matter*, vol. 21, p. 155503, mar 2009.

[29] M. Büttiker, A. Prêtre, and H. Thomas, "Dynamic conductance and the scattering matrix of small conductors," *Phys. Rev. Lett.*, vol. 70, pp. 4114–4117, Jun 1993.

[30] J. H. Shirley, "Solution of the schrödinger equation with a hamiltonian periodic in time," *Phys. Rev.*, vol. 138, pp. B979–B987, May 1965.

[31] F. D. Parmentier, E. Bocquillon, J.-M. Berroir, D. C. Glattli, B. Plaçais, G. Fève, M. Albert, C. Flindt, and M. Büttiker, "Current noise spectrum of a single-particle emitter: Theory and experiment," *Physical Review B*, vol. 85, Apr 2012.

[32] M. Moskalets and M. Büttiker, "Floquet scattering theory of quantum pumps," *Phys. Rev. B*, vol. 66, p. 205320, Nov 2002.

[33] G. Floquet, "Sur les équations différentielles linéaires à coefficients périodiques," *Annales scientifiques de l'École Normale Supérieure*, vol. 2e série, 12, pp. 47–88, 1883.

[34] M. Moskalets and M. Büttiker, "Adiabatic quantum pump in the presence of external ac voltages," *Phys. Rev. B*, vol. 69, p. 205316, May 2004.

[35] M. Moskalets and M. Büttiker, "Magnetic-field symmetry of pump currents of adiabatically driven mesoscopic structures," *Physical Review B*, vol. 72, Jul 2005.

[36] D. Bercioux and P. Lucignano, "Quantum transport in rashba spin–orbit materials: a review," *Reports on Progress in Physics*, vol. 78, p. 106001, sep 2015.

[37] M. Büttiker, "Scattering theory of current and intensity noise correlations in conductors and wave guides," *Phys. Rev. B*, vol. 46, pp. 12485–12507, Nov 1992.

[38] M. Moskalets and M. Büttiker, "Time-resolved noise of adiabatic quantum pumps," *Phys. Rev. B*, vol. 75, p. 035315, Jan 2007.

[39] A.-P. Jauho, N. S. Wingreen, and Y. Meir, "Time-dependent transport in interacting and noninteracting resonant-tunneling systems," *Phys. Rev. B*, vol. 50, pp. 5528–5544, Aug 1994.

[40] M. H. Pedersen and M. Büttiker, "Scattering theory of photon-assisted electron transport," *Phys. Rev. B*, vol. 58, pp. 12993–13006, Nov 1998.

[41] A. Prêtre, H. Thomas, and M. Büttiker, "Dynamic admittance of mesoscopic conductors: Discrete-potential model," *Phys. Rev. B*, vol. 54, pp. 8130–8143, Sep 1996.

[42] C. W. Groth, M. Wimmer, A. R. Akhmerov, and X. Waintal, "Kwant: a software package for quantum transport," *New Journal of Physics*, vol. 16, p. 063065, jun 2014.

[43] R. Winkler, *Spin-Orbit Coupling Effects in Two-Dimensional Electron and Hole Systems*. Springer, 2003.

[44] I. Adagideli, V. Lutsker, M. Scheid, P. Jacquod, and K. Richter, "Spin transistor action from hidden onsager reciprocity," *Phys. Rev. Lett.*, vol. 108, p. 236601, Jun 2012.

[45] I. L. Aleiner and V. I. Fal'ko, "Spin-orbit coupling effects on quantum transport in lateral semiconductor dots," *Phys. Rev. Lett.*, vol. 87, p. 256801, 2001.

[46] P. W. Brouwer, J. N. H. J. Cremers, and B. I. Halperin, "Weak localization and conductance fluctuations of a chaotic quantum dot with tunable spin-orbit coupling," *Phys. Rev. B*, vol. 65, p. 081302(R), 2002.

[47] Y. Tserkovnyak and M. Mecklenburg, "Electron transport driven by nonequilibrium magnetic textures," *Phys. Rev. B*, vol. 77, p. 134407, Apr 2008.

[48] L. S. Levitov, H. Lee, and G. B. Lesovik, "Electron counting statistics and coherent states of electric current," *Journal of Mathematical Physics*, vol. 37, no. 10, pp. 4845–4866, 1996.

[49] B. K. Nikolić, L. P. Zârbo, and S. Souma, "Mesoscopic spin hall effect in multiprobe ballistic spin-orbit-coupled semiconductor bridges," *Phys. Rev. B*, vol. 72, p. 075361, Aug 2005.

[50] M. Büttiker, "Dynamic conductance and quantum noise in mesoscopic conductors," *Journal of Mathematical Physics*, vol. 37, no. 10, pp. 4793–4815, 1996.

[51] M. Lysne, Y. Murakami, M. Schüler, and P. Werner, "High-harmonic generation in spin-orbit coupled systems," *Phys. Rev. B*, vol. 102, p. 081121, Aug 2020.

[52] K. Hamamoto, M. Ezawa, K. W. Kim, T. Morimoto, and N. Nagaosa, "Nonlinear spin current generation in noncentrosymmetric spin-orbit coupled systems," *Phys. Rev. B*, vol. 95, p. 224430, Jun 2017.

[53] O. E. Alon, V. Averbukh, and N. Moiseyev, "Selection rules for the high harmonic generation spectra," *Phys. Rev. Lett.*, vol. 80, pp. 3743–3746, Apr 1998.

[54] E. I. Rashba, "Spin currents in thermodynamic equilibrium: The challenge of discerning transport currents," *Phys. Rev. B*, vol. 68, p. 241315, Dec 2003.

[55] S. Datta and B. Das, "Electronic analog of the electro-optic modulator," *Applied Physics Letters*, vol. 56, no. 7, pp. 665–667, 1990.

[56] S. D. Ganichev, M. Trushin, and J. Schliemann, "Spin orientation by electric current," in *Handbook of Spin Transport and Magnetism* (E. Y. Tsymbal and I. Zutic, eds.), Chapman and Hall, 2 ed., 2016.

[57] M. Dyakonov and V. Perel, "Current-induced spin orientation of electrons in semiconductors," *Physics Letters A*, vol. 35, no. 6, pp. 459–460, 1971.

[58] J. Ohe, M. Yamamoto, T. Ohtsuki, and J. Nitta, "Mesoscopic stern-gerlach spin filter by nonuniform spin-orbit interaction," *Phys. Rev. B*, vol. 72, p. 041308, Jul 2005.

[59] A. G. Mal'shukov, C. S. Tang, C. S. Chu, and K. A. Chao, "Spin-current generation and detection in the presence of an ac gate," *Phys. Rev. B*, vol. 68, p. 233307, Dec 2003.

[60] M. Governale, F. Taddei, and R. Fazio, "Pumping spin with electrical fields," *Phys. Rev. B*, vol. 68, p. 155324, Oct 2003.

[61] P. Sharma and P. W. Brouwer, "Mesoscopic effects in adiabatic spin pumping," *Phys. Rev. Lett.*, vol. 91, p. 166801, Oct 2003.

[62] H. Mathur and A. D. Stone, "Quantum transport and the electronic aharonov-casher effect," *Phys. Rev. Lett.*, vol. 68, p. 2964, 1992.

[63] J. Fröhlich and U. M. Studer, "Gauge invariance and current algebra in nonrelativistic many-body theory," *Rev. Mod. Phys.*, vol. 65, p. 733, 1993.

[64] I. V. Tokatly, "Equilibrium spin currents: Non-abelian gauge invariance and color diamagnetism in condensed matter," *Phys. Rev. Lett.*, vol. 101, p. 106601, 2008.

[65] C. Gorini, P. Schwab, R. Raimondi, and A. L. Shelankov, "Non-abelian gauge fields in the gradient expansion: Generalized boltzmann and eilenberger equations," *Phys. Rev. B*, vol. 82, p. 195316, Nov 2010.

[66] C. Gorini, R. Raimondi, and P. Schwab, "Onsager relations in a two-dimensional electron gas with spin-orbit coupling," *Phys. Rev. Lett.*, vol. 109, p. 246604, Dec 2012.

[67] E. H. Fyhn and J. Linder, "Spin-orbit pumping," *Phys. Rev. B*, vol. 105, p. L020409, Jan 2022.

[68] P. Földi, O. Kálmán, and M. G. Benedict, "Two-dimensional quantum rings with oscillating spin-orbit interaction strength: A wave function picture," *Phys. Rev. B*, vol. 82, p. 165322, Oct 2010.

[69] R. S. M Jonson and O. Entin-Wohlman, "Dc spin generation by junctions with ac driven spin-orbit interaction," *arXiv:1903.03321*, March 2019.

[70] S.-F. Zhang and W. Zhu, "The limit spin current in a time-dependent rashba spin-orbit coupling system," *Journal of physics. Condensed matter : an Institute of Physics journal*, vol. 25, p. 075302, 01 2013.

[71] A. López, Z. Z. Sun, and J. Schliemann, "Floquet spin states in graphene under ac-driven spin-orbit interaction," *Phys. Rev. B*, vol. 85, p. 205428, May 2012.

[72] M. Berdakin, E. A. Rodríguez-Mena, and L. E. F. Foa Torres, "Spin-polarized tunable photocurrents," *Nano Letters*, vol. 21, no. 7, pp. 3177–3183, 2021. PMID: 33819037.

[73] B. Berche, N. Bolívar, A. López, and E. Medina, "Gauge transformations of spin-orbit interactions in graphene," *The European Physical Journal B*, vol. 88, p. 025004, Aug 2015.

[74] I. Adagideli, G. E. W. Bauer, and B. I. Halperin, "Detection of current-induced spins by ferromagnetic contacts," *Phys. Rev. Lett.*, vol. 97, p. 256601, Dec 2006.

[75] I. Adagideli, M. Scheid, M. Wimmer, G. Bauer, and K. Richter, "Extracting current-induced spins: Spin boundary conditions at narrow hall contacts," *New Journal of Physics*, vol. 9, 09 2007.

[76] L. Onsager, "Reciprocal relations in irreversible processes. ii.," *Phys. Rev.*, vol. 38, pp. 2265–2279, Dec 1931.

[77] D. J. Thouless, "Quantization of particle transport," *Phys. Rev. B*, vol. 27, pp. 6083–6087, May 1983.

[78] M. Switkes, C. M. Marcus, K. Campman, and A. C. Gossard, "An adiabatic quantum electron pump," *Science*, vol. 283, no. 5409, pp. 1905–1908, 1999.

[79] J. E. Avron, A. Raveh, and B. Zur, "Adiabatic quantum transport in multiply connected systems," *Rev. Mod. Phys.*, vol. 60, pp. 873–915, Oct 1988.

[80] F. Zhou, B. Spivak, and B. Altshuler, "Mesoscopic mechanism of adiabatic charge transport," *Phys. Rev. Lett.*, vol. 82, pp. 608–611, Jan 1999.

[81] S.-L. Zhu and Z. D. Wang, "Charge pumping in a quantum wire driven by a series of local time-periodic potentials," *Phys. Rev. B*, vol. 65, p. 155313, Mar 2002.

[82] I. L. Aleiner and A. V. Andreev, "Adiabatic charge pumping in almost open dots," *Phys. Rev. Lett.*, vol. 81, pp. 1286–1289, Aug 1998.

[83] J. E. Avron, A. Elgart, G. M. Graf, and L. Sadun, "Geometry, statistics, and asymptotics of quantum pumps," *Phys. Rev. B*, vol. 62, pp. R10618–R10621, Oct 2000.

[84] D. Cohen, "Quantum pumping in closed systems, adiabatic transport, and the kubo formula," *Phys. Rev. B*, vol. 68, p. 155303, Oct 2003.

[85] F. Zhou, B. Spivak, and B. Altshuler, "Mesoscopic mechanism of adiabatic charge transport," *Phys. Rev. Lett.*, vol. 82, pp. 608–611, Jan 1999.

[86] M. L. Polianski and P. W. Brouwer, "Pumped current and voltage for an adiabatic quantum pump," *Phys. Rev. B*, vol. 64, p. 075304, Jul 2001.

[87] C. Tang and C. Chu, "Nonadiabatic quantum pumping in mesoscopic nanostructures," *Solid State Communications*, vol. 120, no. 9, pp. 353–357, 2001.

[88] B. Wang, J. Wang, and H. Guo, "Parametric pumping at finite frequency," *Phys. Rev. B*, vol. 65, p. 073306, Jan 2002.

[89] A. Soori and D. Sen, "Nonadiabatic charge pumping by oscillating potentials in one dimension: Results for infinite system and finite ring," *Phys. Rev. B*, vol. 82, p. 115432, Sep 2010.

[90] P. W. Brouwer, "Scattering approach to parametric pumping," *Phys. Rev. B*, vol. 58, pp. R10135–R10138, Oct 1998.

[91] S. W. Kim, "Floquet scattering in parametric electron pumps," *Phys. Rev. B*, vol. 66, p. 235304, Dec 2002.

[92] S. K. Watson, R. M. Potok, C. M. Marcus, and V. Umansky, "Experimental realization of a quantum spin pump," *Phys. Rev. Lett.*, vol. 91, p. 258301, Dec 2003.

[93] E. R. Mucciolo, C. Chamon, and C. M. Marcus, "Adiabatic quantum pump of spin-polarized current," *Phys. Rev. Lett.*, vol. 89, p. 146802, Sep 2002.

[94] C. Bena and L. Balents, "Spin pumping and magnetization dynamics in ferromagnet–luttinger liquid junctions," *Phys. Rev. B*, vol. 70, p. 245318, Dec 2004.

[95] E. Faizabadi, "Charge and spin pumping in quantum wires by a time-dependent periodic magnetic field," *Phys. Rev. B*, vol. 76, p. 075307, Aug 2007.

[96] E. H. Fyhn and J. Linder, "Spin-orbit pumping," 2021.

[97] A. G. Mal'shukov, C. S. Tang, C. S. Chu, and K. A. Chao, "Spin-current generation and detection in the presence of an ac gate," *Phys. Rev. B*, vol. 68, p. 233307, 2003.

[98] Y. Avishai, D. Cohen, and N. Nagaosa, "Purely electric spin pumping in one dimension," *Phys. Rev. Lett.*, vol. 104, p. 196601, May 2010.

[99] C. Li, Y. Yu, Y. Wei, and J. Wang, "Nonadiabatic quantum spin pump: Interplay between spatial interference and photon-assisted tunneling in two-dimensional rashba systems," *Phys. Rev. B*, vol. 75, p. 035312, Jan 2007.

[100] C.-H. Lin, C.-S. Tang, and Y.-C. Chang, "Nonmagnetic control of spin flow: Generation of pure spin current in a rashba-dresselhaus quantum channel," *Phys. Rev. B*, vol. 78, p. 245312, Dec 2008.

[101] H. Pan and Y. Zhao, "Spin pumping and spin filtering in double quantum dots with time-dependent spin-orbit interactions," *Journal of Applied Physics*, vol. 111, no. 8, p. 083703, 2012.

[102] Y.-C. Xiao, W.-Y. Deng, W.-J. Deng, R. Zhu, and R.-Q. Wang, "Quantum pump in a system with both rashba and dresselhaus spin–orbit couplings," *Physics Letters A*, vol. 377, no. 10, pp. 817–821, 2013.

[103] F. Romeo and R. Citro, "Adiabatic pumping in a double quantum dot structure with strong spin-orbit interaction," *Phys. Rev. B*, vol. 80, p. 165311, Oct 2009.

[104] M. Yama, M. Tatsuno, T. Kato, and M. Matsuo, "Spin pumping of two-dimensional electron gas with rashba and dresselhaus spin-orbit interactions," *Phys. Rev. B*, vol. 104, p. 054410, Aug 2021.

[105] U. Bajpai, B. S. Popescu, P. Plecháč, B. K. Nikolić, L. E. F. F. Torres, H. Ishizuka, and N. Nagaosa, "Spatio-temporal dynamics of shift current quantum pumping by femtosecond light pulse," *Journal of Physics: Materials*, vol. 2, p. 025004, mar 2019.

[106] L. E. F. Foa Torres, "Mono-parametric quantum charge pumping: Interplay between spatial interference and photon-assisted tunneling," *Phys. Rev. B*, vol. 72, p. 245339, Dec 2005.

[107] F. N. Gürsoy, P. Reck, C. Gorini, K. Richter, and I. Adagideli, "Dynamical spin-orbit-based spin transistor," 2021.